



NTNU – Trondheim
Norwegian University of
Science and Technology

Acoustic Emission from Arctic Steels

Andreas Vrenne Larsen

Mechanical Engineering

Submission date: June 2015

Supervisor: Christian Thaulow, IPM

Norwegian University of Science and Technology
Department of Engineering Design and Materials

THE NORWEGIAN UNIVERSITY
OF SCIENCE AND TECHNOLOGY
DEPARTMENT OF ENGINEERING DESIGN
AND MATERIALS

**MASTER THESIS SPRING 2015
FOR
STUD. TECHN. ANDREAS VRENNE LARSEN**

Acoustic Emission from Arctic Steels

Akustisk emisjon fra arktiske stål

Brittle fracture in steel is a process that is intricately linked to the microstructure in the material. Usually the fracture starts somewhere in front of the macroscopic crack, often associated with some kind of second phase particle. The local crack may propagate to become a global crack or it could possibly be arrested when facing microstructural barriers to further crack growth. The latter is a very interesting phenomenon; however, it is difficult to analyze just based on the traditional mechanical testing, as the events often are too small to cause any visible signs in the load-displacement curves. The use of Acoustic Emission (AE) offers a means to monitor this microcracking activity in more detail. There are several features that can be measured. The number of AE signals (stemming from microcrack nucleation) generated represents the rate of microcrack nucleation. However, recent research carried out also has demonstrated that the amplitude of the AE signal can be linked to the size of the arrested microcrack, allowing more quantitative data to be extracted from the testing. Thus, AE can be a valuable tool to better understand which microstructural features could lead to local crack arrest, and eventually provide valuable input to models for describing brittle fracture in steels.

During the work the candidate shall cooperate closely with stud techn Cathrine Gjerstad Hartwig who will focus on fractographic investigations of the AE samples.

The scope of the project thesis is:

- Summarize results obtained from the project work and present models to be investigated during the Master Thesis.
- Develop an experimental test setup to be able to detect arrested defects and perform tests. This can also include AE monitoring during nanomechanical testing
- Linking of the results to theoretical models for brittle fracture/FE modelling of microcracks, including estimation of local crack arrest values

Link between microstructure and observed AE behaviour

Formal requirements:

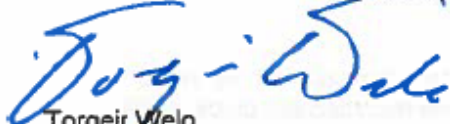
Three weeks after start of the thesis work, an A3 sheet illustrating the work is to be handed in. A template for this presentation is available on the IPM's web site under the menu


"Masteroppgave" (<http://www.ntnu.no/ipm/masteroppgave>). This sheet should be updated one week before the master's thesis is submitted.

Risk assessment of experimental activities shall always be performed. Experimental work defined in the problem description shall be planned and risk assessed up-front and within 3 weeks after receiving the problem text. Any specific experimental activities which are not properly covered by the general risk assessment shall be particularly assessed before performing the experimental work. Risk assessments should be signed by the supervisor and copies shall be included in the appendix of the thesis.

The thesis should include the signed problem text, and be written as a research report with summary both in English and Norwegian, conclusion, literature references, table of contents, etc. During preparation of the text, the candidate should make efforts to create a well arranged and well written report. To ease the evaluation of the thesis, it is important to cross-reference text, tables and figures. For evaluation of the work a thorough discussion of results is appreciated.

The thesis shall be submitted electronically via DAIM, NTNU's system for Digital Archiving and Submission of Master's theses.


Torgeir Welo
Head of Division


Christian Thaulow
Professor/Supervisor

 NTNU
Norges teknisk-
naturvitenskapelige universitet
Institutt for produktutvikling
og materialer

Preface

This report is the result of the master thesis carried out spring 2015 at the Norwegian University of Science and Technology. The master thesis is weighted 30 credits and is a continuation of the project thesis carried out during the third semester of the 2-year master program at the Department of Engineering Design and Materials.

This thesis is written for the Department of Engineering and Materials in cooperation with DNV GL and SINTEF. The main objective has been to investigate the relationship between Acoustic Emission (AE) amplitude and arrested cleavage microcrack size. A theoretical relationship presented by Lysak (1996) and further developed by Østby et al. (2012) forms the basis for this thesis. In addition, fractographic investigation has been carried out. Furthermore, improvements to the procedure for post processing of the AE signals have been made. In the early stage of investigation of fracture facets different events were observed and devoted attention. Keeping a steady progress has proved difficult as the two rounds of testing were both delayed between six and eight weeks, in addition to frequent breakdown of key equipment like the SEM.

Prior to this master thesis I had no knowledge of the lab work performed in this thesis or the equipment used, except for the AE equipment. A large amount of time has therefore been used learn the different equipment. The combination of practical lab work and theoretical analysis has been demanding and time consuming, but also very educational.

A large part of the time has been used to sort the results from both AE and EDS and investigation of the fracture surface in SEM. A large quantity of the work performed in this process is not presented in this thesis. A USB stick with all the data, except for the CTOD spreadsheet provided by SINTEF, has been delivered to Professor Christian Thaulow at the department. It is highly recommended that anyone who wishes to do further work at this field acquire this data.

In addition, the master thesis of Axel Louis Legouy Kvaal and Brage Dahl Snartland can be of interest as they investigate the R50A 420 steel from Rukki.

I would like to thank Odd Magne Akselsen at SINTEF, Erling Østby at DNV GL and Christian Thaulow at the department for proposing this interesting master thesis and valuable input and advice during the master thesis. Tore Andre Kristensen from SINTEF also deserves credit for helping me understand the AE equipment and how the tests are carried out. Finally I would like to thank Cathrine Gjerstad Hartwig for the cooperation in writing this thesis.

10.06.2015, Trondheim



Andreas Vrenne Larsen

Abstract

As the search for hydrocarbons moves into the Arctic regions new materials are required to meet the new challenges due to the harsh environment. Arctic Materials 2, is a cooperation between SINTEF, NTNU, DNV GL, several material manufactures and Oil&Gas companies. Brittle fracture initiated in the Heat Affected Zone (HAZ), which is created by welding, in low temperatures is of interest.

When a material is welded the microstructure changes due to heat transmitted from the welding, and the transition temperature is significantly reduced. The three main factors which primarily decide the toughness of the material after welding are the base material chemical composition, the maximum temperature from welding and the rate of cooling. This transformation of microstructure combined with low temperatures makes it vulnerable to brittle fracture, even though the base material is ductile.

Brittle fracture in steel is linked to the microstructure in the material with respect to initiation, propagation and arrest of cracks. Traditional testing is often not accurate enough to cause any visible signs in the load displacement curves at microcracking. Acoustic Emission (AE) makes this possible.

The main objective has been to investigate the relationship between Acoustic Emission (AE) amplitude and the arrested cleavage microcrack size based on a theoretical relationship presented by Lysak (1996) and further developed by Østby et al. (2012). This relationship may provide quantitative data as input for development of the micromechanical based cleavage fracture models for steel. In this context the Multiple Barrier Model is used as a model to describe a cleavage fracture initiated at M-A particles (Lambert-Perlade et al., 2004) and (Martin-Meizoso et al., 1994).

Fractographic investigation has been carried out with SEM and EDS. In addition, AE signals have been analyzed and linked to arrested microcrack. Furthermore, improvements to the procedure for post processing and analysis of the AE signals have been made.

Only one arrested microcrack was found which could be connected to AE amplitude, but it deviated from the curve presented in Østby et al. (2012). The reason might be differing perceptions of how to measure and what to measure. Further on were large scatter in the fracture toughness observed. This might be linked to presence of upper bainite and autotempered martensite.

The formation of M-A phases was reduced due to the low amount of carbon. No initiations observed in M-A particles were observed. The Multiple Barrier Model could not be linked to initiation in M-A particles, but different stages were seen at larger inclusions. Smooth surfaces observed on the fracture surface, were investigated, but not identified.

Further testing and localization of arrested microcracks is necessary to confirm its relationship to AE amplitude.

Sammendrag

Ettersom søken etter hydrokarboner beveger seg in i arktiske områder er nye materialer nødvendig for å møte de utfordringene det harde klimaet fører med seg. Arktiske Materialer 2 er et samarbeid mellom SINTEF, NTNU, DNV GL, flere materialprodusenter og andre olje&gass bedrifter. Sprøbrudd i den varmpåvirkede sonen (HAZ) som dannes ved sveising, er i lave temperaturer av interesse.

Når et material blir sveiset endrer mikrostrukturen seg på grunn av varme som blir overført fra sveisingen, og omslagstemperaturen blir markant redusert. Det er tre hovedfaktorer som bestemmer seigheten til materialet etter sveising. Disse er grunnmaterialets kjemiske sammensetning, den høyeste varmen fra sveisingen og avkjølingshastigheten. Denne forandringen i mikrostruktur i kombinasjon med lave temperaturer gjør den utsatt for sprøbrudd, selv om grunnmaterialet er duktilt.

Sprøbrudd i stål er koblet opp mot mikrostrukturen i materialet med hensyn til dannelse, vekst og stans av sprekker. Tradisjonell testing er ofte ikke nøyaktig nok til å kunne se synlige tegn på last-forskyvningskurven ved mikrosprekking. Akustisk Emisjon (AE) gjør dette mulig.

Hovedoppgaven har bestått i å undersøke sammenhengen mellom amplituden fra Akustisk Emisjon (AE) og størrelsen på den stansede mikrosprekken basert på et teoretisk forhold presentert av Lysak (1996) og vireutviklet av Østby et al. (2012). Denne sammenhengen kan vise seg å tilføre kvantitativ data for utvikling av modeller for mikromekanisk basert kløvningsbrudd i stål. I denne sammenheng er «Multiple Barrier Model» brukt for å beskrive et kløvningsbrudd som er startet i M-A partikler (Lambert-Perlade et al., 2004) og (Martin-Meizoso et al., 1994).

Undersøkelser av bruddflaten har blitt gjennomført med SEM og EDS. I tillegg har AE signalene blitt analysert og knyttet til stansede mikrosprekker. Videre har det blitt gjort forbedringer av prosedyren for etterarbeid og analyse av AE signaler.

Kun en stanset mikrosprekk ble funnet som kunne knyttes til en AE amplitude, men den avvek fra kurven presentert i Østby et al. (2012). Årsaken kan være at det er forskjell i oppfattelsen av hvordan den skal måles og hva som skal måles. Videre var det stor spredning i bruddstyrken som ble observert. Dette kan muligens knyttes opp mot tilstedeværelse av øvre bainitt og autotemperert martensitt.

Dannelsen av M-A faser ble redusert på grunn av det lave innholdet av karbon. Ingen sprekkdannelser som kunne knyttes til M-A partikler ble observert. «Multiple Barrier Model» kunne ikke knyttes opp mot sprekkdannelse i M-A partikler, men forskjellige faser ble sett på større inneslutninger. Glatte flater som var observert på bruddflaten, ble undersøkt men ikke identifisert.

Videre testing og lokalisering av stansede mikrosprekker er nødvendig for å bekrefte sammenhengen til AE amplitude.

List of Acronyms

AE = Acoustic Emission

AF = Acicular Ferrite

Al = Aluminum

ASTM = American Society for Testing and Materials

AWS = American Welding Society

BCC = Body Centered Cubic

C = Carbon

Ca = Calcium

BCT = Body-Centered Tetragonal

CCT = Continuous Cooling Transformation

CE = Carbon Equivalent

CGHAZ = Coarse grained Heat Affected Zone (one welding cycle)

CMOD = Crack Mouth Opening Displacement

Co = Cobalt

Cr = Chromium

CTOD = Crack Tip Opening Displacement

EDS = Energy-dispersive X-ray spectroscopy

eV = electron voltage

FCC = Face Centered Cubic

Fe = Iron

$H_V/(HV)$ = Vicker hardness

HAZ = Heat Affected Zone

HCP = Polycrystalline Hexagonal Close - Packed

HSLA steel = High Strength Low Alloy steel

ICCGHAZ = Intercritically reheated CGHAZ (two welding cycles)

IIW = International Institute of Welding

IPM = Institutt for Produktutvikling og Materialer (Department of Engineering Design and Materials)

LM stands = Lath Martensite

MBM = Multiple Barrier Model

M_s = Martensite (start)

Mo = Molybdenum

NDT = Non Destructive Testing

Ni = Nickel

O = Oxygen

P = Phosphorus

S = Sulfur

SEM = Scanning Electron Microscope

Si = Silicon

TEM = Transmission Electron Microscope

TTT = Time-Temperature Transformation

wt% = % by weight

Contents

Preface.....	iii
Abstract	iv
Sammendrag	v
List of Acronyms	vi
Contents	viii
List of Figures.....	xiii
List of Tables.....	xv
1 Introduction	1
1.1 Background.....	1
1.2 Objective.....	1
1.3 Structure of the report	2
2 Theory	3
2.1 Scanning Electron Microscope (SEM).....	3
2.1.1 Key settings	3
2.1.2 Backscatter	4
2.1.3 Energy-dispersive X-ray spectroscopy	4
2.2 Plate manufacturing	6
2.2.1 Hot rolling.....	6
2.2.2 Cold rolling	7
2.2.3 Microstructure effects from hot and cold rolling	7
2.2.4 Controlled rolling.....	8
2.2.5 Annealing.....	9
2.3 Delamination in steel.....	9
2.4 Weldability.....	10
2.5 Multiple barrier model	11
2.6 From CMOD to CTOD.....	14
2.6.1 Calculation of CTOD by plastic hinge model	14
2.6.2 From CMOD to CTOD by SINTEF spreadsheet	15
2.7 Microstructures	16
2.7.1 Precipitation (utfelling)	16
2.8 Hardness testing	16

3	Acoustic Emission - AE	19
3.1	Theory.....	19
3.1.1	Area of use	19
3.1.2	Waveform.....	19
3.1.3	Sensors	20
3.1.4	Amplifier.....	20
3.2	Equation from (Østby et al., 2012)	21
3.2.1	Lysak	21
3.2.2	Østby et al. (2012).....	24
3.2.3	Link between Lysak (1996) and Østby et al. (2012)	26
3.3	AEwin – the software.....	27
3.3.1	Startup.....	27
3.3.2	Post processing.....	29
3.3.3	From AEwin to Microsoft Excel	31
3.3.4	The most important parameters in excel.....	32
3.4	Sorting the data	33
3.4.1	Sorting of data in Excel.....	33
3.4.2	Suggestion to sorting code.....	34
3.4.3	Reason for sorting	34
3.5	Different types of signals and situations	36
4	Testing.....	41
4.1	Material properties.....	41
4.1.1	Mechanical properties	41
4.1.2	Chemical composition (%).....	42
4.1.3	Different alloys and effect on mechanical properties	42
4.2	E-modulus.....	43
4.3	Are both materials considered weldable?	43
	Weldability for R50A 420	43
4.4	Preparation of specimens before testing.....	44
4.4.1	Extraction from plate	44
4.4.2	Weld simulation	44
4.4.3	Common preparation.....	44

4.5	Mounting of AE – hardware and equipment.....	46
4.5.1	Sensors	46
4.5.2	Pre amplification	46
4.5.3	Threshold.....	46
4.5.4	Data Lookup Display	47
5	Preparation before examination	49
5.1	Cutting	49
5.2	Preparation for SEM – fracture surface.....	49
5.3	Preparation for light microscope – microstructure.....	49
5.4	Hardness testing	50
5.5	Measurement of crack depth	52
6	Results from SEM, EDS, Hardness, Microstructure	55
6.1	Microstructure.....	55
6.1.1	M-A phases.....	59
6.1.2	Hardness.....	63
6.2	Tests run to complete fracture.....	64
6.2.1	Cleavage zone and possible initiation points.....	66
6.3	Test stopped after first signal	68
6.3.1	Cleavage facet	68
6.3.2	Fatigue line	72
6.4	Inclusions	74
6.5	Bridge.....	78
6.6	Dimples in ductile zone	79
6.7	Smooth surfaces	80
6.7.1	Smooth surface and AE correlation	81
6.8	Straight cracks	87
7	Results AE.....	91
7.1	Amplitude vs CMOD	91
7.2	Deformation	95
7.3	Further observations	96
7.4	Calculation of CTOD.....	96
7.5	Relation between AE signal amplitude and arrested micro crack size	99

7.5.1	How to measure area?	99
7.5.2	The constant “k” and power law	101
8	Discussion.....	103
8.1	Relationship between arrested microcrack and AE amplitude.....	103
8.1.1	Cleavage facet	103
8.1.2	Smooth surfaces and straight secondary cracks	103
8.2	The Multiple Barrier Model	103
8.3	Different observation on fracture surface	105
8.4	Arrested microcracks.....	105
8.5	Welding effect and temperature effect on material toughness	106
8.6	Experience of theoretical relationship between AE amplitude and arrested microcrack	106
8.6.1	Correlation to Arctic Materials 1 (AM1).....	107
9	Conclusion.....	109
10	Further work.....	111
11	References.....	113
12	Appendix.....	115
12.1	Master contract	115
12.2	Risk assessment	117
12.3	Test setup SENB	121
12.4	AE equipment	122
12.5	Geometrical factor used in SINTEF spreadsheet	123
12.6	Line display setup	124
12.7	Other parameters in AEWIn	125
12.8	Power law	126
12.8.1	General procedure	126
12.8.2	From Østby et al., 2012	127
12.9	Overview all SENB05 tests	128
12.9.1	From project thesis	128
12.9.2	Conducted during writing of master thesis.....	129
12.10	EDS - Average values, smooth and rough surfaces.....	134
12.12	EDS of inclusion in arrested microcracks – test no 167	137

12.13	EDS of fracture of inclusion – test no. 167	138
12.14	EDS on unknown facet – test no. 217	138
12.15	X80 TPI.....	139
	Weldability for X80 TPI	139
12.16	Additional pictures taken in SEM.....	140
	12.16.1 Missing inclusion.....	140
	12.16.2 Deformed edge	140
	12.16.3 Test no. 217 – smooth surface enlarged.	141
12.17	Form for crack depth measurement.....	142
12.18	Calculated CTOD	143

List of Figures

Figure 1 - Electron beam	3
Figure 2 - EDT - Alpha and Beta X-rays	5
Figure 3 - EDS spectrum	6
Figure 4 - The four stages of MBM (Lambert – Perlade, 2004).....	12
Figure 5 - Temperature vs crack propagation (by Håkon Gundersen).....	13
Figure 6 - Geometrical factor SENB (Anderson 2006).....	14
Figure 7 - Signal shaping chain - (Hellier, 2001).....	20
Figure 8 - Cleavage facet and graph from Østby et al. (2012)	25
Figure 9 - AEwin layout.....	28
Figure 10 - AE Hardware Setup	29
Figure 11 - AEwin - acquire/replays	29
Figure 12 - Replay window	31
Figure 13 - Graphical display of parameters	33
Figure 14 - Difference between high and low RISE	35
Figure 15 - Waveform with to high RISE value.....	36
Figure 16 - Burst signal	37
Figure 17 - Continuous signal	37
Figure 18 - Pop in, test no 54 - 5sec1cyc 0c	38
Figure 19 - Double signal – Test no 180 – 15sec1cyc -60c.....	39
Figure 20 - Special signals.....	39
Figure 21 -ASTM notation for tested specimen	44
Figure 22 - Notch for pinch gauge and spark eroded crack	45
Figure 23 - Photo of notch for pinch gauge and spark eroded crack.....	45
Figure 24 - Fatigue.....	45
Figure 25 - Cross section of SENB05 specimen after finished testing.....	45
Figure 26 - Pre-amplification.....	46
Figure 27 - Data Lookup Display.....	47
Figure 28 - MicroWiZhard Hardness Testing Machine.....	50
Figure 29 - Technical 2 for crack depth measurement	52
Figure 30 - Crack depth measurement.....	53
Figure 31 - Micrographs of the specimens with different weld simulations	56
Figure 32 – Micrograph - Test no 7 - 1cyc15sec.....	57
Figure 33 - Micrograph - Test no. 12 - 2cyc15sec	57
Figure 34 - Micrograph - Test no 31 - 1cyc5sec	58
Figure 35 - Micrograph of base material - Test no 12 - 2cyc15sec	58
Figure 36 - Micrograph of base material -Test no. 12 - 2cyc15sec	59
Figure 37 - SEM micrograph LePera etched for approx. 20 sec. - Test no. 7 (1cyc15sec)	60
Figure 38 - SEM micrograph, LePera etched for approx. 20 sec -Test no. 12 - 2cyc15sec	61
Figure 39 - SEM micrograph LePera etched for approx. 20 sec - Test no. 7 - 1cyc15sec.	61
Figure 40 - SEM micrograph LePera etched for approx. 20 sec - Test no. 12 1cyc15sec	62

Figure 41 - Test no. 24 (2cyc 10sec -60 °C) – 110X - fracture zones in ductile specimen.....	64
Figure 42 - Pre-fatigue to SENB surface	65
Figure 43 – Possible initiation sites - Test no. 12 (2cyc 15sec -60 °C)	66
Figure 44 - Crack initiation overview, test no 7 - 1cyc 15sec -60c.....	67
Figure 45 - Crack initiation magnified - Test no. 7 - 1cyc 15sec -60c.....	67
Figure 46 - Cleavage facet - Test no. 167 - 5sec1cyc-30c.....	68
Figure 47 - Magnification on inclusions, cleavage facet	69
Figure 48 - Inclusions at cleavage facet – Test no. 167 – 5 sec1cyc-30c.....	69
Figure 49 - Inclusion on cleavage facet - test no 167.....	70
Figure 50- Test no. 217 – 2cyc5sec -60c.....	71
Figure 51 - Test no. 217 - 2cyc5sec -60c	72
Figure 52 - Fatigue line from cleavage facet	73
Figure 53 - Fatigue line from cleavage facet	73
Figure 54 – Crack through inclusion. Test no. 167 - 5sec1cyc-30c	74
Figure 55 – Crack trough inclusion. Test no. 180 - 15sec1cyc-60c.....	75
Figure 56 - Different inclusions	76
Figure 57 - EDS on inclusions.....	77
Figure 58 - EDS on "Crack through inclusion". Test no. 167 - 5sec1cyc-30c.....	77
Figure 59 - Bridge	78
Figure 60 - Test no. 7 - ductile zone	79
Figure 61 - Smooth surfaces.....	80
Figure 62 - 217 - Smooth surface with pits, inclusion, elevations and plastic deformation....	81
Figure 63 - Smooth surface - Test no. 126	82
Figure 64 - First smooth surface - Test no. 180.....	83
Figure 65 - Firs smooth surface - Test no 217	83
Figure 66 - First smooth surface - Test no. 339.....	84
Figure 67 - Backscatter on smooth surface - Test no. 167.....	85
Figure 68 - Etched smooth surface - Test no. 180	86
Figure 69 - Straight secondary cracks - Test no. 7.....	87
Figure 70 - Straight secondary crack - Test no. 7	88
Figure 71 - Straight crack, from Jr et al. (2013).....	89
Figure 72 - Straight crack – EBSD map - Jr et al. (2013)	90
Figure 73 - CMOD vs Amplitude -30c	92
Figure 74 - CMOD vs Amplitude -60c	93
Figure 75 - CMOD vs Temperature - interrupted tests	94
Figure 76 - Fracture toughness 1cyc	95
Figure 77 - Fracture toughness 2cyc	95
Figure 78 - Load deformation curve from AEwin	98
Figure 79 - Measurement of arrested microcrack - Test no. 167	99
Figure 80 - Relation between the microcrack size and the AE signal amplitude.....	100
Figure 81 - AE amplitude linked to creation of microcrack - Test no 167.....	101

List of Tables

Table 2-1: Crystal structure	8
Table 3-1 - Data related to continuous signal	37
Table 4-1- Mechanical properties	41
Table 4-2 - Chemical composition	42
Table 6-1 - Vickers Hardness R50A 420.....	63
Table 7-1 - Table over calculated CTOD	97
Table 7-2 – AE amplitude VS a_micro.	100
Table 12-1 - Attempts to acquire a power law based on Østby et al., 2012	127
Table 12-2 - Overview of tests run to macroscopic fracture – project.....	128
Table 12-3 - Overview - SENB 05 tests run to macroscopic fracture - master.....	130
Table 12-4 - Overview - SENB 05 Interrupted tests – master	133
Table 12-5 - EDS on smooth and rough surfaces - Test no. 126	134
Table 12-6 - EDS on smooth and rough surfaces - Test no. 180	134
Table 12-7 - EDS on smooth and rough surfaces - Test no. 339	135
Table 12-8 - EDS on smooth and rough surfaces - Test no. 167	135
Table 12-9 - EDS on smooth and rough surfaces - Test no 217	136
Table 12-10 - EDS on lower inclusion – Test no. 167	137
Table 12-11 - EDS on upper inclusion – Test no. 167.....	137
Table 12-12 - EDS on fracture of inclusion - Test no. 167	138
Table 12-13 - EDS on unknown facet – Test no. 217	138
Table 12-14 - Vickers Hardness X80 TPI	139

1 Introduction

1.1 Background

As the search for hydrocarbons moves into the Arctic regions new materials are required to meet the new challenges due to the harsh environment. Today the Norwegian oil and gas industry base their activity on the NORSOK standard which covers temperatures down to -14°C. The Arctic regions need a standard which covers much lower temperatures. Arctic Materials 2, is a cooperation between SINTEF, NTNU, DNV GL, several material manufactures and Oil&Gas companies, where the challenges posed by the environment are investigated. Brittle fracture initiated in the Heat Affected Zone (HAZ), which is created by welding, in low temperatures is of interest.

When a material is welded the microstructure changes due to heat transmitted from the welding and the transition temperature is significantly reduced. The three main factors which primarily decide the toughness of the material after welding are the base material chemical composition, the maximum temperature from welding and the rate of cooling. Two materials have been tested, P-TPI X80 (pipeline steel) and R50A – 420 (steel plate) but with large emphasis on the latter. Due to this, the P-TPI is not mentioned further in the thesis, but included in the appendix. This is to avoid confusion. Both materials are High Strength Low Alloy (HSLA) steel. This transformation of microstructure combined with low temperatures makes it vulnerable to brittle fracture, even though the base material is ductile.

Brittle fracture in steel is linked to the microstructure in the material with respect to initiation, propagation and arrest. Traditional testing is often not accurate enough to cause any visible signs in the load displacement curves. Acoustic Emission (AE) makes this possible.

1.2 Objective

The main objective has been to investigate the relationship between Acoustic Emission (AE) amplitude and the arrested cleavage microcrack size based on a theoretical relationship presented by Lysak (1996) and further developed by Østby et al. (2012). In addition, fractographic investigation has been carried out. Furthermore, improvements to the procedure for post processing of the AE signals have been made. Based on the study performed in the project thesis, it has been decided to use the Multiple Barrier Model (MBM) to explain crack initiation, propagation and arrest of a microcrack. It assumes crack initiation in M-A particles, but the low carbon content in the 420 steel from Ruukki should prevent blocky M-A phase to form.

Three other master students have also been writing their master thesis in association with the Arctic Materials 2 project. Parts of this work have been performed in co-operation with Cathrine Hartwig and will therefore recommend to read her master: Acoustic emission from arctic steels and fractographic investigation.

1.3 Structure of the report

The report consists of two parallel parts which are invariable connected, microstructure and Acoustic Emission (AE). The subdivisions of the thesis allows the reader to maintain an overview throughout the thesis.

In chapter 2 theory related to the different equipment used and theory related to the microstructure is presented. This theory will later be linked to the results, discussion and conclusions.

In chapter 0 theory and essential papers related to AE are outlined. In addition, the procedure for sorting the AE data generated during the work with this thesis is presented.

Chapter 4 covers the whole testing procedure and merge what is directly related to AE with the material dependencies of the specimen.

Chapter 0 and 7 covers respectively the results linked to the specimen and AE signal. In chapter 0 the microstructure are defined and the fracture surface investigated. To comment the events observed at the fracture surface is it necessary with some linking to the accompanying AE signal. Chapter 7 investigates Acoustic Emission on a more general plane and defines the material properties based on results from the data recorded by the software AEwin.

In chapter 8 the results are discussed before conclusions are made in chapter 0.

The last chapter before the appendix is recommendations for further work.

The appendix consists of some selected tables of results from AE monitoring, Energy-dispersive X-ray spectroscopy (EDS), crack depth measurement and CTOD calculation. These are referred to in the text.

2 Theory

Theory regarding weld simulation, crack initiation and propagation in addition to microstructure is described in the project thesis, "Acoustic emission from brittle fracture".

2.1 Scanning Electron Microscope (SEM)

In 1876 Abbé showed that there was a lower limit of 2000\AA for resolution in a microscope with his theory about how light spreads (Helen, 1989). This limit was due to the way that light is transmitted as waves and the solution to achieve a better resolution was to use light with reduced wavelength.

In a regular light microscope the light will have wavelengths at several thousand \AA . Electrons which are accelerated through a potential of, i.e. 30kV achieve a wavelength at $0,07\text{\AA}$. Those electrons are then used as light and the resolution is considerably increased.

The surface which is examined is exposed to a thin focused beam of electrodes. The beam may be stationary or scan. When the beam hits the surface multiple signals can be detected. These are Auger electrons, characteristic x-ray radiation, secondary electrons, backscattered electrons and photons with different energies. The signals can give information about the specimen's chemical composition, surface roughness, crystallography etc.

X-ray, backscattered electrons and secondary electrons are most applicable signals in SEM. When the specimen is exposed to the beam of electrons the emission of secondary electrons will vary depending on the topography of the surface.

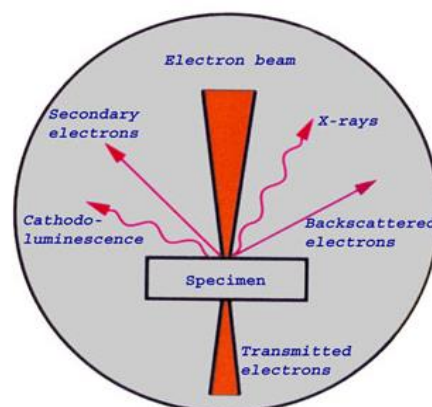


Figure 1 - Electron beam

2.1.1 Key settings

Acceleration voltage: In theory will an increase in accelerating voltage result in a higher signal and lower noise in the image. On the other hand it gives a reduction in structural details of the specimen surface, increased electron build up (causing dark areas) and increased heating and the possibility of damaging the sample.

Increased acceleration will allow the electrons to penetrate deeper into the specimen, and in addition give a brighter image due to increased number of backscattered electrons.

Spot size: This is the cross section diameter that the cone of the beam makes when it hits the specimen. This affects both the resolution of the image and the number of electrons generated. At low magnification a larger spot size is used as opposed to high magnification.

Stigmator: By adjusting the stigmator the shape of the probe is adjusted from circular to elliptic. It can be used to correct for major lens distortions and are usually not used before magnification is larger than 1000X.

2.1.2 Backscatter

This feature can be used to identify if an area consists of different chemicals. It displays areas with heavy atoms (high atom number) as bright as they reflect atoms more strongly than the lighter atoms (lower atomic number). The lighter atoms are represented with darker areas-

The backscatter electrons are of high energy which originally was emitted as a part of the electron beam before they were reflected due to collision with the specimen's atoms. This interaction is called elastic scattering interactions with specimen's atoms.

2.1.3 Energy-dispersive X-ray spectroscopy

Energy-dispersive X-ray spectroscopy (EDS, EDX or XEDS, depends on the producer. SEM is used to analyze the chemical composition. The technology is based on the principle that every element has a unique atomic structure which allows a unique set of peaks on the X-ray emission spectrum.

A high energy beam of charged electrons is emitted from an SEM (or TEM - Transmission Electron Microscope) towards a selected area. When this beam hits the specimen surface X-ray waves are sent back. These X-ray waves are characteristic of the elements present in the area.

Before the specimen is exposed to the emitted beam, the atoms electrons are in what is called a ground state (they are unexcited) and are in their "orbit" or shell. The electrons in the inner shell(s) have lower energy than the outer one(s). When the atom is hit by the charged electrons the electrons at the inner shells excite and jump out of their shell which leaves an "empty space". This space is filled when an electron from the outer orbit jumps in to the inner shell to stabilize the atom. The difference in energy between the electrons from the outer and inner orbit is emitted as X-ray waves.

The X-ray beam is then detected by an Energy Dispersive detector. The x-ray beam need to pass through a thin layer of beryllium and in to a refrigerated lithium doped silicon crystal. The signal is displayed as either a spectrum or histogram with intensity, number of X-rays, versus X-ray energy. The elements that the specimen consists of are identified by the energies of the characteristic X-rays.

The spatial resolution of EDS analysis performed in the SEM depends on the size of the interaction volume which is linked to the accelerating voltage and the mean atomic number

of the specimen. Both the spatial resolution and the depth resolution are in the order of a few microns.

The detection limit of EDS in SEM is in the range of 0.1-0.5 wt% and depends on the composition of the specimen.

After the different elements are identified utilizing X-ray, they can be plotted separately into a map to show how the concentration of one element varies across an area. Red colors indicate higher concentration, while blue represent a lower concentration. Quantitative analysis may be performed to find the concentration of major and minor elements (weight percentages) on different phases in the sample. This is determined by comparison with standard reference materials.

Depending on the samples density and the accelerated voltage a depth of 0.5 to 2 microns into the specimen can be investigated.

The different X-rays are named depending on which shell that are filled and which shell the electron comes from. The letters (K, L, M, N) describe which shell that are filled, Alpha indicates an electron which jumped from one shell to the next one while Beta indicates an electron that has jumped past one shell.

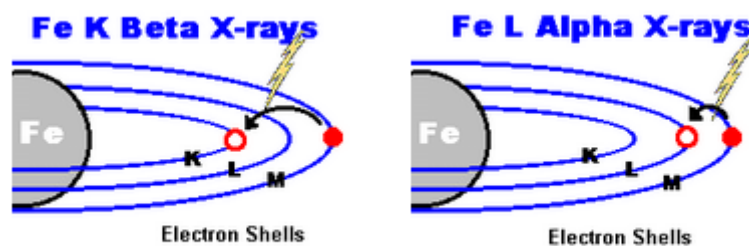


Figure 2 - EDT - Alpha and Beta X-rays

Reading/understanding the results

The x-axis, see Figure 3, indicates the energy (KeV) while y-axis describes the intensity, or the number of X-rays detected. The number of peaks is related to the number of shells. For instance will carbon never have more than one peak, while an element with higher atom number might display several peaks. The software used for analyzing the x-ray signal performs a gaussian fit of the element peaks selected before the area under the peaks are calculated.

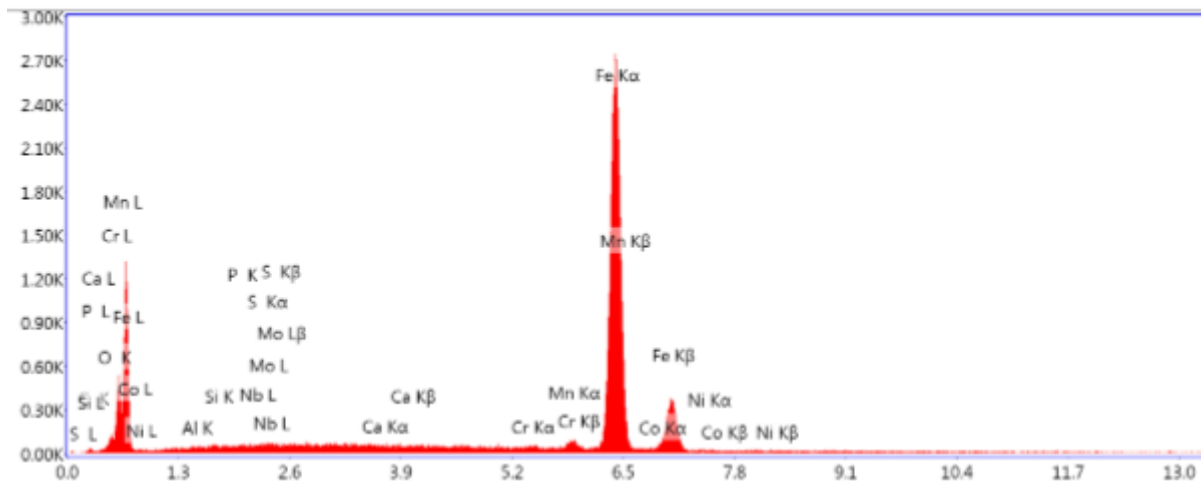


Figure 3 - EDS spectrum

2.2 Plate manufacturing

A steel plate is manufactured in many steps which greatly affect its mechanical properties. They are divided into two groups, hot rolled (thermomechanical) and cold rolled. The temperature which defines hot and cold rolling is set to be recrystallization temperature (Askeland and Phulé, 2006). The steel from Ruukki is hot rolled and quenched and will therefore be emphasized in this chapter. Delamination is discussed in chapter 2.3, where the link between finish temperature and mechanical behavior is addressed and is a prolongation of this chapter.

Regardless of how the steel is treated to obtain its final shape and properties it will most likely go through the following steps:

1. Heating: The steel is heated up to 1800 °C and to speed up melting process carbon, oxygen, fuel gas mixtures etc. are added.
2. Removal of carbon and injecting additional alloying elements in an Argon Oxygen Decarburization converter, Vacuum Oxygen Decarburization etc.
3. Secondary metallurgical treatment to adjust the chemical compositions.
4. The liquid steel is cooled down and later cut to manageable pieces called slabs. The next step is the flat hot rolling mills.

2.2.1 Hot rolling

Hot rolling is performed at a temperature above recrystallization temperature. In this process the cast microstructure is broken down and deformed. During the hot work, the metallic material is continually recrystallized causing a microstructure where the grains have approximately the same size.

The necessary number of series with milling depends on how much the thickness is reduced. Normal practice is to start with a temperature well above the recrystallization temperature. High temperature gives the material low yield strength and high ductility. The last step is performed just above recrystallization temperature allowing a large percentage of deformation in order to produce the finest possible grain size (Askeland and Phulé, 2006).

Positive effects of hot rolling are elimination of some imperfections in the original metallic material. Gas pores can be closed and composition differences can be reduced as the surface and the center of the plate is brought closer.

Negative effects are that the final properties are not isotropic since the surfaces are cooled more rapidly than the center of the plate. Much of this can be related to the rolling wheels which hold much lower temperature than the steel plate. This gives the surface much finer grains than the center and a fibrous structure is produced because inclusions and second phase particles are elongated in the working direction.

2.2.2 Cold rolling

Cold rolling can be put under the collective term cold work. Each time it's processed the plate is deformed to a thinner plate. The mechanical effects are an increase in yield and tensile strength and a reduction in the ductility. The number of dislocations is increased due to deformation. The mechanical explanation is that when a stress greater than yield strength, dislocation begin to slip. As the dislocation begins to move on its slip plane it encounters obstacles which locks the ends of the dislocation line. As more stress is applied the dislocation will try to move by bending its center and may end up creating a loop. When this loop touches itself a new dislocation is created and may continue to create new dislocations.

As the number of dislocation increase they will start to interfere with their own motions. This is called strain hardening and is a result of cold work or work hardening.

2.2.3 Microstructure effects from hot and cold rolling

In the process of rolling the grains become oriented in a preferred crystallographic direction and plane which gives a sheet texture. The result of this is that the mechanical properties depend on the direction which is measured. The strengthening that occurs by the development of anisotropy or of a texture is known as texture strengthening.

The E – modulus depends on crystallographic directions.

According to Askeland and Phulé (2006) up to 10% of the applied stress is stored within the plate as a tangled network of dislocations. This is named residual stress and increases the total energy of the structure. This is often a result of cold working and not always desirable. It can be removed or reduced by heat treatment known as stress-relief anneal.

The residual stresses are uniform through the material meaning that high compressive residual stresses may be present at the surface while high tensile stresses might be stored in the center. If some material is removed from one side it might only contain compressive residual stresses and the plate needs to be distorted to restore balance.

A compressive residual stress at the surface of a component might be beneficial with respect to mechanical properties since any crack or flaw on the surface will not likely grow.

Crystal structure	Sheet or rolling texture
FCC = Face Centered Cubic	{110} Planes parallel to rolling plane <112> Directions parallel to rolling directions
BCC = Body Centered Cubic	{001} Planes parallel to rolling plane <110> Directions parallel to rolling directions
HCP = Polycrystalline Hexagonal Close	{0001} Planes parallel to rolling plane <1120> Directions parallel to rolling directions

Table 2-1: Crystal structure

2.2.4 Controlled rolling

The purpose with controlled rolling is to produce steel with fine microstructure. To do this, it's required to have a starting point with austenitic structure with a high number of grain boundaries. This is ensured by aborting the rolling at a low temperature, often close to the transformation temperature to ferrite and by close control of the relationship between deformation and temperature.

For standard CMn (Carbon - Manganese) steel spontaneous recrystallization will appear/ be initiated at temperatures above 800 °C. The rate of recrystallization will increase with the grade of deformation and with increasing temperature.

Ti (titanium), V (Vanadium) or Al (Aluminium) will reduce the rate of re-crystallization and the precipitated particles will have a significant effect to the rate of grain growth.

Nb (Niobium) has proven to have the best effect when appearing in austenite. It reduces the rate of re-crystallization considerably and eliminates recrystallization during deformation at temperatures below 390 °C.

The procedure can be described in the following way:

After the first rolling at high temperature the plate is cooled until the final rolling is done. It is usually cooled until the plate has reached somewhere in between 930 – 800 °C. Nb prevents recrystallization until the last round with rolling which result in elongated austenitic grains with a large number of dislocations. One prerequisite for acquiring this shape is that sufficient deformation was applied during the last round of rolling. Elastic tensions are created which gives favorable conditions for nucleation of ferrite. The areas of austenitic grains are large and the ferrite grains are prevented from growing due to the elongated form of the austenitic grains. This gives the fine ferrite structure.

There are two weaknesses to the procedure: Powerful rolling equipment are required due to large deformations at low temperatures and the aborted rolling (due to cooling) is space consuming and time demanding.

Good control is important since aborting the rolling at a too high temperature will lead to a mix of recrystallized and deformed grains with large variation of grain size and the finished

product. A too low temperature during rolling can create areas of ferrite. This ferrite will give improved dislocation density and have other qualities than the ferrite created after rolling.

2.2.5 Annealing

This is a process used to eliminate some or all of the effects of cold working. The annealing temperature depends on the purpose which can be divided into *recovery*, *recrystallization* and *grain growth*.

No separate annealing is needed if the steel has been hot rolled.

Recovery, low-temperature

The microstructure is composed of deformed grains which contains a large number tangled dislocation after being cold worked. When the metal is reheated the energy allows the dislocations to move and form a polygonised subgrain structure but at the same time keeping the dislocation density. Residual stresses are reduced or eliminated while the mechanical properties are unchanged. This low-temperature treatment is typically done between 150 °C - 250 °C.

Recrystallization, higher temperature

When heated above a certain temperature, which depends on factors like amount of cold work and annealing time, the metal will undergo recovery phase at a higher speed. As the recovery phase is completed the microstructure will go over to nucleation of small grains at cell boundaries of the polygonised structure. This will eliminate most of the dislocation. This lack of dislocations results in low strength and high ductility.

Grain growth, high temperature

At this temperature the recovery and recrystallization phase are completed at a high rate and a fine recrystallized grain structure is produced. The grains begin to grow with the favored grains consuming the smaller ones in a process driven by the reduction in grain boundary area. Grain growth is not related to cold working and will be initiated if exposed to sufficient high temperature. Recovery and recrystallization are not needed for grain growth to occur.

2.3 Delamination in steel

Delamination is an event which is mainly associated with tensile testing and Charpy testing. However tensile stress also occurs in SENB testing. When load is applied to the specimen, compressive forces appear on the side where the load is applied and tensile stress appear on the other side where the notch is placed, see appendix, chapter 12.3. This tensile stress is the driving force behind both crack growth and delamination. There is nevertheless a large difference between a cleavage fracture and delamination.

Very low carbon steel is investigated with Charpy V-notch testing and tensile testing, (Bramfitt and Marder, 1976), are delamination found to be caused by cracks propagating between pancake grains parallel to rolling plane. The theory was that the mechanism is

decohesion of grain boundaries which are independent of the texture of the material. In addition was it discovered that the number of splitting increased with decreasing finishing temperature and test temperature. A review of the part with Charpy testing follows.

!!!Several theories exist and the following can be named: grain - boundary failure, distribution and morphology of carbides or cleavage along {100} planes. Necking and cup and cone which appear at tensile testing are delamination!!!

Bramfitt and Marder (1976) test with Charpy showed that the delamination always occurred parallel with rolling plane, independent of the Charpy V-notch position. It is therefore possible to conclude that the delamination is associated with a plane of weakness along the rolling planes. It was also experienced that when the finishing temperature were reduced the shelf energy also dropped. This led to decreased transition temperature and the ductile-brittle transition zone disappears. When testing a plate finished at 707 °C, an doubling of delamination were experienced when the test temperature went from room temperature to -18 °C before dropping to zero incidents at -73 °C, the surface were 100% cleavage fracture. The results vary with the finish temperature, test temperature and if the specimen is transverse or longitudinal, where the transverse exhibited more laminations for an equivalent temperature.

In (Herø et al., 1975) it is stated that the process of delamination is associated with some microstructural feature other than elongated inclusions. Further on is delamination said to not develop from a predominantly cleavage mode because of the nature of the fracture surface developed by delamination and the cube on edge texture in the tests. Further are other types of weak interfaces which can result in delamination discussed. For instance that decohesion at prior austenite boundaries because of local chemical inhomogeneities.

2.4 Weldability

The amount of carbon affects the weldability since martensite can form in the Heat Affected Zone (HAZ) easily which lead to a low toughness. Nevertheless, carbon steels generally have good weldability (Palmer and King, 2008). In low carbon steels, the strength in the welded regions are higher than in the base material due to the fine pearlite microstructure that forms during cooling of the HAZ (Askeland and Phulé, 2006) (Easterling, 1992). In addition will retained austenite along ferrite grain boundaries limit recrystallization which helps to retain a fine grain size. Nevertheless, it is not said that low carbon content is a guarantee for a good welding result. If the cooling is done too fast the formation of pearlite and quasi-polygonal ferrite will be reduced and the result is increased hardness (Jun et al., 2005).

Two of the most used methods for calculation of weldability based on the Carbon Equivalent (CE) are from the American Welding Society (AWS) and the International Institute of Welding (IIW). CE is a way to express hardenability of the steel, (Bhadeshia and Honeycombe, 2006). As the formula from the IIW is described to have a poor prediction of hardenability when it

comes to low carbon steels while AWS is largely used for pipeline steels where the carbon content will be in the range 0.15-0.2%.

The first formula is the one recommended by IIW and should according to Bhadeshia and Honeycombe (2006) be used when the carbon content is larger than 0.18 wt%.

$$CE = C + \left(\frac{Mn + Si}{6}\right) + \left(\frac{Cr + Mo + V}{5}\right) + \left(\frac{Cu + Ni}{15}\right) \quad [wt\%] \quad 2-1$$

The formula recommended by AWS can be found in API Specification 5L. According to Palmer and King (2008) is the maximum CE for pipelines in the range 0.32-0.39 while for forgings and flanges are a CE of 0.45 acceptable. According to Easterling (1992) can a material be considered weldable when $CE < 0.4$.

$$CE = C + \frac{Mn}{6} + \frac{Cr + Mo + V}{5} + \frac{Ni + Cu}{15} \quad [wt\%] \quad 2-2$$

For steels with carbon content lower than 18 wt% or 0.1% is it necessary to use the Ito-Bessyo formula. This formula calculates the Parameter for Crack Measurement (PCM) and provides a more realistic representation of the weldability. The PCM should not exceed 0.18-0.2 (Bhadeshia and Honeycombe, 2006), (Palmer and King, 2008).

$$PCM = C + \frac{Si}{30} + \left(\frac{Mn + Cr + Cu}{20}\right) + \frac{Ni}{60} + \frac{Mo}{15} + \frac{V}{10} + 5B \quad [wt\%] \quad 2-3$$

The Ito-Bessyo formula reduces the effect of the alloys compared with the formula from IIW and AWS.

2.5 Multiple barrier model

In the project thesis the Beremin model, Master Curve and Multiple Barrier Model (MBM) was investigated. The difference between these models is that the Beremin model and Master Curve assume that the cleavage is done in one step. This is not observed experimentally. The MBM assumes that the cleavage consists of four different steps, illustrated in Figure 4, (Lambert-Perlade et al., 2004) (Martin-Meizoso et al., 1994). Based on what was learned in the project thesis will the master thesis focus be on the MBM. The steps are as follows:

Stage 1

It is assumed that the crack initiates at or near an M-A particle which is assumed to be brittle. This can be done by either particle/matrix interface decohesion or brittle fracture of the M-A particle. This depends on the rate of stress acting on the particle.

Stage 2

If the crack is initiated in the particle the brittle fracture will immediately split the particle and reach the matrix interface which is the first barrier.

Stage 3

The microcrack breaks through the barrier and propagates across the matrix until it reaches the matrix/matrix boundary, for instance a grain boundary or a high angle packet boundary.

Step 4

The microcrack continues to propagate across the matrix/matrix interface leading to a macroscopic and final fracture.

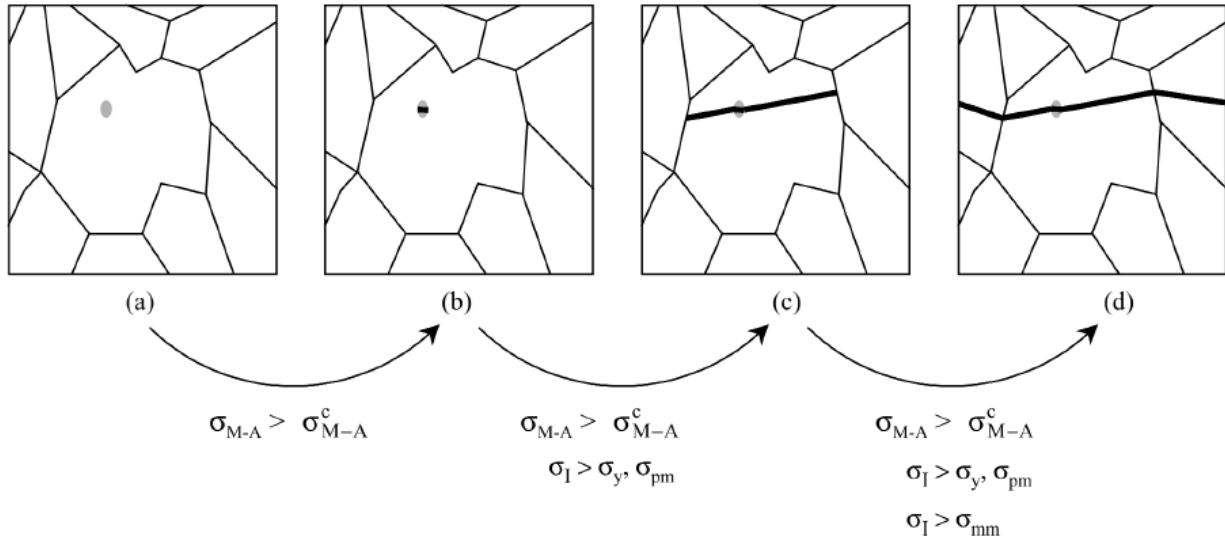


Figure 4 - The four stages of MBM (Lambert – Perlade, 2004)

The weakest link assumption is used and the fracture probability of the specimen is given by combining the different conditional probabilities for the crack to propagate from stage 1 to stage 4. This means that all the conditions shown in Figure 4 needs to be fulfilled at the same location in the specimen. The different stresses needed to propagate depend on the temperature, i.e. the arrest toughness depends on temperature. In Lambert – Perlade is it said that σ_{mm} depends on temperature and is reduced as the temperature is reduced. With high enough temperature is it said to be higher than σ_{pm} , which is the strength of the M-A/bainite phase boundary. σ_y is defined to be the material yield stress and σ_I or σ_{M-A} is defined to be the local maximum stress (in the M-A particle). The temperature effect on the failure micromechanism can then be split into four different temperature ranges as shown in Figure 5.

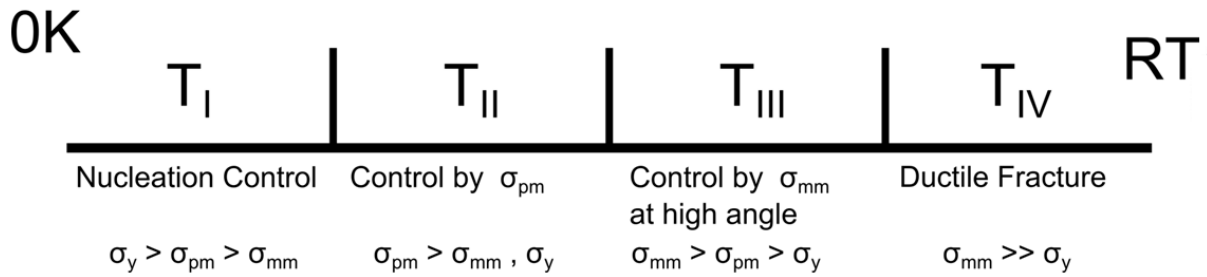


Figure 5 - Temperature vs crack propagation (by Håkon Gundersen)

1. At very low temperatures will $\sigma_{mm} < \sigma_{pm} < \sigma_y$, but as soon as $\sigma_{M-A} \geq \sigma_y$ locally the first particle cracking event will lead to macroscopic fracture as the local value of σ_I is larger than the yield strength, σ_y , and the other microstructural barriers (σ_{pm} and σ_{mm}). In this temperature range the fracture will be nucleation controlled.
2. As the temperature increase it enters zone two where still $\sigma_{mm} < \sigma_{pm}$ but $\sigma_y < \sigma_{pm}$. As load is added the σ_I increases and become larger than the yield strength but is still less than the strength of the M-A/bainite phase boundary. As soon as $\sigma_{M-A} > \sigma_{M-A}^c$ a microcrack initiate at the particle and propagate until it stops at the particle/matrix boundary. For it to continue the local stress needs to be higher than the M-A/bainite phase boundary, σ_{pm} , and when it is it will propagate through the particle/matrix interface. The situation can now be described as $\sigma_I > \sigma_{pm} > \sigma_{mm}$ which means it is able to propagate across the matrix/matrix interface and go to final failure.
3. In the next temperature range the strength of the matrix/matrix interface is high, $\sigma_y < \sigma_{pm} < \sigma_{mm}$. When load is applied and σ_I increases microcracks are initiated in particles, $\sigma_{M-A} > \sigma_{M-A}^c$, and propagate through the particle/matrix interface until it stops at the matrix/matrix interface. When sufficient load is applied it will continue through the matrix/matrix boundary until final failure. In this temperature range the failure is controlled by the strength of matrix/matrix interfaces, for example high – angle bainite packet boundaries.
4. In zone four is σ_{mm} very high and ductile fracture, which might initiate at M-A particles, will occur before cleavage fracture develops into the bainitic matrix.

This can be summed up to that propagation controlled fracture will happen in zone one and two with initiation at M-A constituents. The cleavage fracture will propagate trough the M-A/bainite interface and under right conditions be arrested at high angle bainite packet boundaries.

2.6 From CMOD to CTOD

Crack Mouth Opening Displacement (CMOD) and Crack Tip Opening Displacement (CTOD) are two different ways to measure deformation as the load is applied. The reason both methods are used is for practical reason. It is usually easier to measure CMOD since the equipment is placed on the surface and not in the crack.

Sometimes it's necessary to transform the CMOD values to CTOD values and vice for comparison. The plastic hinge model will be shown since this method was used by Østby and it was calculated after BS 7448 (1991). In addition will a method used by SINTEF be briefly explained as it has been used in relevant papers published by them. It's important to use the same method for relevant comparison.

Note that when running SENT tests double pinch gauge must be used.

2.6.1 Calculation of CTOD by plastic hinge model

$$\delta = \delta_{el} + \delta_{pl} = \frac{K_I^2}{m\sigma_{YS}E'} + \frac{r_p(W-a)v_p}{r_p(W-a) + a} \quad 2-4$$

To find the K_I it's necessary to use a formula specific for this kind of test.

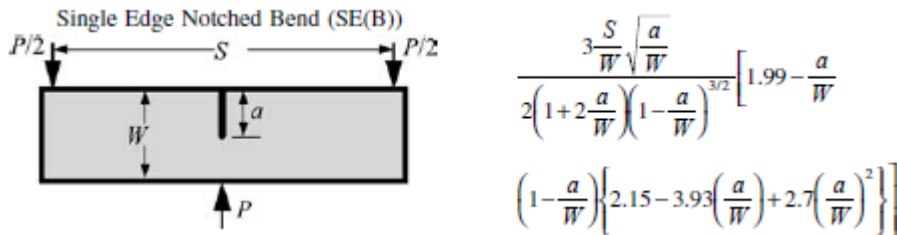


Figure 6 - Geometrical factor SENB (Anderson 2006)

The following parameters are as follows:

- S = distance between supports [m]
- W = height of plate [m]
- a = crack depth [m]

By inserting this into the formula shown on the right side of the picture of SENB the ratio number $f\left(\frac{a}{W}\right)$ is found. There are also graphs and tables where this value can be found.

$$K_1 = \frac{P}{B\sqrt{W}} \times f\left(\frac{a}{W}\right) \quad 2-5$$

- P = applied load at fracture [kN]
- B = plate thickness [m]

This gives the stress intensity factor $K_1 = [MPa \times \sqrt{m}]$

- m = dimensionless constant dependent on material properties and stress states. It is approximately 1.0 for plane stress and 2.0 for plane strain (Anderson, 2005).
- $E' = E$ for plane stress
- ν = Poisson number

$E' = \frac{E}{1-\nu^2}$ for plane strain

- δ_{YS} = Yield strength [MPa]
- r_p = Plastic rotational factor for SENB after BS 7448-1:1991 = 0.4 (0.44 ASTM 1290 (1993))
- E = Elastic modulus, see chapter 4.1.3.

$$CMOD = V_P = \left(\delta - \frac{K_1^2}{m \times \delta_{YS} \times E'} \right) + \frac{r_p(W - a) + a}{r_p(W - a)} = [m] \quad 2-6$$

$$CTOD = \delta = \frac{K_1^2}{m \times \delta_{YS} \times E'} + \frac{r_p(W - a) \times V_P}{r_p(W - a) + a} \quad 2-7$$

2.6.2 From CMOD to CTOD by SINTEF spreadsheet

The spreadsheet developed by SINTEF depends on measured crack depth and the stress – displacement curve in addition to:

- yield strength
- Poisson number
- E-modulus
- Dimensionless constant “m”.
- SENB span
- Knife height for pinch gauge
- Geometrical properties

In addition are the crack depth measured, explained in chapter 5.5, and the complete load – deformation curve which is recorded on an independent PC parallel with the recording Acoustic Emission (AE).

Further on are the $f\left(\frac{a}{W}\right)$ calculated from another formula, shown in appendix 12.5.

The procedure of measurement of crack depth is shown in chapter 5.5.

2.7 Microstructures

Low carbon steel is defined to have a carbon quantity lower than 0.2%.

2.7.1 Precipitation (utfelling)

A prerequisite for formation of fine grained microstructure is control with size of the austenitic grains. The ferrite/bainitic structure is mainly formed on the austenitic grain boundaries. An fine austenitic structure with a high number of grain boundaries per volume will be the basis for a fine grained ferrite/bainitic structure. Micro alloy elements give precipitation of small and stable particles in the austenite and this will affect the austenite structure. The precipitated particles will have different effect depending on if they are precipitated in the austenitic phase or after the transformation in ferrite/bainitic phase.

- Precipitation in austenitic phase will give grain refinement.
- Precipitation in ferrite/bainitic phase will give precipitation strengthening.

During rolling and during normalization will there be a strong tendency to grain growth. This can be prevented by precipitates from the micro alloy elements which create a fine network of particles which lock the austenitic borders. The particles will largely precipitate on the grain boundaries since this gives the lowest total surface energy. During grain growth are the border surface forced to either drag or release the particles while new particles get caught by the border surface until the number of particles are large enough for the structure to stabilize. Stabilization of austenite presupposes that the particles are not to coarse. The maximum particle size can be calculated by:

$$r = 10f \frac{d}{2} \quad 2-8$$

r = radius of particle

f = volumefraction of particles

d = diamter of grain

2.8 Hardness testing

Only Vickers hardness test will be described as this is the method used in the master thesis.

This method which was developed in 1921 is one of many ways to test the hardness of a material, but might be the most convenient one as the calculations are independent of the size of the indenter. In addition may the indenter be used for all materials, independent of the hardness.

The hardness is measured based on the resistance to plastic deformation. The shape of the indenter is made so the impression is geometrically similar regardless of size. The tip of the indenter is a square-based diamond which satisfies two criteria. First, the diamond has a

high resistance to self-deformation as it's the hardest of all natural minerals. Second, the shape of the tip gives well defined points which are easy to measure.

The Vickers Pyramid Number (HV) is found by dividing the applied force on the created area, $HV = F/A$.

Vickers hardness number is reported on the form xxxHVyy.

- xxx = the hardness number
- HV = the hardness scale – Vickers
- yy = load used in kgf

See the ISO 6507-1 standard or the ASTM E384 standard for guidance when running the test.

Calculate force from Newton to Kilogram force.

$1.8544 \times F_1 = 0.1891 \times F_2$ where:

- $F_1 = \text{force in kg}$
- $F_2 = \text{force in N}$

$$F_1 = \frac{0.1891 \times F_2}{1.8544}$$

2-9

3 Acoustic Emission - AE

3.1 Theory

Acoustic emission occurs when discontinuities in components release energy as the component is subjected to mechanical loading or stress. This energy travels in the form of high-frequency stress waves. These waves or oscillations are received with the use of sensors (i.e. transducers) that in turn convert the energy to voltage. This voltage is electronically amplified and with the use of timing circuits is further processed as AE signal data. Analysis of the collected data comprises the characterization of the received voltage (i.e. signals) according to their source location, voltage intensity and frequency content (Hellier, 2001). Sources to acoustic emission can be:

- Crack growth
- Crack initiation
- Crack jumps
- Plastic deformation
- Dislocation motion in large numbers – yielding and buckling
- Friction during crack opening and closing
- Twins

3.1.1 Area of use

There are several areas where AE is useful. As it provides “real time” monitoring it can be used to monitor internal combustion engines to discover faults early gives the source location and detect leakage in a high pressure vessel. Furthermore, is used for NDT (Non Destructive Testing) as it gives comprehensive information on the origination of flaws and the development of it. Finally it is used in science when it comes to understanding the mechanisms in a material which is applied load and stress. It gives information of the rate of microcrack nucleation and the distribution of arrested cleavage microcrack sizes, (Østby et al., 2013).

3.1.2 Waveform

How the signal is displayed depends on four stages, see Figure 7. The signal starts as a short pulse which is affected by the structure of the material as it travels towards the sensor. The shear and compressional forces supported by the specimen leads to a variation of waves which can be excited simultaneously. For a propagating crack the signal will be strongest perpendicular to the plane it grows. As the signal reaches the sensor will it change shape once more. The chosen type of sensor, broad or narrow band, will greatly affect this.

Broadband SENSORS offers higher fidelity and picks up a wide range of frequencies, but also much background noise. The narrowband is more sensitive, less expensive and operate in a known and well established frequency band. It can be optimized when dealing with wave fading or background noise. The frequency bandpass of the amplifier/filter combination in the AE instrument is normally set to match the sensor.

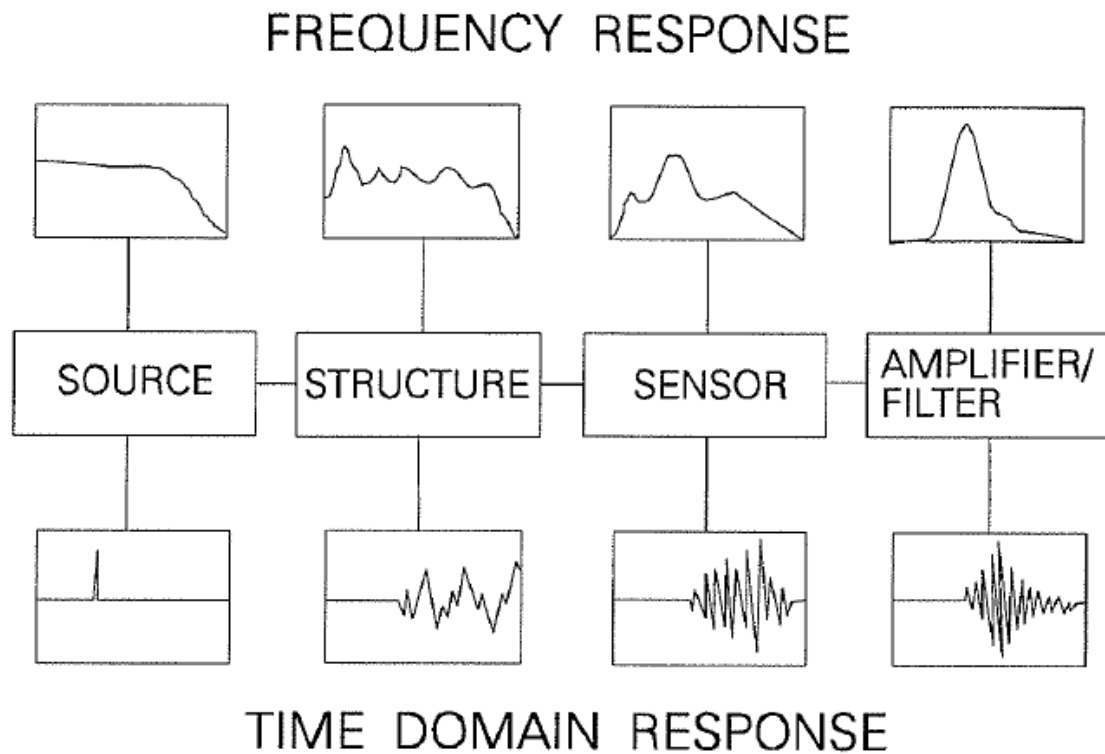


Figure 7 - Signal shaping chain - (Hellier, 2001)

3.1.3 Sensors

As mentioned in chapter 3.1.2 the sensors are of great importance. It consists of a piezoelectric element where a crystal, often quartz (SiO_2), is used to transform the pressure variation (from soundwaves/stresswaves) into an electric charge which oscillates with the incoming waves. Quartz is a material with a charged atom structure that consists of one positive and one negative pole. When its thickness is changed the voltages also changes. This means that it does not need an external power supply.

To ensure good quality of the signals is it important that the surface are plane and that a binder which ensure smooth transition of the waves to the piezoelectric element.

3.1.4 Amplifier

As the signal leaving the sensor has strength of a few micro voltage is it necessary to amplify it. It is important that the amount of noise in the amplifier is low and the soundwaves are therefore often filtered with “highpass” or “bandpass” as it enters.

High frequencies will be damped more rapidly than the low frequencies meaning that signals with higher frequencies will contain less background noise. Unfortunately will this affect the width of detection and vice versa for low frequencies.

See chapter 3.3 for information about software, parameters and the different signals.

3.2 Equation from (Østby et al., 2012)

In Østby et al. (2012) an equation linking the amplitude of the AE signal to the arrested cleavage microcrack size is presented. It is largely based on an article written by M. V. Lysak from the Physico – Mechanical Institute of the Ukrainian Academy of Sciences (MIUAS). A review of these two articles is presented in this chapter.

3.2.1 Lysak

The background for the paper, assumptions, theories and relevant definitions are presented in the following chapter.

Background for the paper

Determination of the defect parameters from AE data was at the “working out” stage when the article was written due to a lack in universal, physically grounded dependencies between parameters of the defects and the AE signal. The radiation of elastic waves in a material occurs when a crack grows by jumps. The sequence of AE signals starts at the moment when a crack initiates and ends when the elastic waves are transformed into electrical signals. This is the subject of the fracture mechanics study. Thereafter the study can be separated into two closely connected stages.

1. The condition and situation in a material which precede local failure are grounded in the basis of physical and chemical fracture mechanics. Analysis of stress – strain state and the physical – chemical situation at the crack are important keywords and these results will be used as input for the next stage.
2. With the data from the previous stage models are created and the boundary conditions for the problems of crack initiation and propagation are formulated and thereby solved by dynamical fracture mechanics.

The theoretical basis for the AE method requires formulation of the calculation models of crack initiation and growth, investigation of the displacement field which is caused by these dynamic processes and establishment of the dependence of the mechanical and electrical AE vibration.

Development of models

The theory of the AE – method relies on capability of solving the dynamic problems of elasticity with boundary and initial conditions, shown in the paper. The model and the correct initial and boundary conditions for the problems of crack propagation are chosen. This should take into account the material characteristics, geometry and the size of structural elements in addition to the modern level of the mathematical apparatus for solving the respective problems of the elastic theory. Previous models have simplified the problem by specifying the instantaneously applied static displacement on the crack surface. It is thereby modelled by means of concentrated strain and atomic bond break which in some cases allows for taking into account of the free surface of the elastic solid. Unfortunately they do not consider the vibration of the whole crack surface. To incorporate

the conditions causing fracture three hypothesis were formed to create a new approach for modelling.

1. Local fracture of the material begins in the zone where the maximal stresses or strain act depending on the strength properties of the material.
2. When the crack forms or jumps over its newly formed surface the instantaneous unloading from the initial defectless level to zero occurs, which results in the acoustic emission.
3. At the moment of the crack formation or its jump the dynamic field of displacement is determined by the methods of the linear elasticity theory

Further on are three more assumptions made:

1. Since the newly formed crack is much less than the size of the solid to be investigated it is assumed that the crack was formed in an infinite solid.
2. The third hypothesis states that the problems are linear which makes it possible to use the principle of the stress-strain state superposition and to divide the formulated problem into two subproblems, a static and a dynamic one.
3. Since the AE transducer record only the dynamic component of the displacements field, only dynamic problems are considered.

The relationship between microcrack size and behavior and AE amplitude

The following section is linked to Mode 1 cracking. The equations presented have the purpose of graphically display of relations and for linking with Østby et al. (2012).

It is assumed that the amplitudes, A , of the electrical AE signals are proportional to the amplitudes of elastic waves, u , i.e. $A = \alpha u$ where α is the proportionality factor and the longitudinal wave amplitudes $u = 1.57\sigma_0 l^3 (1 - 2\varepsilon^2 \cos^2 \theta) / \pi \rho c_1^2 \sqrt{r}$.

Through crack

$$A = \frac{\sigma_0 l^3 \phi(\theta)}{\pi \rho c_1^2 \sqrt{r}} \quad 3-1$$

Radiation direction angle

$$\phi(\theta) = 1.57(1 - 2\varepsilon^2 \cos^2 \theta) \quad 3-2$$

Penny shaped internal crack

$$A = \frac{\alpha \sigma_0 r_0^2 \phi(\eta)}{\rho c_1^2 R} \quad 3-3$$

$$\phi(\eta) = 2(1 - 0.68 \cos^2 \eta) \quad 3-4$$

$$\eta = tg^{-1}\left(\frac{z}{r}\right), \quad R = (x^2 + y^2 + z^2)^{1/2}$$

The equations for spatial distribution of the AE signal amplitudes from a penny shaped crack was compared with the equation for AE signals amplitudes from a through crack. It showed that with distance the amplitudes will decrease more rapidly for the penny shaped crack, see equation 3-1 and 3-3. Further on is it stated that the dependence of crack size will vary for the two cases. The penny shaped crack will have AE signals amplitudes which correspond to the crack area, while for a through crack it will be proportional to the crack length to the power of 3/2. The dependencies between AE signal amplitudes and crack location angle will be similar, see equation 3-2 and 3-4.

Equation 3-3 is re-written for comparison with Østby et al.

$$A = \frac{\alpha\sigma_0\phi(\eta)}{\rho c_1^2} \left(\frac{r_0^2}{R}\right) \quad 3-5$$

Where $\phi(\eta)$ is the function for the radiation direction angle.

Link between AE signal and CTOD

Lysak states, based on hypothesis 1 and a solution of the elastic-plastic problem, that the maximal stresses or strains are achieved at a distance from the crack tip proportional to the CTOD. Further on is the process of a single jump of a macrocrack split into two stages which starts with the initiation of a microcrack at the point of maximal stresses or strains and ends with it growing towards the macrocrack. The break of the ligament between the micro- and macrocrack will be the crack jump and it will be proportional to the CTOD as the opening will be proportional with the square of the stress intensity factor.

$$\Delta l = aK_1^2 \quad 3-6$$

$\Delta l = \text{Value of crack jump}$

$a = \text{Experimentally determined material constant}$

Further on is the relation between number of AE events (crack jumps) and the stress intensity factor found and formula, 3-7, which describes dependence between geometrical parameters of cracks and the parameters of the AE signals created.

$$\Delta l = \left[\frac{\sigma_0\phi(\theta)}{\alpha\rho c_1^2\sqrt{r}} \right]^{2/3} \sum_{k=1}^k A_k^{2/3} \quad 3-7$$

Δl is the full increment of the crack in process of its subcritical growth, A_k is the AE amplitude at the k-th jump and $\phi(\theta)$ is the function of acoustic emission direction at the crack jump.

Generalization of results for the case of the non through crack

An arbitrary crack is simplified into the shape of penny-shaped crack. The jump form will be presented as a semicircle. When a penny-shaped crack is formed the AE signal amplitude is proportional to its area. Since the functional dependence of the AE signal for a through crack, both in formation and in a jump of the crack, are similar, it is according to Lysak (1996) rightful to suppose that in formation and growth of a plane three – dimensional crack it will be similar as well. Based on these assumptions the area of the crack jump in its subcritical growth is related to the AE signal amplitude through the dependence shown in equation 3-8.

$$\Delta s = \alpha \rho c_1^2 R A / 2 \sigma_0 \phi(\eta) \quad 3-8$$

where $\phi(\eta)$ is the function of the crack orientation angle.

The areas of the crack jump are summed up and the dependence between the full increment of the crack area and the sum of the AE signal can be obtained.

$$\Delta S = d \sum_{k=1}^k A_k \quad 3-9$$

$$d = \alpha c_1 R / 2 \phi(\eta)$$

Again can the geometry be linked to the number of AE events by introducing the following equation:

$$n = g(K_{1eq}) \quad 3-10$$

$g(K_{1eq})$ is a function based on the effective stress intensity factor and the crack single form has the shape of a semicircle.

3.2.2 Østby et al. (2012)

The main subject in the paper Østby et al. (2012) is to perform a quantitative use of AE to estimate the size of microcracking events. It addresses three different theories or challenges which are all connected.

1. The theoretical relation between AE amplitude and arrested microcrack size derived by Lysak (1996).
2. Multiple barrier model introduced by (Martin-Meizoso et al., 1994) and (Lambert-Perlade et al., 2004).
3. Effect by two cycles of welding to get an intercritically reheated coarse grained microstructure in the heat affected zone (ICCGHAZ).

The Multiple Barrier Model (MBM) is discussed in chapter 2.5.

The two steels used in the paper, an API X65 pipeline and a 420 MPa hot rolled plate, are both welded to ICCGHAZ. During cooling of the second cycles martensite – austenite (M-A) phases formed. The microstructure has shown earlier to give a high number of AE signals prior to macroscopic fracture. The specimens pre-fatigued before they were exposed to three point bending until the first signal was recorded. The specimen was then unloaded before subjected to post -fatiguing.

The results in AE signals ranged from 64 – 112 dB and all signals had a “burst” shape which is characteristic for microcracks. An isolated cleavage area was found at or just in front of the pre-test fatigue crack tip. The square root of this area, a_{micro} , was plotted against the AE amplitude, see Figure 8. Further was a load drop observed which can be associated with the higher AE amplitude signals (>110dB), while no visible load drop was observed for the lower amplitude signals. This observation is said to add support to the assumption of a correlation between AE amplitude and the size of the microcrack.

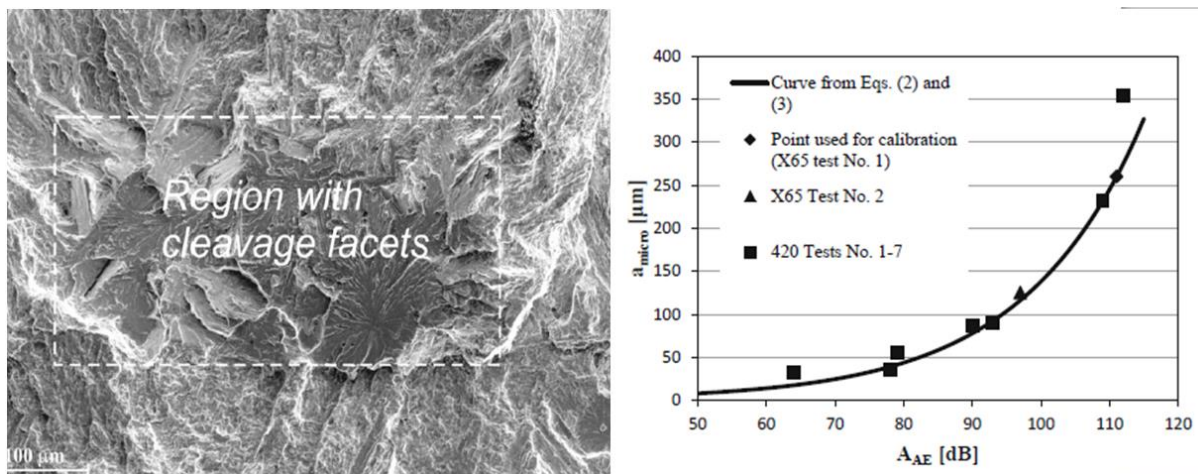


Figure 8 - Cleavage facet and graph from Østby et al. (2012)

The paper concludes the following:

- It's a strong correlation between the measured local cleavage microcrack size and the amplitude of the AE signal recorded.
- The relation between the area of the microcrack and the AE amplitude follows the theoretical relation from Lysak.

In addition is it stated that AE can be used in the following:

- Statistical analysis of the AE data, such as estimated microcrack sizes, could provide information of the relative importance of the different length scales regarding possible arrest of propagating cleavage cracks.
- AE activity during different test temperatures can provide a basis for modelling temperature effect on local crack arrest toughness.

- Information about the size of the arrested microcracks could be linked to modelling aiming at quantifying the local arrest toughness which would be a direct input to the MBM for cleavage crack propagation.
- AE can be used to provide information on the importance of crack nucleation and arrest of microcracks to get the observed constraint effect (geometry and mode of loading) in the fracture toughness data.

3.2.3 Link between Lysak (1996) and Østby et al. (2012)

Østby has re-written the formulation for elastic displacement, D , based on Lysak, equation 3-5. If the signal caused due to a sudden creation of a circular microcrack in a semi-infinite medium is it defined to have the following form.

$$D = F \frac{r^2}{R} \quad 3-11$$

$$D \sim V$$

D = elastic displacement

r = radius of the microcrack

R = distance from microcrack to the point of observations

F = function depending on microcrack orientation etc, see equation 35

The elastic displacement D is related to the voltage, V , produced as the AE signal hits the piezoelectric element. The voltage is then correlated with the amplitude.

Equation 3-12 from (Østby et al., 2012) describes the relation between voltage signal of the AE transducers and the AE signal amplitude.

$$A_{AE} = 20 \log \left(\frac{V_{AE}}{V_{ref}} \right) + A_{pre} \quad 3-12$$

$$\frac{A_{AE} - A_{pre}}{20} = \log \left(\frac{V_{AE}}{V_{ref}} \right)$$

$$10^{\frac{A_{AE} - A_{pre}}{20}} = \frac{V_{AE}}{V_{ref}}$$

$$V_{AE} = 10^{\frac{A_{AE} - A_{pre}}{20}} \times V_{ref} \quad 3-13$$

A_{AE} = dB amplitude of the AE signal

V_{AE} = the largest recorded voltage, see chapter 4.5.4.

$V_{ref} = \text{reference voltage (1}\mu\text{V)}$

$A_{pre} = \text{amplitude of pre – amplifier}$

K – Constant

It is assumed that the relation in Lysak (1996) also applies for finite geometries.

Furthermore, the amplitude of the voltage signals in AE transducers scales with the surface displacement due to the stress waves emitted from the microcrack. It should be possible to use AE measurement to provide a first order estimate of the size of the microcrack event causing the AE signal.

$$V_{AE} = k(a_{micro})^2 \quad \text{3-14}$$

$$a_{micro} = \sqrt{\frac{V_{AE}}{k}} \quad \text{3-15}$$

$k = \text{constant}$

An attempt to define k was made, see chapter 7.5.2, where a power law was created.

3.3 AWin – the software

The AWin software is used before, during and after testing is performed. Before testing it is used to define what should be recorded, during testing it is used to record and display hits and load-displacement curve. After the test is performed, the software is used for post processing and investigation of the results.

There are two main features in the software. The first feature is “Aquire” which is used when running a test. The second one, “Replay”, is used when examining a test that has already been carried out, see Figure 11. As the tests have been performed by SINTEF, the “Aquire” feature will not be emphasized in this chapter. See chapter 0 where the preparation of the testing is described.

3.3.1 Startup

Before the different features are enabled, a layout showing the relevant information and with the right settings should be created. The layout used in this master thesis is shown in Figure 9, and the settings, found by pressing F2, are in the respective tabs the following:

- AE Channel Setup
- AE Timing Parameters:
 - “AE Channel” 1 and 2 is chosen
- Waveform Streaming:
 - “AE Channel for streaming” 1 and 2 are chosen
 - “Enable Streaming2 is chosen

- “Output Filename prefix” is set to PAL demo
- “Manual Trigger (F11 to collect and end *Record Length is not used)” is chosen.
- Data Sets/Parametrics
 - See Figure 10
- Parametric setup:
 - “Source” Parametric 1 with multiplier 3.0000.
 - “Threshold” 3.496V
- Front End Filters: No parameters chosen
- Front End Alarms: No parameters chosen
- DeltaT Filters Setup:
 - “Filter” 1 is chosen

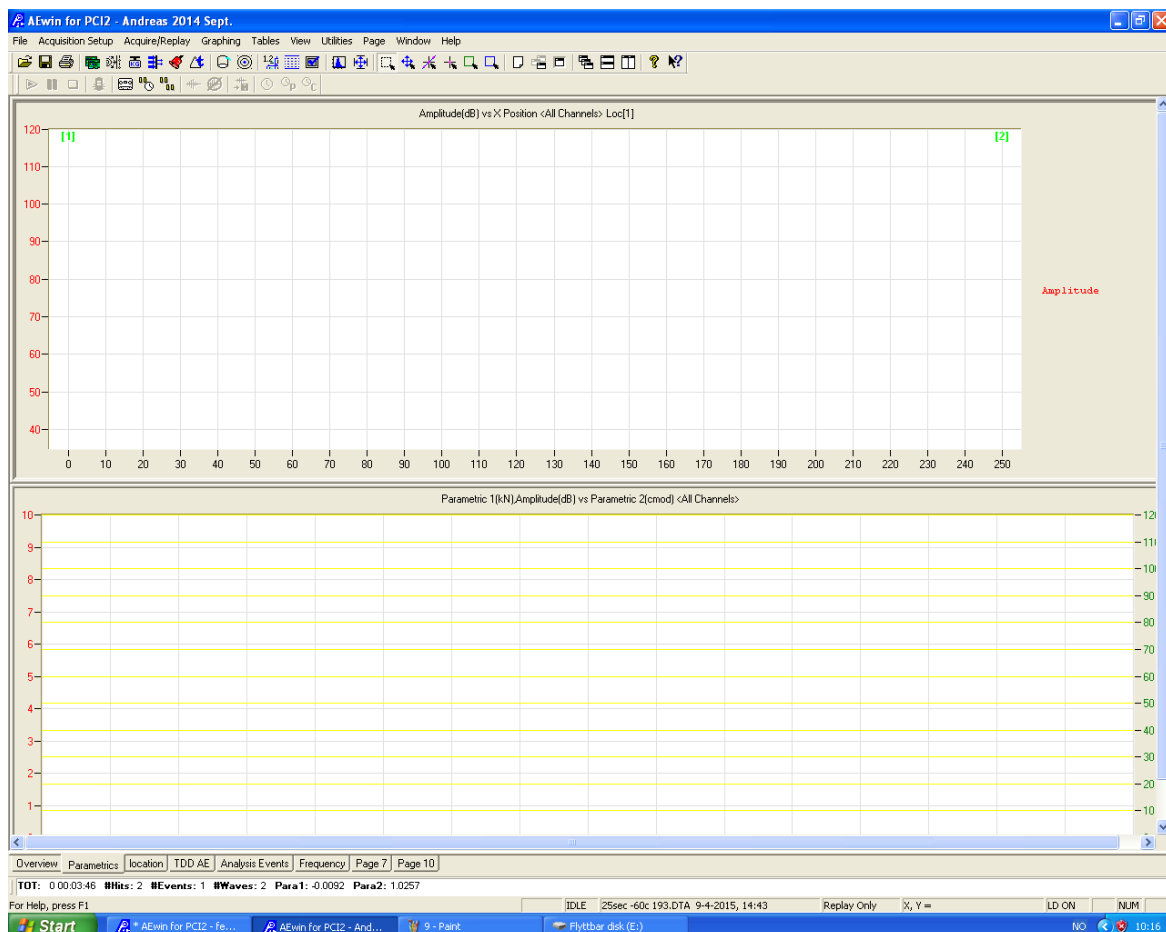


Figure 9 - AEwin layout

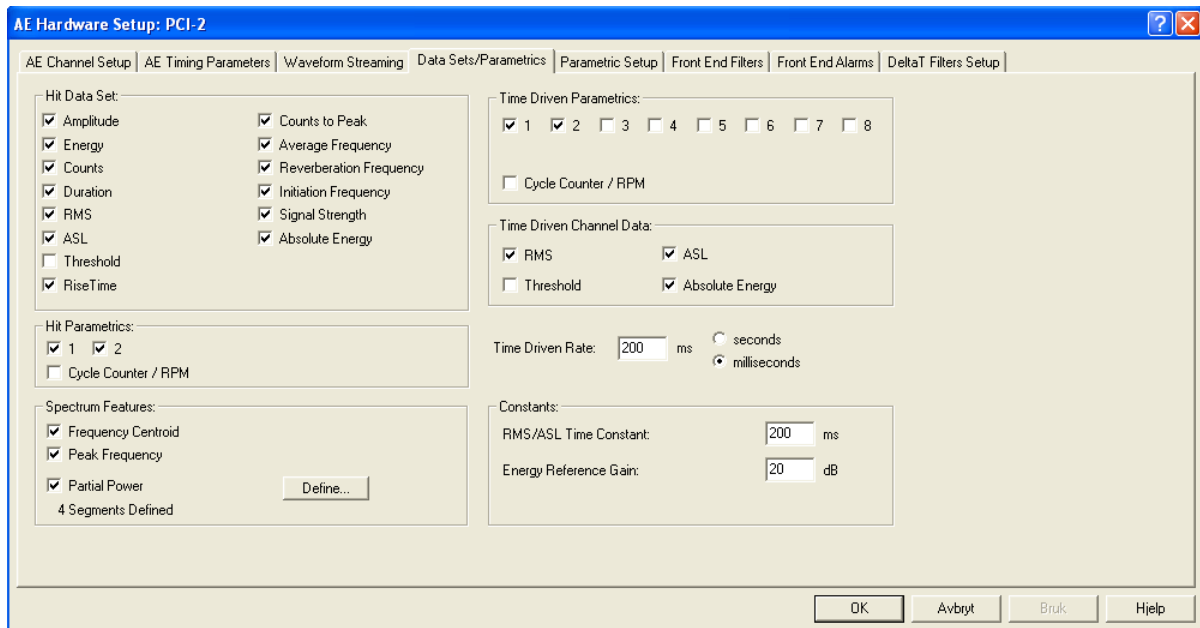


Figure 10 - AE Hardware Setup

3.3.2 Post processing

The replay feature is used when further examination of the test is desired. It is possible to export all the data as a txt file in addition to see the waveform, location of the signal and stress-displacement curve.

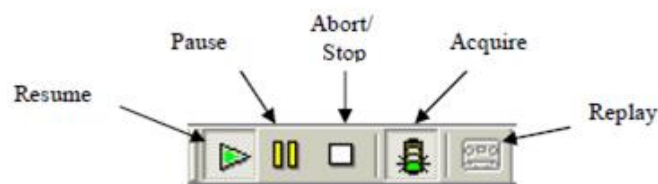


Figure 11 - AEwin - acquire/replays

See Figure 12 to relate the points to the replay window and Figure 13 for graphical display.

- “AE counts”: The number of times the signal has passed the threshold value. Note that if several large deformations appear at the same time is there a possibility that they will appear as one.
- “Hit”: Each waveform registered by a sensor counts as a hit.

- “Event”: One event, or incident, is two hits registered at the same time, one at each of the two channels and linked together.
- “Amplitude”: The amplitude is also the maximum voltage created by the piezoelectric sensor. A signal with high amplitude is more likely to be registered by the software compared with a more continuous signal as it is more likely to exceed the threshold value. The link between voltage and dB is shown in chapter **Error! Reference source not found..**
- For PARA 1 and PARA 2 see chapter 3.3.4.

Other parameters are described in appendix 12.7.

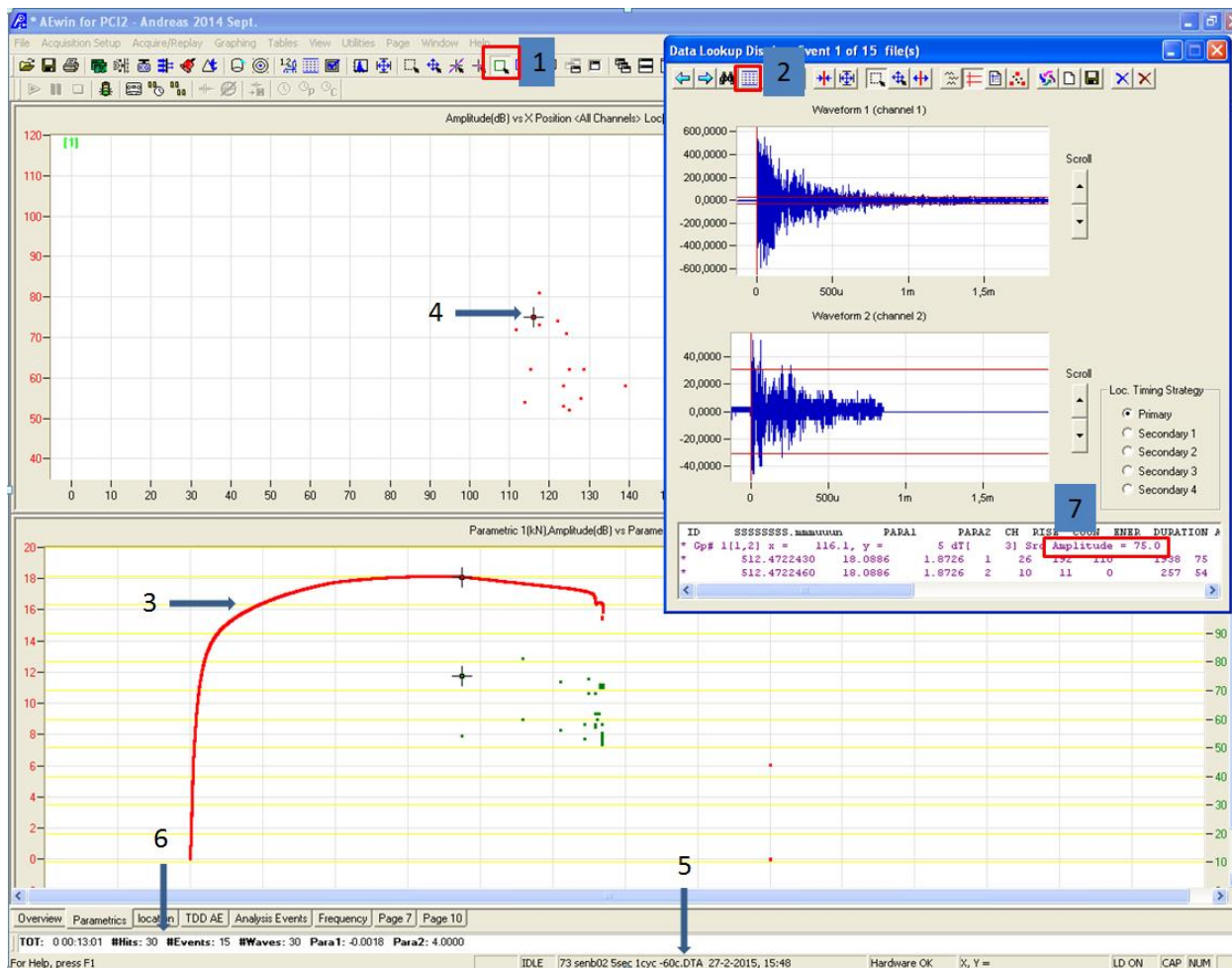


Figure 12 - Replay window

Figure 12 shows the replay window in the software. The numbered items represent the following:

1. Makes it possible to mark all signals in the upper window. The result is the window in the right corner.
2. Gives access to the data in text format.
3. Stress – deformation curve. The investigated event is displayed whit a cross.
4. The investigated event location relative to sensors (x-direction) and amplitude in dB (y-axis)
5. Test identification
6. Information of hits, events etc.
7. Amplitude

3.3.3 From AEwin to Microsoft Excel

Data achieved from AEwin exported to Excel for post-processing in the following procedure below. Numbers in clamps refers to the numbers in Figure 12.

1. Define which data that should be recorded in the “Line display setup”, see appendix 12.6. This stage is discussed more thoroughly in the project thesis.

2. Select all the points [4] after clicking button [1]. This will make the window in the upper right corner appear.
3. Click button [2] and copy all the data. Paste this into a text document.
4. Open this document in excel and use the "Text Import Wizard". Define new vertical lines before clicking "finish".

3.3.4 The most important parameters in excel

- PARA1 = the load applied at the SENB test. Measured in kN.
- PARA2 = CMOD [mm].
- CH = Channel, one for each sensor.
- RISE = Rise time is the time from the signal first exceeds the threshold value and until maximum amplitude is reached.
- ABS-ENERGY = Absolute energy which is released when the crack propagates.
- DURATION = time from the first signal passes the threshold value to the last
- AMP = amplitude. The amplitude can be linked to the size of the arrested microcrack. The magnitude of the amplitude corresponds to the amount of energy needed to drive the crack forward. The amplitude is used as both lower and upper threshold.
- C-FRQ = Center Frequency or average frequency in the signal.
- GP = Ground Position, gives information about the cracks location relative to the location of the sensors.

Other parameters are described in appendix 12.7.

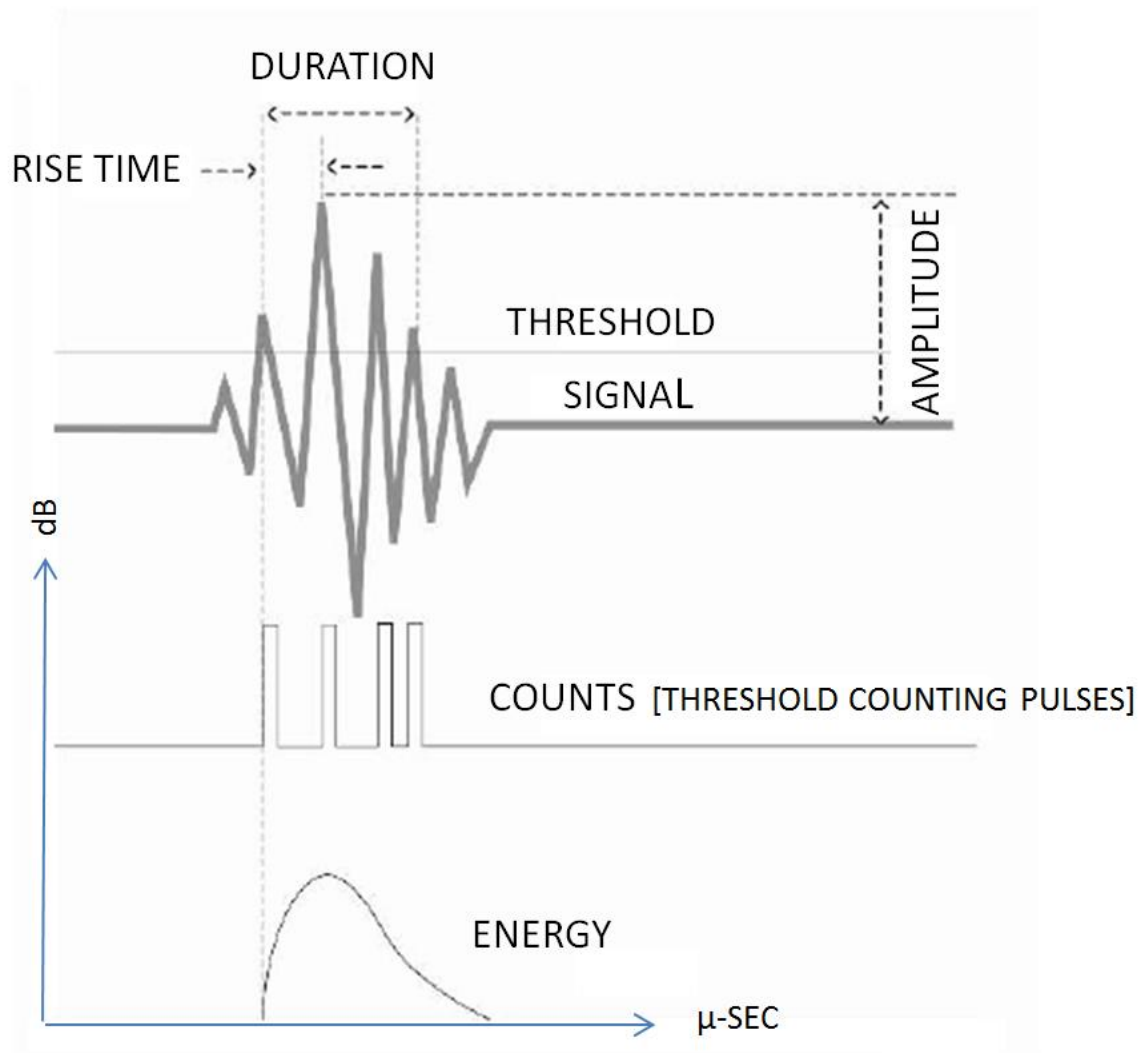


Figure 13 - Graphical display of parameters

3.4 Sorting the data

3.4.1 Sorting of data in Excel

The signal should be deleted if channel 1 or channel 2 meets any of the following requirements.

1. If the amplitude is equal or larger than 113dB, all data from that signal is to be deleted.
2. Delete every signal recorded after the one with 113dB.
3. Delete every signal with negative values of PARA1 (load).
4. Find the largest value of PARA1 and delete every signal with PARA1 value less than 30% of this value.
5. Delete every signal with a C-FRQ value equal or above 1000.

6. Delete every signal with a RISE value equal or above 160dB. Every signal between 150dB and 160dB should be investigated manually. See chapter 0 for closer explanation
7. Delete the signal if the x – coordinate is less than 10 or larger than 15.
8. Detect the x – coordinates, copy and paste it under column Z, GP.
9. Each signal contains data from sensor 1 and sensor 2, the largest signal should be used

3.4.2 Suggestion to sorting code

1. Check if the amplitude is equal or larger than 113dB. If yes delete all data from that signal.
2. Delete every signal recorded after the one with 113dB.
3. Delete every signal with negative values of PARA1 (load).
4. Find the largest value of PARA1 and delete every signal with PARA1 value less than 30% of this value.
5. Delete every signal with a C-FRQ value equal or above 1000.
6. Delete every signal with a RISE value equal or above 160dB.
7. Every signal between 150Db and 160db is marked for further investigation
8. If the x – coordinate is less than 10 or larger than 15 then delete that signal.
9. Detect the x – coordinates, copy and paste it under column Z, GP.
10. Each signal contains data from sensor 1 and sensor 2. Move the one with the lowest amplitude to the right side at the same row as of the signal from the other sensor
11. Move the Gp# information to the right side of the row.

3.4.3 Reason for sorting

This list is based on information given by Erling Østby (DNV GL), Tore Kristensen (SINTEF) and experience from testing.

PARA1 (LOAD)

It was observed that AE signals were recorded at very low loads and it was interpreted that this was a result from the load configuration. In other words, the recorded signals were emitted when the specimen was going into stable position as the load was added. To filter out these signals it was decided to remove every signal which was recorded before the load had reached 30% of maximum value.

Amplitude (AMP)

If the signal has an amplitude equal or larger than 113 dB it means that the final fracture have happened.

C-FRQ (CENTEROID FREQUENZY)

For signals assumed to be noise, typically signals with less than one or very few “spikes”, which is a high signal, had a typically value more than 1000 kHz. For “burst” signals the C-FRQ is typically lower than 1000 kHz. See chapter 3.5 for a typical signal without any “spikes”.

RISE

Signals with another form than burst signals, but with the same total energy (ABS-ENERGY) and amplitude was observed. It was discovered that these signals had a longer RISE time compared with the “Burst” signals. These signals were typically observed at low temperatures and it was therefore a large possibility that these were caused by cracking and deformation of ice on the specimen.

As outlined in chapter 3.4.1, there is in special cases necessary to investigate the form of the signal and not just the value. Closer investigation of signals in the range between 150 – 160dB shows some interesting points. As seen in Figure 14, there is a large difference between the signals on the left and right side. Channel 2, see the left picture, have an RISE value of 958 while channel 1 only have a RISE value of 36. The event is approved according to the sorting described in chapter 3.4, except for the high RISE value on channel 2, but the effect on the signal is clear. The RISE values for the signal in the right picture are 7 and 5.

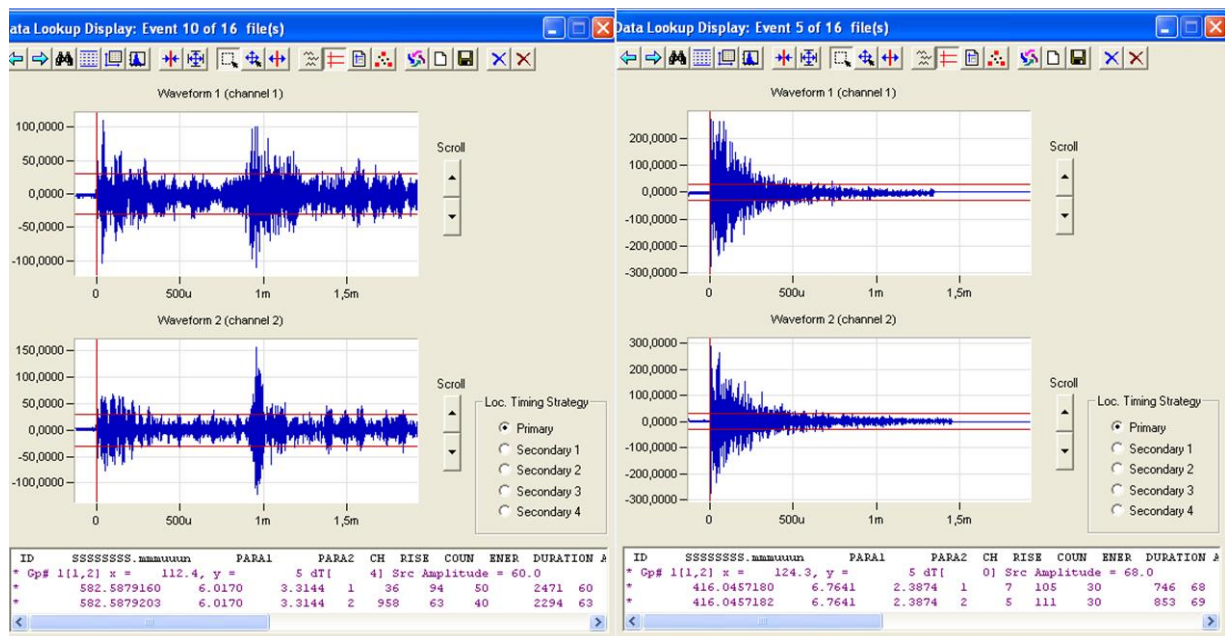


Figure 14 - Difference between high and low RISE
Both signals are from test no. 134 - 25sec 1cyc -60c

The signal in Figure 15 would be deleted after the original requirements as channel 1 have a RISE of 151 while channel 2 have a RISE of 2. The event meets all of the requirements, and additionally is the largest amplitude is recorded at channel 2. This situation is observed in several cases and can also be seen at Figure 19.

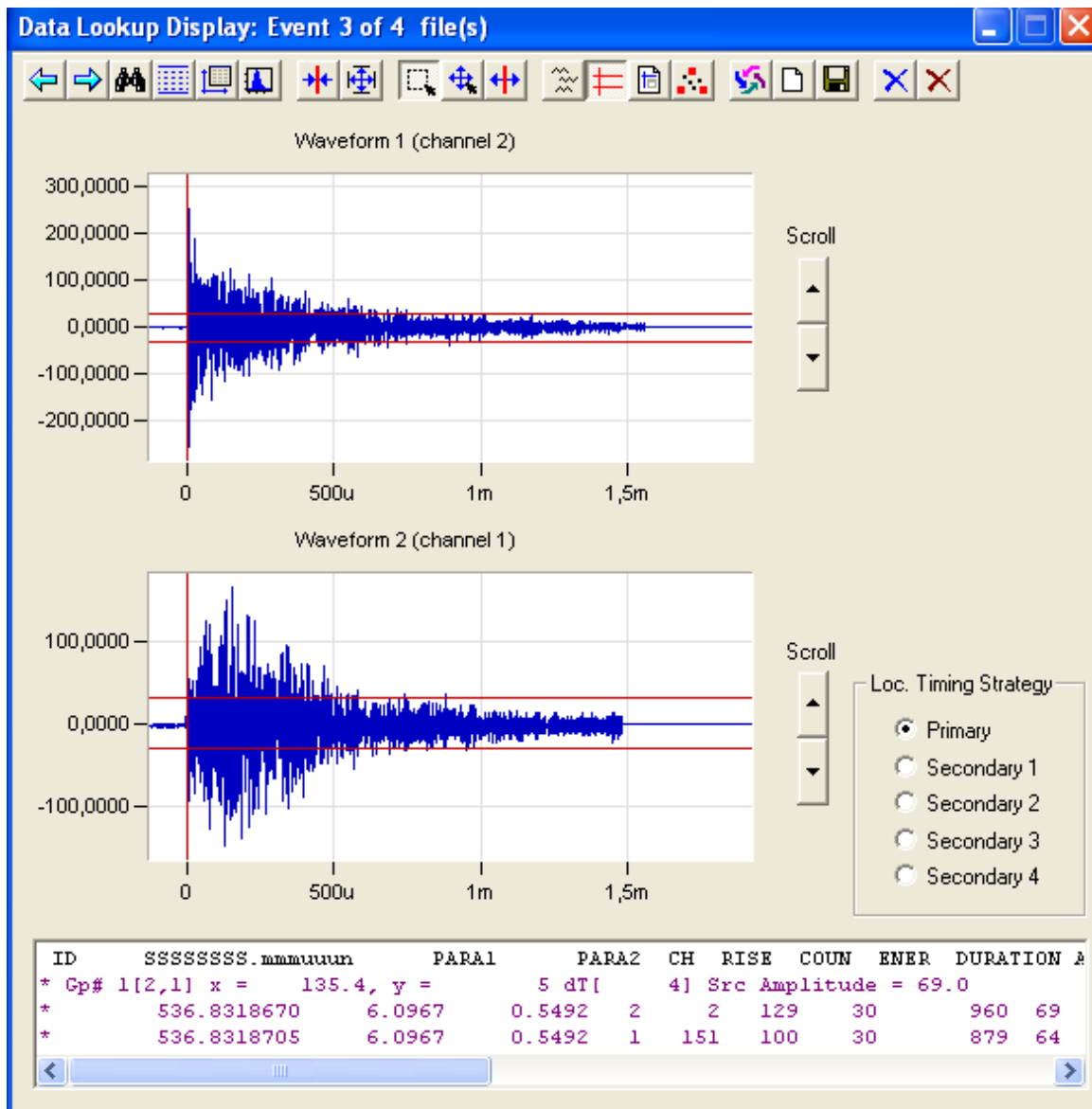


Figure 15 - Waveform with to high RISE value
Signal no. 130 - 25sec 1cyc -30c

3.5 Different types of signals and situations

Burst

Burst signal is the common signal for micro cracking and it indicates initiation and arrest properties. The high rise, seen at the left hand side of the x-axis in Figure 16, comes from signals that have hit the sensors directly from the source. Moving further to the right, the graph represents signals which have been reflected back and forth. It can be seen that the highest amplitude occur shortly after the rise starts as it consists of interference between several signals. Some waves will also be reflected at the surface and continue to affect the specimen and might be recorded by the sensors several times before they disappear.

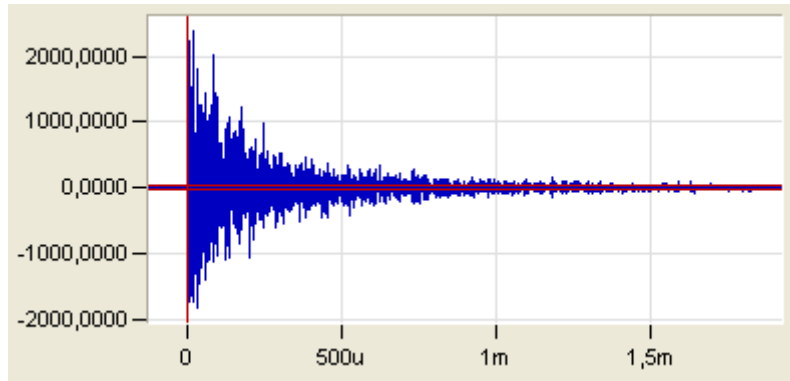


Figure 16 - Burst signal

Continuous

A continuous signal is often a result of noise and can be characterized as a signal with macroscopic fracture or a high RISE value.

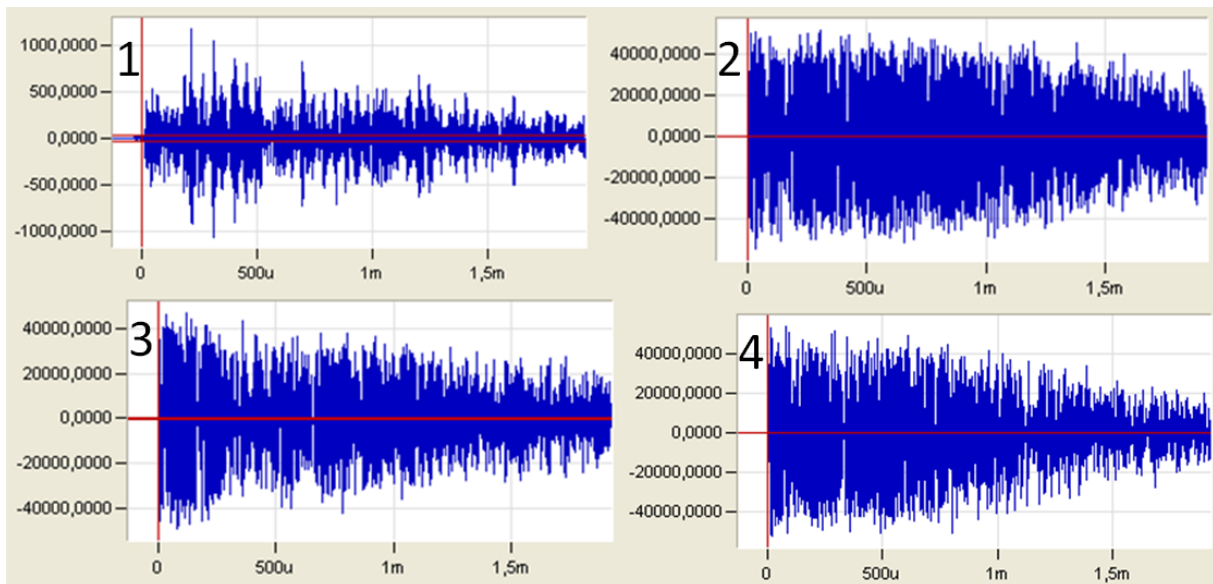


Figure 17 - Continuous signal

1. Test no. 150, 2. Test no. 51, 3. Test no. 144, Test no. 88

Table 3-1 shows data related to continuous signals with different sensors

Type	Para1	Para2	RISE	Duration	AMP	C-FRQ	GP
150 - SENB02-25sec1cyc-60c	16.3	2.65	196	7712	83	196	11.24
51 - SENB05 - 5sec1cyc -30c	4.9	0.14	33	48805	115	553	12.50
144 - SENB02 - 25sec1cyc -90c	15.4	0.36	183	13185	114	523	12.43
88 - SENB05 - 15sec1cyc - 30c	4.8	0.12	261	42339	114	578	12.57

Table 3-1 - Data related to continuous signal

Pop-in

Pop in can be observed as a sudden drop at the load – displacement curve and is associated with higher AE amplitude (>110, Østby et al. (2012)) or macroscopic fracture which results in an amplitude equal or larger than 113dB. In Figure 18, three pop-ins are observed but with amplitude of 56dB and no macroscopic fracture.

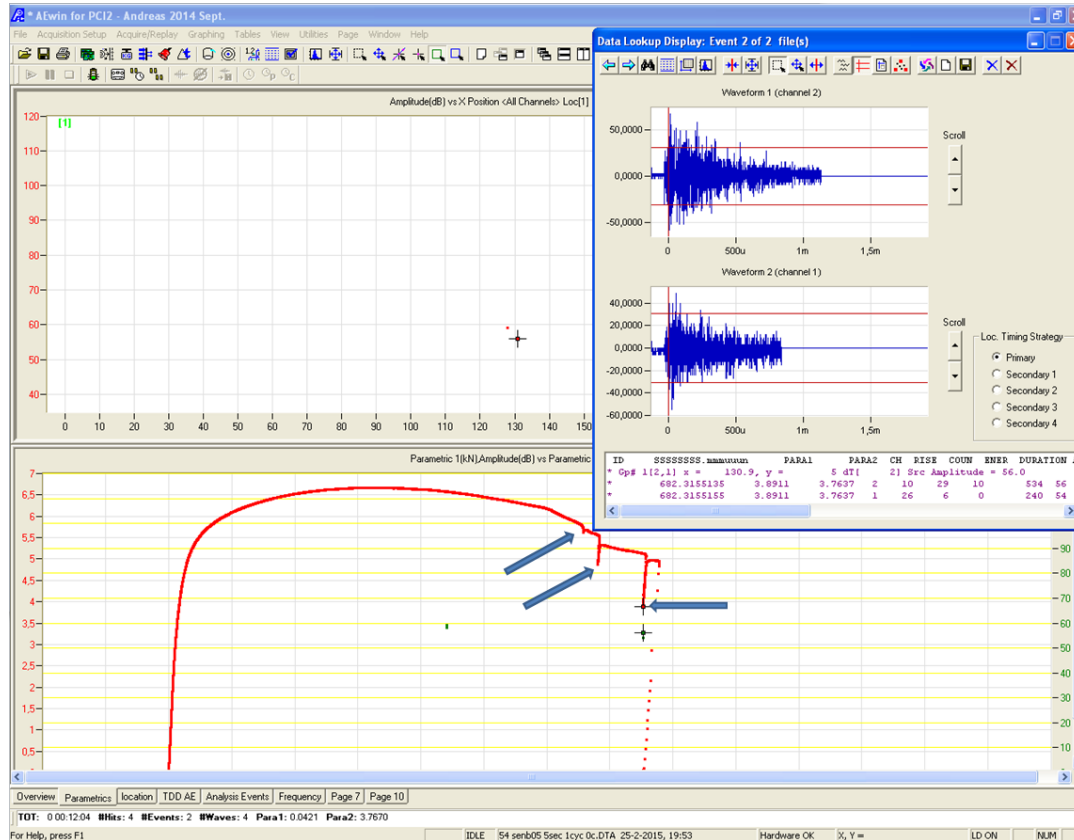


Figure 18 - Pop in, test no 54 - 5sec1cyc 0c

Double signal

A double signal has only been observed one time and has not been correlated to any source. The signal shown in Figure 19 is from a test stopped after the first signal. The signal in the upper window (channel 1) has three distinct areas where a descending amplitude can be observed. The signal recorded at channel 2 has an RISE value of 157, exceeding the allowed value. A possible explanation for this signal may be multiple small initiations at the same area, reflection in the matrix causing the signals to hit the sensor at the same time or noise (high RISE value).

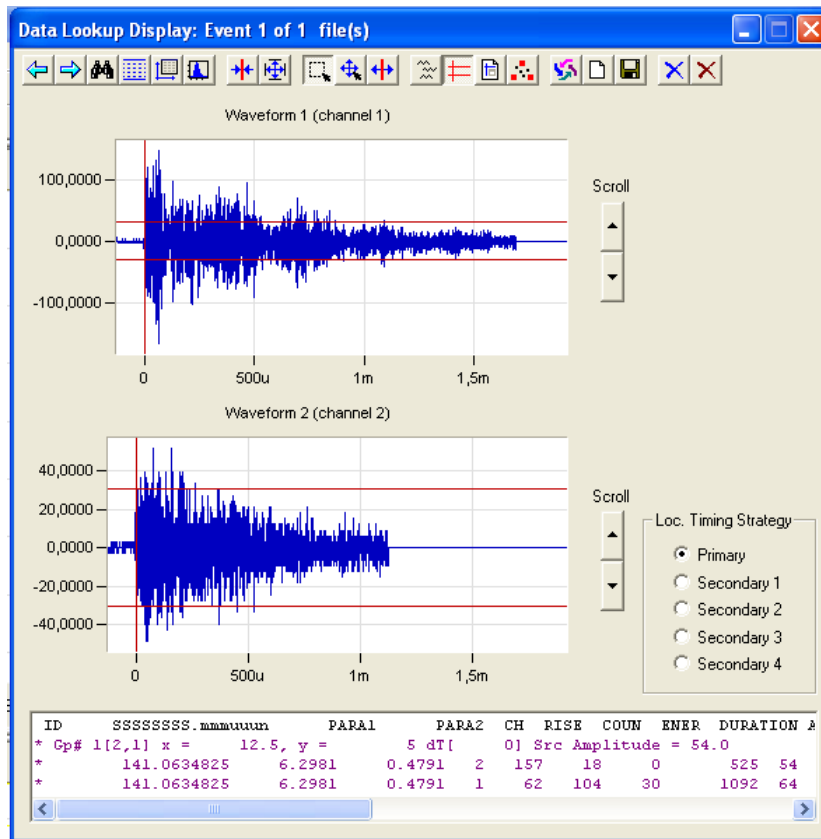


Figure 19 - Double signal – Test no 180 – 15sec1cyc -60c

Other special signals connected to noise

After sorting the data accompanying this signals recoded by AEwin, are these signals defined to be noise.

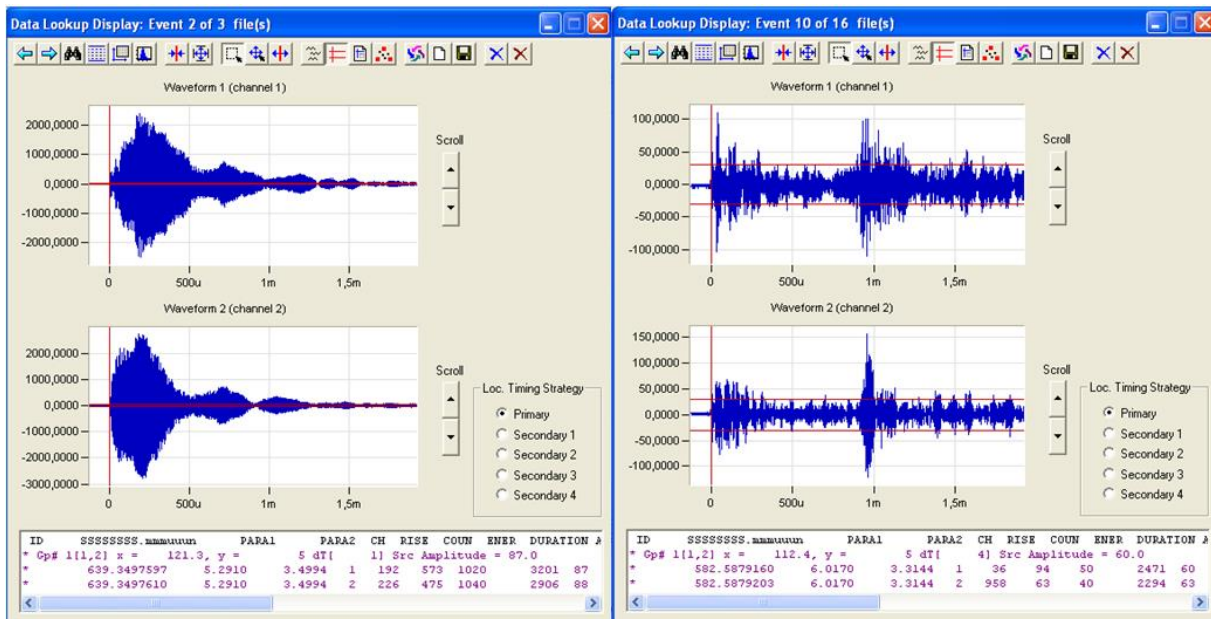


Figure 20 - Special signals

Left: Test no. 93 – 15sec1cyc 0c – amp 88. Right: Test no. 134 – 25sec1cyc .60c – amp 60.

4 Testing

The material tested in this master thesis is the same as in the project thesis, P-TPI X80 from Posco and R50A 420 from Ruukki. Unlike the project thesis, this thesis will emphasize on the R50A 420 steel from Ruukki.

4.1 Material properties

4.1.1 Mechanical properties

Ruukki – mechanical properties								
Tensile tests						Charpy-V impact test at – 60°C		
Plate no.	Thickness [mm]	Test direction	Rp0,2 [N/mm ²]	Rm [N/mm ²]	A5 [%]	Test direction	Impact energy [J]	
							individual	avg
76676-022	20	transverse, head	462	558	25,9	transv., head	304, 322, 333	320
		transverse, tail	477	564	25,4			
72722-041	50	transverse, head	498	580	23,9	transv., head	350, 362, 330	347
		transverse, tail	505	581	24,1			

Rp0,2 = Yield Strength [N/mm²], Rm = Tensile Strength [N/mm²], A5 = Strain [%], measured at a given area of the parallel length.

Posco – mechanical properties									
Transverse direction					Longitudinal direction				
YP	TS	YR	EL	U_EL	YP	TS	YR	EL	U_EL
MPa		%			MPa		%		
603	657	92	45	10	568	632	90	43	9
Impact toughness									
DWTT Shear Area at -20°C (%)					Charpy energy at -60°C (J)				
1	2	Average			1	2	3	Average	
90	90	90			336	337	332	335	

Table 4-1- Mechanical properties

YP = Yield Point, TS = Tensile Strength, YR = Yield Response, EL = Elongation, U_EL = Undeformed Elongation

4.1.2 Chemical composition (%)

Ruukki																		
Plate no	PC M	C	SI	MN	P	S	AL	NB	V	TI	CU	CR	NI	MO	N	B	SN	PB
72722 50 mm	,15	,019	,25	1,59	,008	,002	,027	,037	,012	,011	,0257	,23	,34	,206	,003	,0002	,003	,000
76676 20 mm	,13	,025	,22	1,46	,009	,003	,023	,036	,014	,008	,030	,22	,05	,208	,005	,0000	,003	,002
$PCM = C+(MN+CU+CR)/20+SI/30+NI/60+MO/1.5+V/10+5*B$																		
Posco (P-TPIX80) In addition in contains C-Eq = 0,43 *Present, but not specified.																		
	0,17	0,05	0,2	1,8			*	*		*		*	*	*				
High Strength Low Alloy (HSLA) from (Lambert-Perlade et al., 2004)																		
		,07	,32	1,5	,012	,001	,03	,014			,16	,06	,47	,12	,006			

Table 4-2 - Chemical composition

4.1.3 Different alloys and effect on mechanical properties

Some of the elements which were thought to have a larger influence on the events observed on SEM are listed below.

Phosphorus – P: In (Kunishige et al., 1979) is it proved that an increase of phosphorus lead to an higher intensity of separations. Separation is used as an collective term for both cleavage type and grain boundary type of fracture.

Sulfur – S: Can be a source to inclusions

Calcium – Ca: Applied to reduce the needed quantity of S. Remaining S will attach itself to Ca, creating CaS inclusions which retain its round shape after rolling.

According to (Thaulow and Valberg, 2012) are all modern steels based on a combination between thermo mechanical treatment and added micro alloy elements.

Small amounts with Al combined with normalization gives a grain refinement which increase the yield strength and reduce the transition temperature.

By adding the micro alloy elements Nb, V and Ti is it possible to further increase the yield strength. These elements can provide/give very fine precipitation in the ferrite, but on the downside reduce impact resistance. To maximize the effect one has to combine this with thermo mechanical work.

In addition to provide/lead to precipitation the micro alloy elements greatly affect the transformation mechanisms, especially the relationship between the grade of deformation, temperature and recrystallization. Nb is indispensable when it comes to development of controlled rolling, with or without accelerated cooling. Nb helps to keep control with the microstructure and ensure a fine grained micro structure.

A prerequisite for achieving a fine grained structure is to control the austenite grain size. Ferrite/bainite structure are mainly formed at the austenitic grainborder. A fine autenitic

structure with a high number of grain boundaries per volume will be the basis for a fine grained ferrite/bainite structure.

The particles will have completely different effect depending if they are precipitated in the austenitic phase, which result in grain refinement, or after the transformation in ferrite/bainite phase, which gives precipitated strength

During hot rolling and normalization which is described in chapter 2.2 will there be a strong tendency to grain growth. Precipitations from the micro alloy elements will then create a fine network of particles with the ability to lock the austenitic borders to prevent grain growth.

Thermodynamic gives a tendency for particles to precipitate particles at the grain boundaries since this gives the lowest total surface energy. As the grains grow the surface needs to drag with or free itself from the particles while new particles are captured by the border face. When the number of particles are large enough the structure are stabilized.

4.2 E-modulus

No data about the E-modulus is delivered from Ruukki and no tests have been carried out to determine it.

4.3 Are both materials considered weldable?

See chapter 4.1 for material properties and chapter 2.4 for theory about weldability.

Weldability for R50A 420

After IIW

$$CE = C + \left(\frac{Mn + Si}{6}\right) + \left(\frac{Cr + Mo + V}{5}\right) + \left(\frac{Cu + Ni}{15}\right) \quad [wt\%]$$

$$CE = 0.019 + \left(\frac{1.59 + 0.25}{6}\right) + \left(\frac{0.23 + 0.206 + 0.012}{5}\right) + \left(\frac{0.257 + 0.34}{15}\right) = 0.46$$

After AWS

$$CE = C + \frac{Mn}{6} + \left(\frac{Cr + Mo + V}{5}\right) + \left(\frac{Cu + Ni}{15}\right) \quad [wt\%]$$

$$CE = 0.019 + \frac{1.59}{6} + \left(\frac{0.23 + 0.206 + 0.012}{5}\right) + \left(\frac{0.257 + 0.34}{15}\right) = 0.41$$

The CE = 0.41 is somewhat more than what Palmer (2008) recommend for a pipe steel (range 0.32- 0.39) but is below what is recommended for flanges and forgings (0.45). In the datasheet provided by Ruukki for the 50mm R50A 420 steel are PCM = 0.15 which is below what he stated as a maximum which is 0.18 – 0.2.

4.4 Preparation of specimens before testing

4.4.1 Extraction from plate

Two plates are welded together with a one sided weld (half V notch) before the specimens are machined out from outside the HAZ. One specimen is retrieved from each side of the plate in the thickness direction, a few millimeters beneath the surface. The specimen's orientation is perpendicular on the rolling direction.

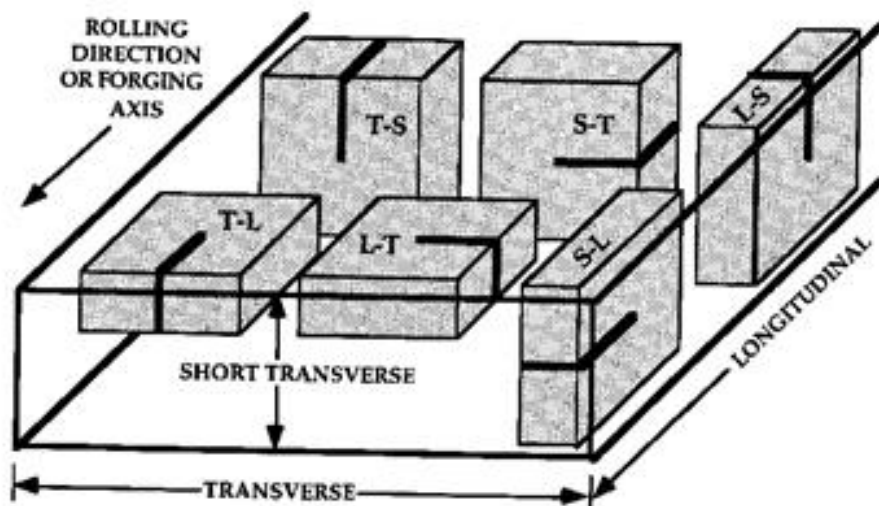


Figure 21 -ASTM notation for tested specimen

The specimens were cut from the base metal with their length axis perpendicular to the plate rolling direction and with cross section 11x11mm and length 100 mm.

4.4.2 Weld simulation

It is then weld simulated with a Smithweld TCS 1500 weld thermal simulator. The two following different microstructures are obtained:

Coarse Grained Heat Affected Zone (CGHAZ) which is the result from one welding cycle. It is done with four different rates of cooling, denoted $\Delta t_{8/5}$. A higher $\Delta t_{8/5}$ means slower cooling.

Peak temperature 1350° C with a cooling time between 800 and 500° C $\Delta t_{8/5} = 5s, 10s, 15s$ and 25s.

Inter Critically Coarse Grained Heat Affected Zone (ICCGHAZ) which is the result from two welding cycles. It is done with the same rates of cooling as CGHAZ.

1. Peak temperature 1350° C with a cooling time between 800 and 500° C $\Delta t_{8/5} = 5s, 10s, 15s$ and 25s (first cycle)
2. Peak temperature 780° C with a cooling time between 800 and 500° C $\Delta t_{6/4} = 5s, 10s, 15s$ and 25s (second cycle)

4.4.3 Common preparation

The specimen is then machined down to a cross section of 10mm x 10mm before a notch for the pin gauge is machined. The straight crack is spark eroded and the depth depends on the

type of SENB test. The sparked eroded crack is placed parallel to the rolling direction. The specimen is denoted T-S after the ASTM standard due to how it is how it's extracted and forged.

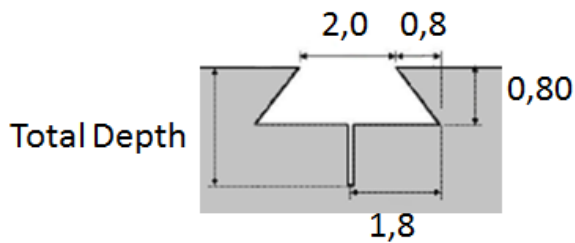


Figure 22 - Notch for pinch gauge and spark eroded crack



Figure 23 - Photo of notch for pinch gauge and spark eroded crack

Figure 22 shows the geometry used when only one pinch gauge is needed. For SENB02 the total depth is 0.2 mm and for SENB05 will the total depth be 0.5. Pre-fatigue is done to achieve an “infinite” sharp crack and is done until the right depth is reached.

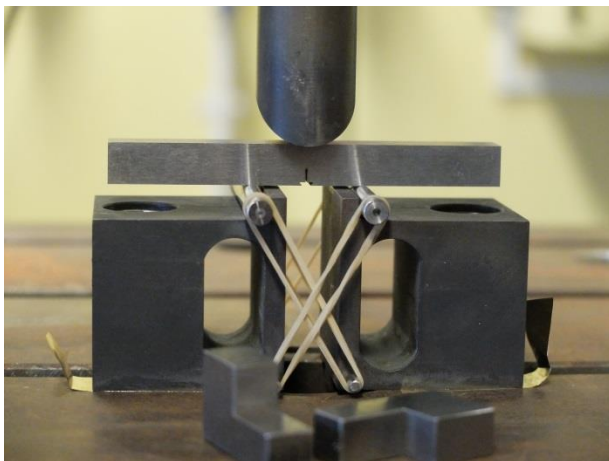


Figure 24 - Fatigue

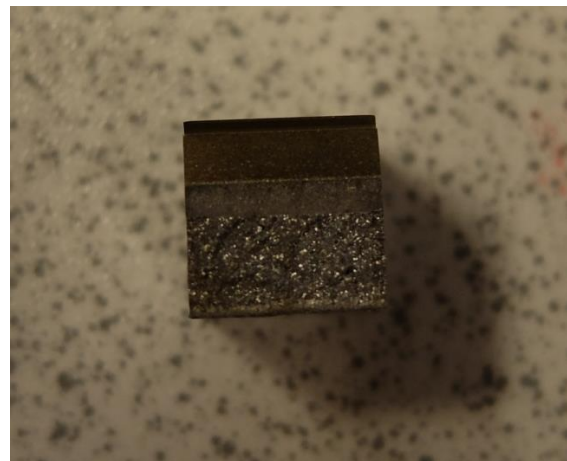


Figure 25 - Cross section of SENB05 specimen after finished testing

See attachment 12.3 to see a picture of the specimen mounted before the test is performed. The specimen is then mounted in the chamber on top of two circular bars with diameter 10 mm and with a predefined distance center – center, see Figure 24. The sensors are then mounted on top and fastened by magnets.

4.5 Mounting of AE – hardware and equipment

The acoustic emission was recorded and measured with equipment from Physical Acoustic Corporation.

4.5.1 Sensors

The sensors used were PICO Ultra-mini wide-band, see appendix 12.3. Two sensors were mounted with a distance 25mm, both 12.5 mm from the crack plane. See chapter 3.1.3. Between the sensors is a low temperature cream of the brand Molykote used. It can stand temperatures down to - 73 °C.

4.5.2 Pre amplification

A pre amplification 2/4/6 with built inn 100kHz high pass filter was used. It can deliver 20, 40 or 60dB amplification but 20dB is chosen as it gives the best dynamic between weak and strong signals. A higher amplification will in addition to amplifying the signal, amplify the noise. It has a noise level of 2 μ V.

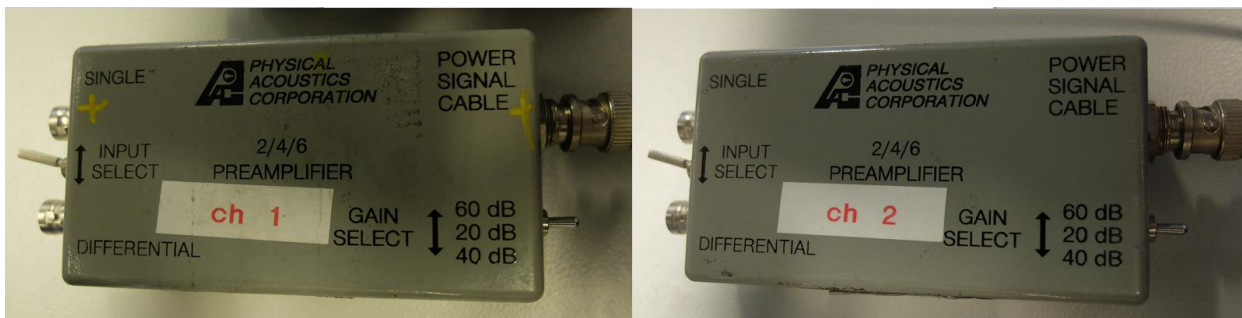


Figure 26 - Pre-amplification

4.5.3 Threshold

Threshold is chosen with respect to the lowest amplitude desired to record. A too low threshold may result in too many signals which may result from background noise or microcracks which is impossible to find. It might also lead to zero recorded signals because the sensors are jammed by too many signals. The threshold value was set to 50dB. A threshold of 30dB and 40dB was also tried but was discarded since no signals were recorded. This is set in the AEwin software, see chapter 3.3.

4.5.4 Data Lookup Display

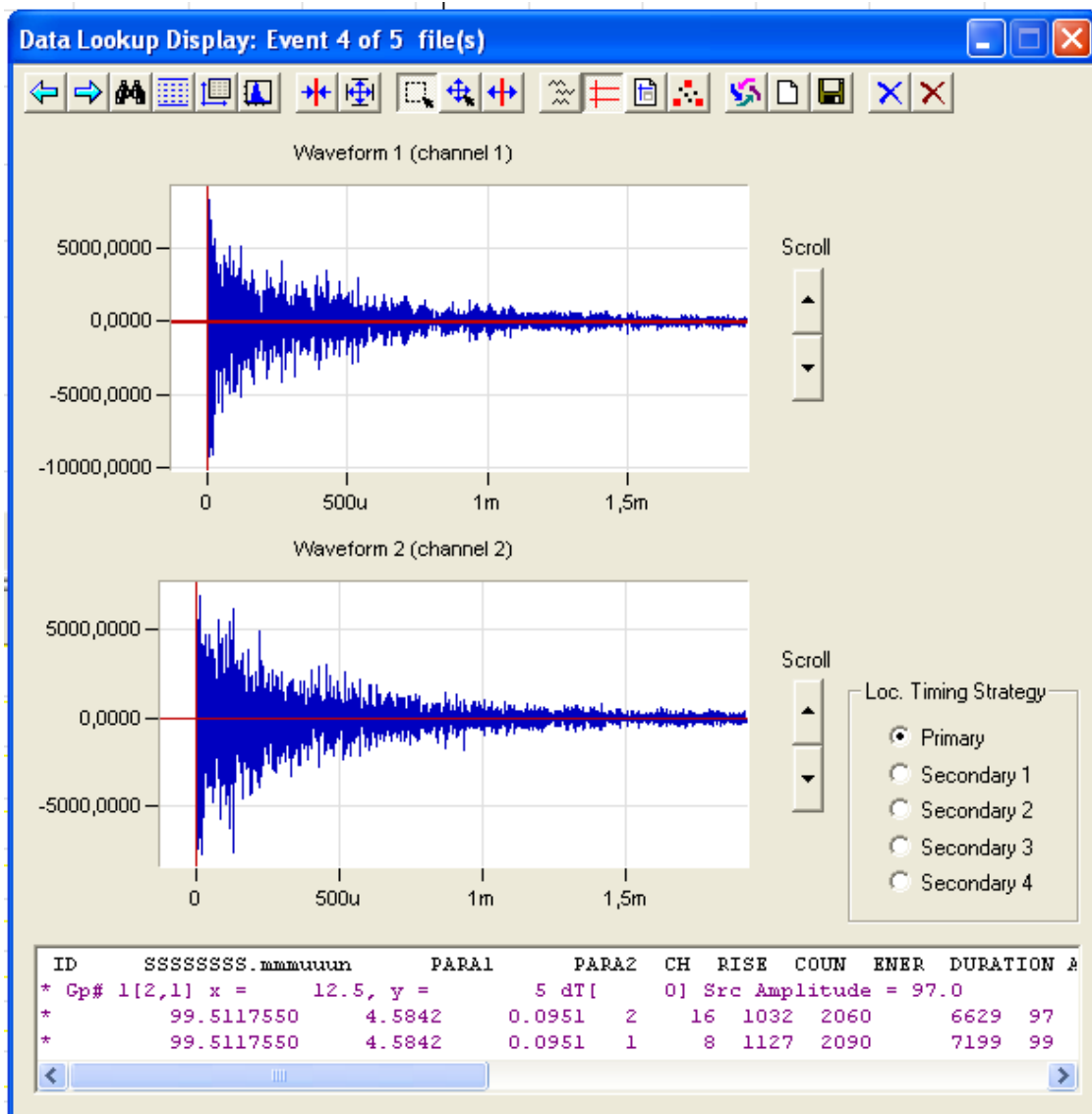


Figure 27 - Data Lookup Display

X – Axis: time in micro and milli seconds

Y – Axis: size of amplitude in volt. This value is a result of the following equation, see page 16 in (SOFTWARE, 2004):

$$\text{Displayed Value} = (\text{Measured Voltage} \times \text{Multiplier}) + \text{Offset}$$

With the help of equation 3-13 can the minimum amplitude voltage needed for detection be calculated to 31.6V. This assumes an threshold value of 50dB and a pre-amplification of 20dB.

5 Preparation before examination

5.1 Cutting

The specimens were first cut in a manual cutting machine, but the result was not satisfactory. It was experienced that the method had high demands to the operator to keep a slow and steady motion during cutting. The result varied from each time and in to many cases the heat generation was too large. It was therefore decided to use an automatic cutting machine.

The rest of the specimens were cut in automated cutting machine with an aluminum oxide abrasive cut of wheel (Struers 30A15). It was done with rotation to improve the cut. In the cases where fracture surface were of interest the fracture surface were flushed with Ethanol prior to cutting to reduce the risk of corrosion. All the specimens were rinsed with ethanol after cutting and dried with a hairdryer.

5.2 Preparation for SEM – fracture surface

After the specimen is cut and rinsed with Ethanol the edges which were deformed from cutting is grinded down. Coarse grinding paper wetted with water was used. Grinding machine was not used to reduce further exposure to water. The edges were grinded to make it possible to insert the specimen into the clamp for tilting. In addition it was experienced that if the specimen was not steady the quality of the picture was drastically reduced, most likely due to small vibrations in the specimen.

All the R50 420 specimens were put in ultra-sonic bath for two minutes. It was not observed any visible reduction of dirt and two minutes is assumed to be enough.

5.3 Preparation for light microscope – microstructure

Grinding and polishing

The specimens were grinded with Waterproof Silicon Carbide Paper, starting with a grain size of 200 μ m and ending with a grain size of 5 μ m. Then they were put in ultra-sonic bath for two minutes before being polished with 3 μ m, new round with ultra-sonic bath and then 1 μ m polishing before ending with ultra-sonic bath to be sure that no dirt is left.

Etching

To see the microstructure in the light microscope the specimen needs to be etched. 2 From (Östberg and Modin) and by advice from Angelika Brink from the Department of Engineering Design and Materials it was decided to use Nital (NaOld). The specimens were etched for 15 seconds before they were washed with Ethanol and dried with hairdryer.

Nital is an electrolytic liquid and a current can be added to change the etching process. This was not done since Nital alone showed satisfactory results.

Martensite will be shown as brown due to coloring from the Nital, as opposed to Bainite and Ferrite which will be displayed as a white and ferrite grain boundaries will be dark.

Specimens who are etched longer than others will be darker. Grain orientation will also affect the final result.

Etching with LePera was done by Chatrine Hartwig alone and the reader is referred to her master thesis.

5.4 Hardness testing

The background for running the hardness test can be divided into two separate goals.

1. Investigate the fracture surface and measure possible difference at the smooth surfaces and the surrounding fracture surface.
2. Determine the hardness on the machined surfaces to make it easier to define the microstructure.

Hardness testing was performed with a MicroWiZhard – HM-200 Hardnes Testing Machine from Mitutoyo. The machine calculates the hardness based on the Vickers Pyramid Number (HV). It is equipped with three different magnifications, 10X, 50X and 100X. 100X was used when defining the surface area. The load control were set at loading = 4, duration = 15, unloading = 4 with test force = HV0.1. According to the manual can this be written as 100gf or 0.1kgf ($980.7 \cdot 10^{-3} \text{N}$). The measurement of the area is done manually and the HV is calculated automatically.



Figure 28 - MicroWiZhard Hardness Testing Machine

Fracture surface

At first the fracture surface were investigated to measure possible difference at the smooth surfaces and the surrounding fracture surface. This was aborted after several attempts as the microscope had problems with getting good picture due to the difference in height on the surface. It was not possible to spot the smooth surfaces and this testing was therefore aborted.

It was discussed with the person responsible for the Nanomechanical lab if there was possible to determination the hardness by a nanoindenter. The conclusion was that this would be difficult because demands that the surface is perpendicular to the indenter.

Machined surfaces

At the first tested specimen were three faces tested were one of those were an etched surface. It turned out that the etched surface provided a better result than the other, which means that the mark left from the indenter leave a clear square mark. The rest of the tests were therefore preformed on the etched surfaces only. Furthermore were the hardness test run at two different locations at each specimen, the first approximately 1mm from the fracture surface and the second approximately 15 mm from the fracture surface. Seven indentations were made at each "line" manually with an approximate distance between the points of 1mm.

Some of the first specimens showed a tendency were the hardness changed as the indenter moved from the spark eroded crack to the brittle fracture zone and vice versa. But after this were recorded systematically no clear tendency were recorded. More indentations would also be necessary to achieve a satisfactory result and therefore are no conclusion made.

5.5 Measurement of crack depth

The specimens tested consist of a machined track and a pre-fatigued crack, see chapter 4.4.3. The depth of the crack is measured by a Technical 2 provided by Carl Zeiss.



Figure 29 - Technical 2 for crack depth measurement

The procedure follows the following steps and the result are listed in forms, see appendix 12.17:

1. Reset the digital measuring device at point 1 and 2, see Figure 30. Point 1 is placed at the edge in the center of the specimen and point 2 at the edge where the pre-fatigue end. This point can be hard to find when the specimen is stopped after the first signal as the transition between pre- and post-fatigue can be hard to spot.
2. Measure the distance in y-direction at 1%, 12.5%, 25%, 37.5%, 50%, 62.5%, 75%, 87.5% and 99% of the width.
3. When large plastic deformation is present is it necessary to measure the width and calculate new points. In addition is it necessary to make two measurements in x-direction, one to where the fatigue ends and one two where the plastic deformation stops.

4. The average value of the measurement is found with the following equation:

$$a_0 = \frac{\left(\frac{y(1)+y(99)}{2}\right)+y(12.5)+y(25)+y(37.5)+y(50)+y(62.5)+y(75)+y(87.5)}{8}$$

The numbers in parenthesis denotes the percentage where the measurements are done. As can be seen in the equation are the contribution from “1%” and “99%” half of the contribution from the other points.

5. If an extra measurement is done due to plastic deformation will an average of this two values be used.

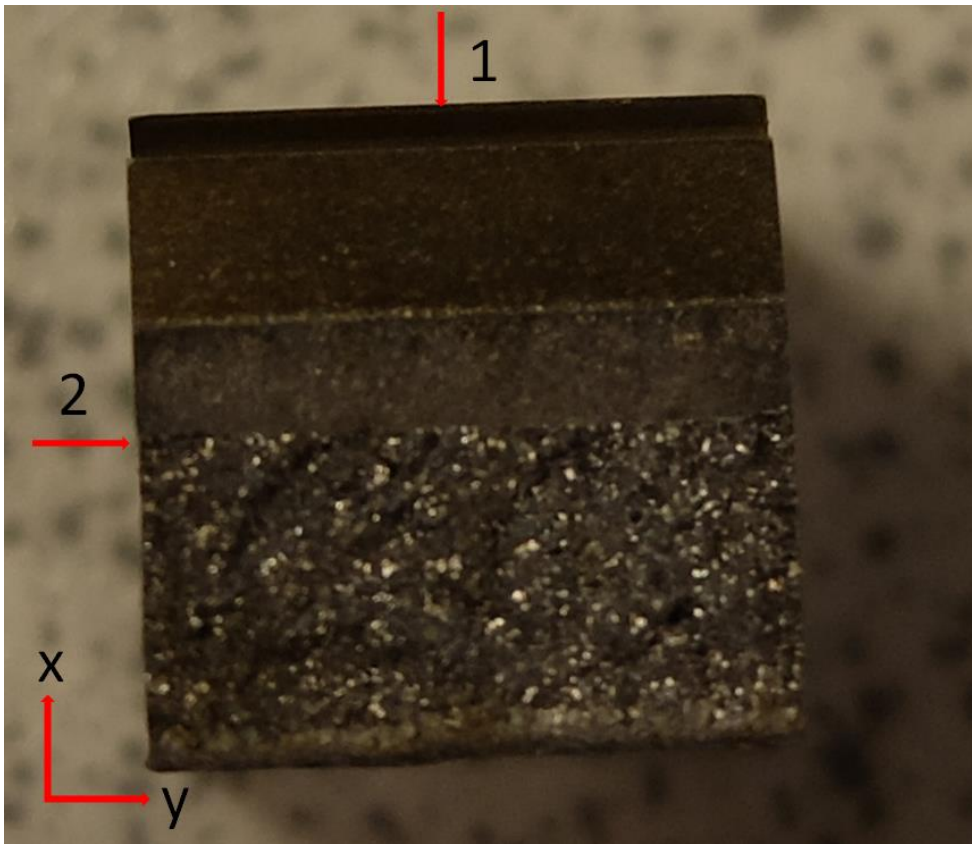


Figure 30 - Crack depth measurement

A table over the measurement can be found in the appendix, chapter **Error! Reference source not found.**

6 Results from SEM, EDS, Hardness, Microstructure

The EDS equipment is provided by “EDAX” – X1 ANALYZER from the (A)METEK – Materials Analysis Division. The software used is named “TEAM: Texture & Elemental Analytical Microscopy”.

All investigation in the SEM has been performed at the IPM – Nanolab. The SEM is provided by EDAX and of type Quanta Feg 650. Software is xT Microscope control.

The fracture surface is investigated in the SEM with two different treatments as described in chapter 0. The working distance was set to 10 (+0.5/-0.1) mm. Higher HV and spot when investigating holes and cracks. High vacuum was used in all time.

6.1 Microstructure

Analysis of microstructure in microscope has been performed by Chatrine Hartwig .For more information see her master thesis.

The microstructure is examined in a light microscope from ZEISS and the pictures are taken with the software LAS from Leica.

The material is highly inhomogeneous and is therefore difficult to classify the microstructure. This is valid for both the base material and the material exposed to weld simulation.

Almost all of the specimens examined had an average prior austenite grain size of $100\mu\text{m} \pm 30\mu\text{m}$. The general microstructure for all the specimens can be defined to be a mixture of upper bainite and martensite with a varying degree of auto tempering in addition to some ferrite. It is believed to be auto – tempered martensite present because the steel have a high M_s . There seem to be a coarsening in the microstructure as the cooling time increases, and a tendency to form more upper bainite than martensite, as can be seen in Figure 31.

In test no 7, Figure 32, which have a CGHAZ 15sec simulated microstructure, is the microstructure mostly upper bainite with dotted lines due to the small amount of carbon. There are some areas which are believed to be auto tempered martensite appearing as white with black dots. The reason for uncertainty is that it might also be bainite with grain orientation in/out of the plane. All of these microstructures are indicated in Figure 32. Sample 12, see Figure 33, which has an ICCGAZ 25sec simulated microstructure, is very similar except that it seem to contain more auto-tempered martensite. It is difficult to determine any difference in the microstructure for sample 17 and 24, ICCGAZ 10sec simulated microstructure, which seems to be a bit over-etched.

The base material for sample 12, see Figure 35 and Figure 36, have elongated grains in longitudinal rolling direction. Some large white grains can be seen, but higher magnification, Figure 36, indicates that they can be further divided into smaller grains. The thin, almost

invisible lines, indicate that they could be bainite or martensite. Ferrite on the other hand should not contain any black particles due to the low solubility of carbon. Further can it be stated that there is a large scatter in grainsize, with the smallest down to 2µm.

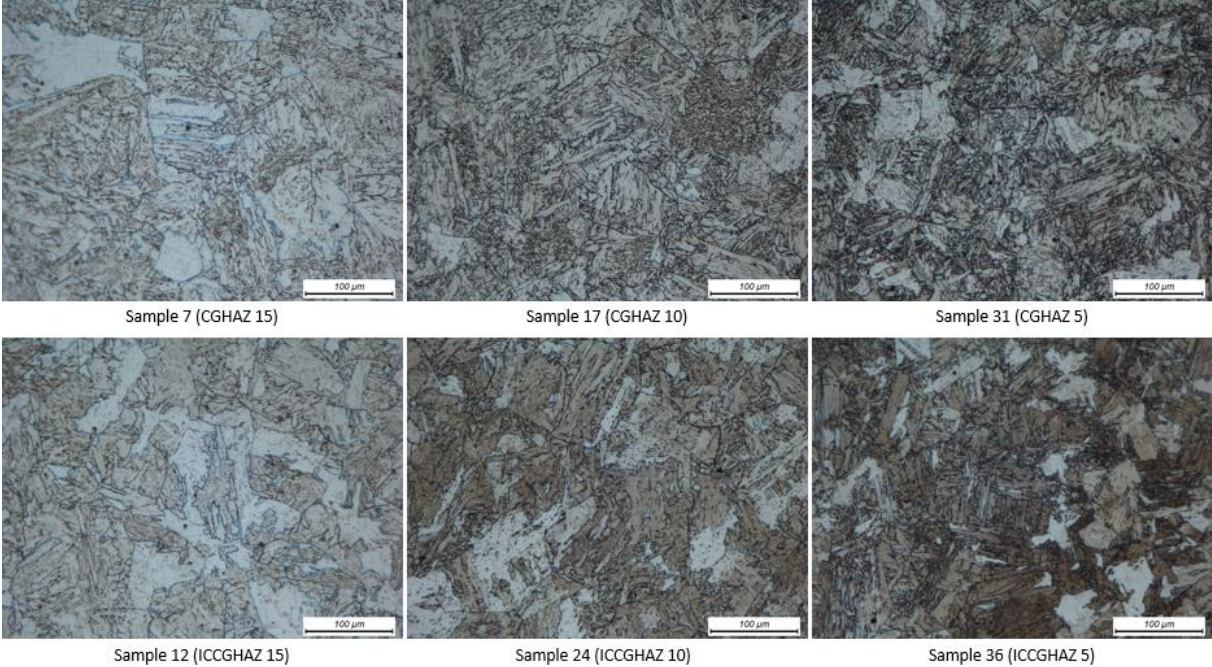


Figure 31 - Micrographs of the specimens with different weld simulations

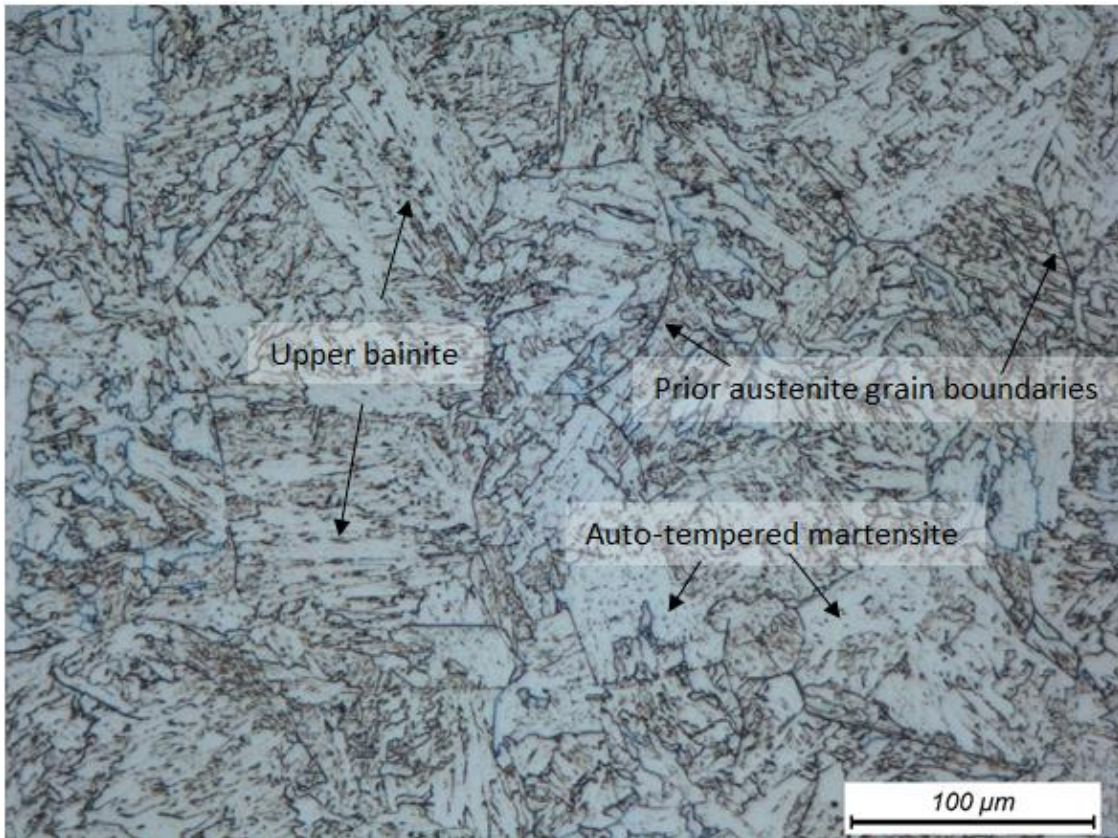


Figure 32 – Micrograph - Test no 7 - 1cyc15sec

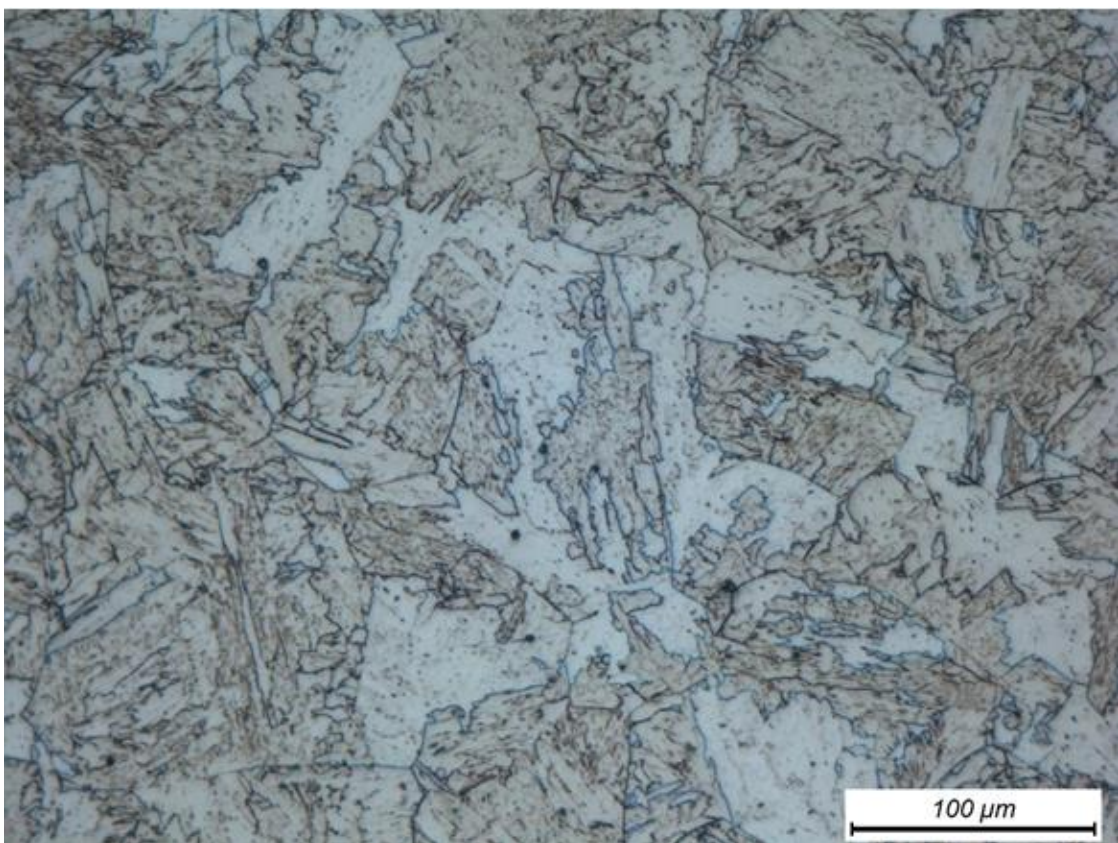


Figure 33 - Micrograph - Test no. 12 - 2cyc15sec

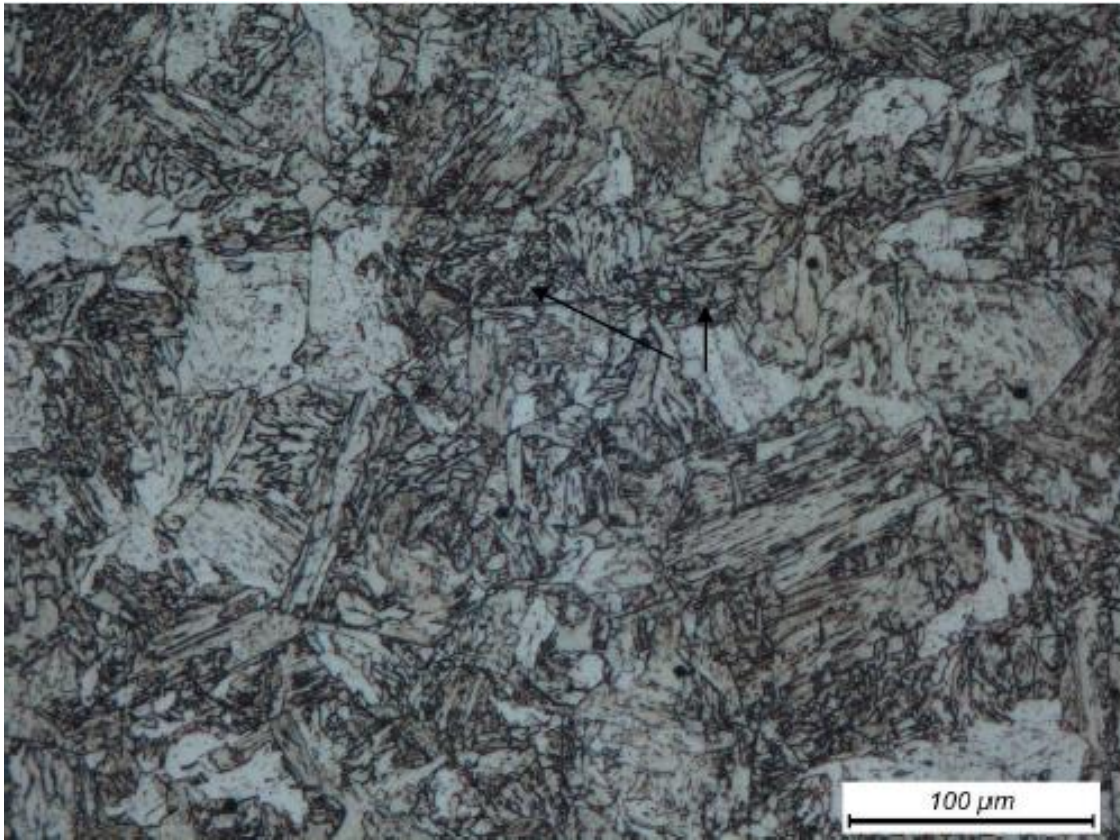


Figure 34 - Micrograph - Test no 31 - 1cyc5sec

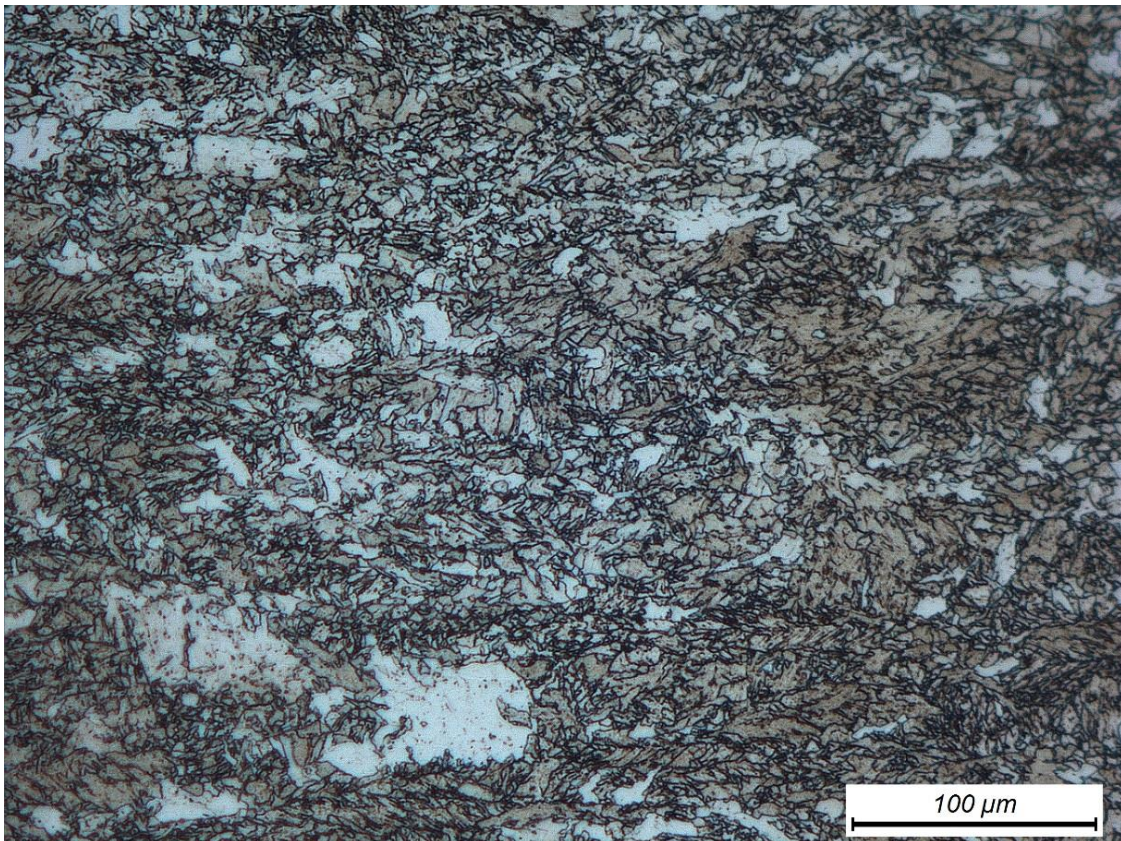


Figure 35 - Micrograph of base material - Test no 12 - 2cyc15sec

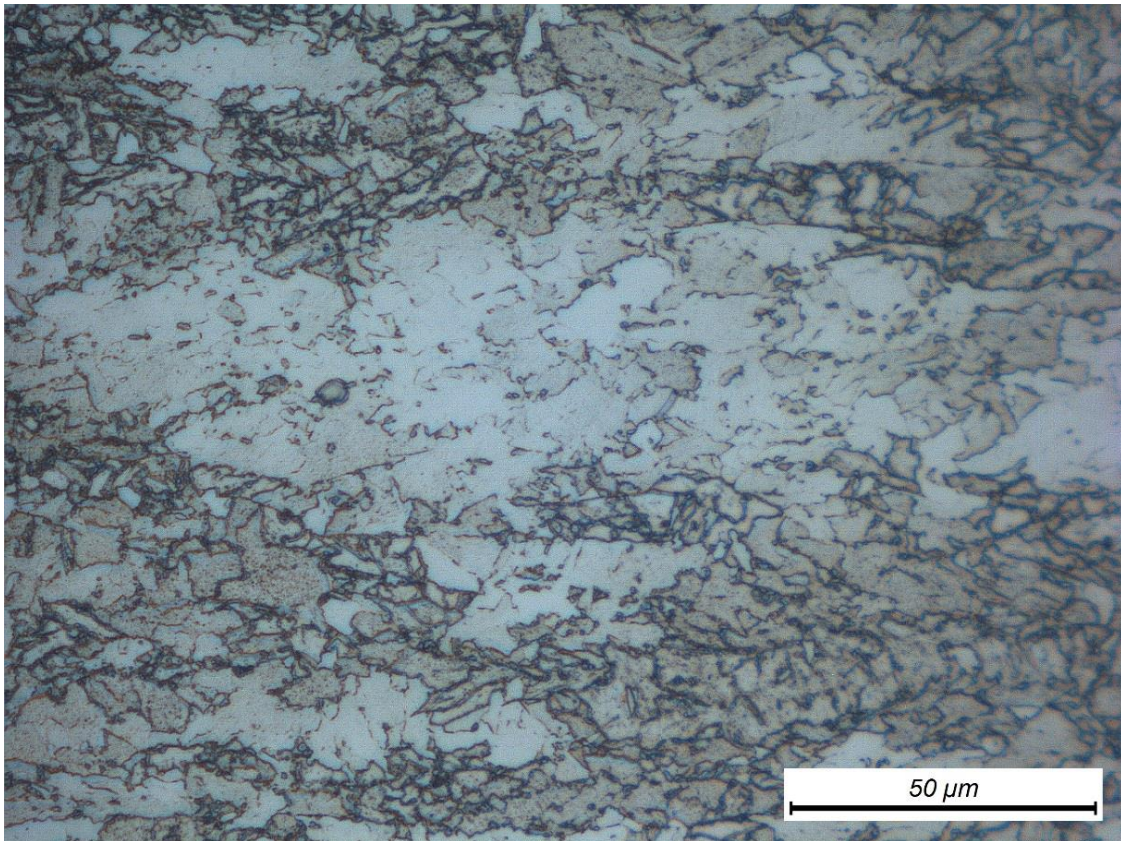
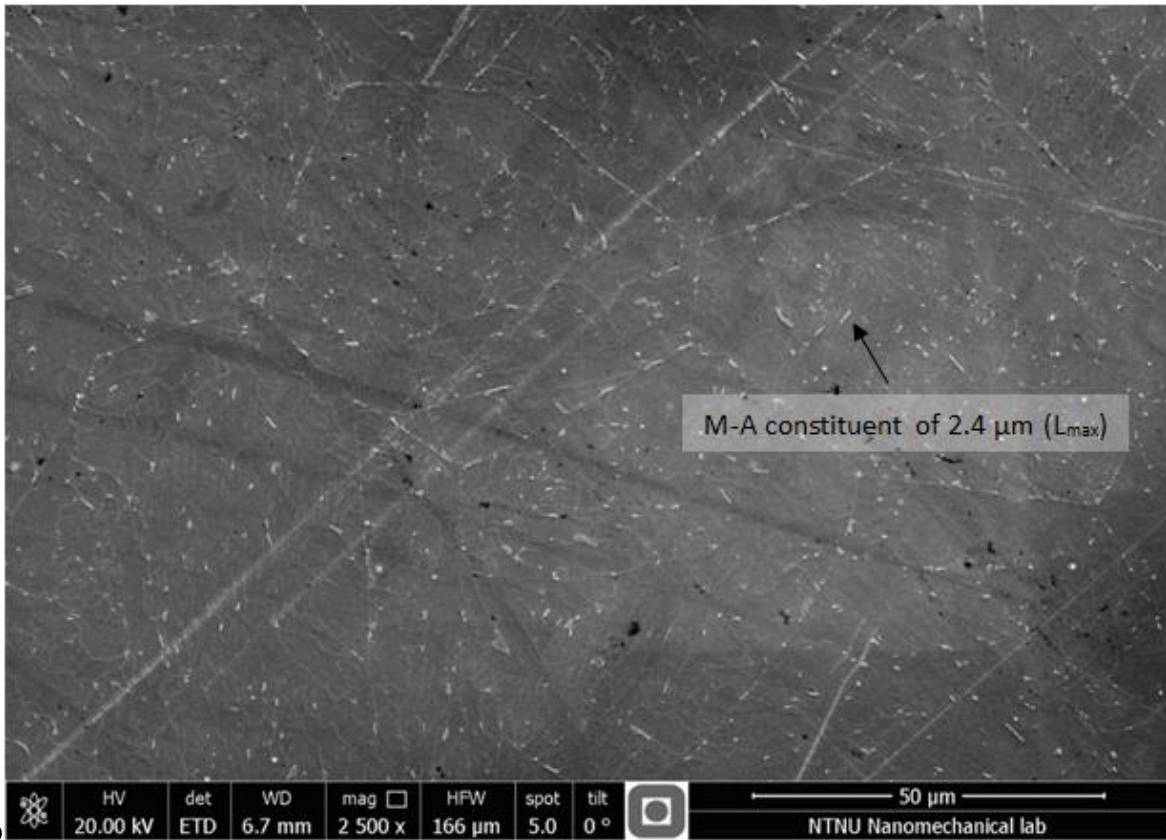


Figure 36 - Micrograph of base material -Test no. 12 - 2cyc15sec

6.1.1 M-A phases

The LePera etched samples shows a similar amount of M-A and morphology in both the CGHAZ 15sec and ICCGAZ 15sec specimen and the following description apply for both samples. The M-A phases is distributed approximately as seen in Figure 37 through Figure 40. As can be seen are there little M-A constituents on the prior austenite grain boundaries for both samples. The M-A constituents were mostly short elongated stringers or very small blocky particles located between bainite or martensite laths. L_{max} for the blocky particles is typically less than 1μm, while for stringer 2μm which is similar to the one indicated in Figure 37.

These results comply with the results achieved by Aksel Louis Legouy Kvaal and Brage Dahl Snartland's master theses which were written simultaneously as this. They are conducting nanomechanical testing on weld simulated specimen from the same steel and with the same treatment as the one investigated in this master thesis. Their specimens are respectively CHGAZ 15 sec and ICCGAZ 15sec. No larger M-A constituents were found in their work, in contrast to what have been discovered in this thesis. Some stringer M-A constituents were found to have a L_{max} up to 7μm in addition to a few blocky M-A islands around 3 μm. These were found on both intergranular and prior austenite grain boundaries, indicated in Figure 39 and Figure 40.



Fo

Figure 37 - SEM micrograph LePera etched for approx. 20 sec. - Test no. 7 (1cyc15sec)

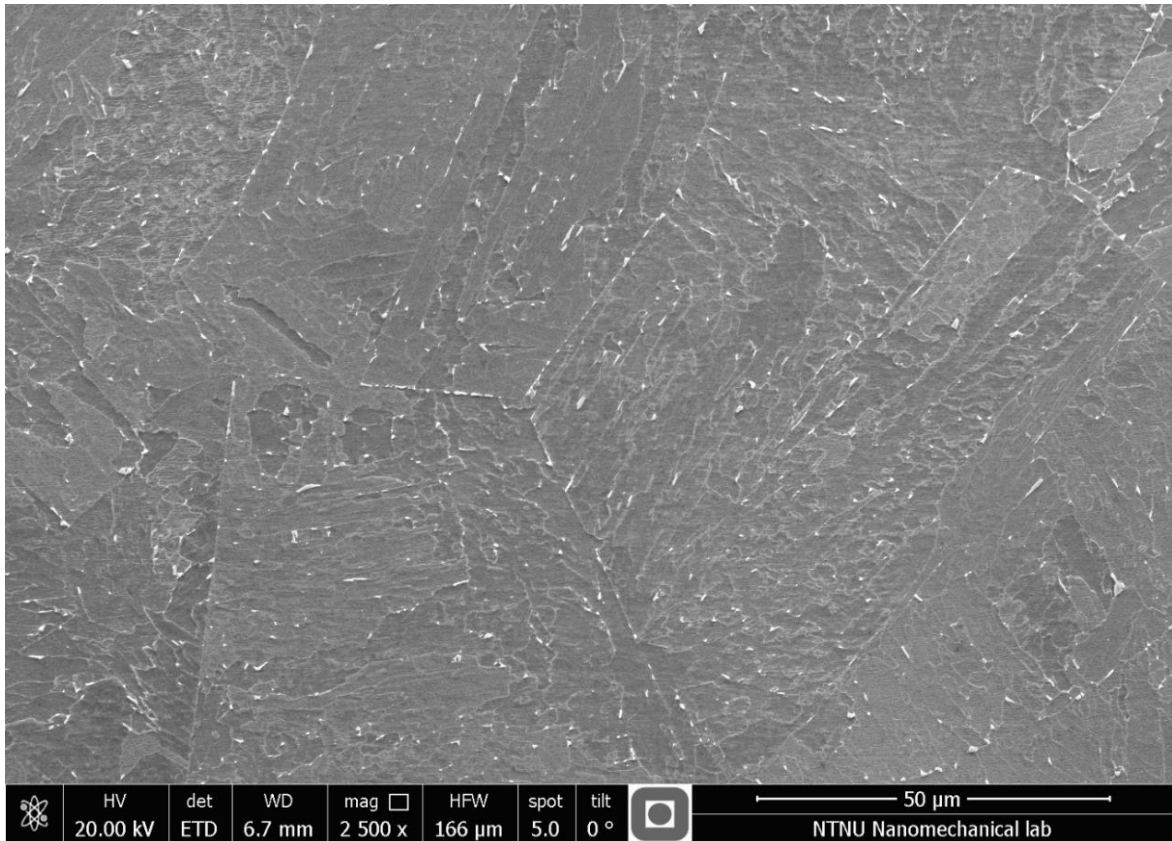


Figure 38 - SEM micrograph, LePera etched for approx. 20 sec - Test no. 12 - 2cyc15sec

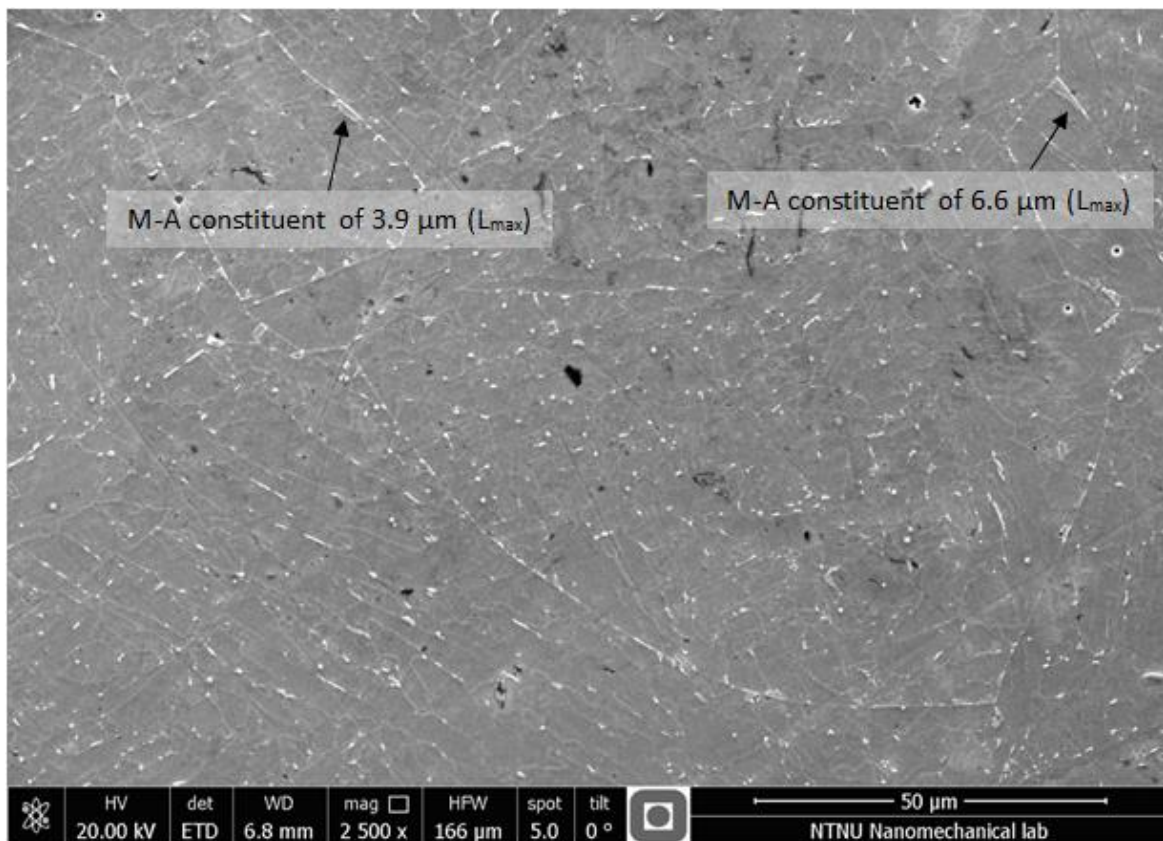


Figure 39 - SEM micrograph LePera etched for approx. 20 sec - Test no. 7 - 1cyc15sec.

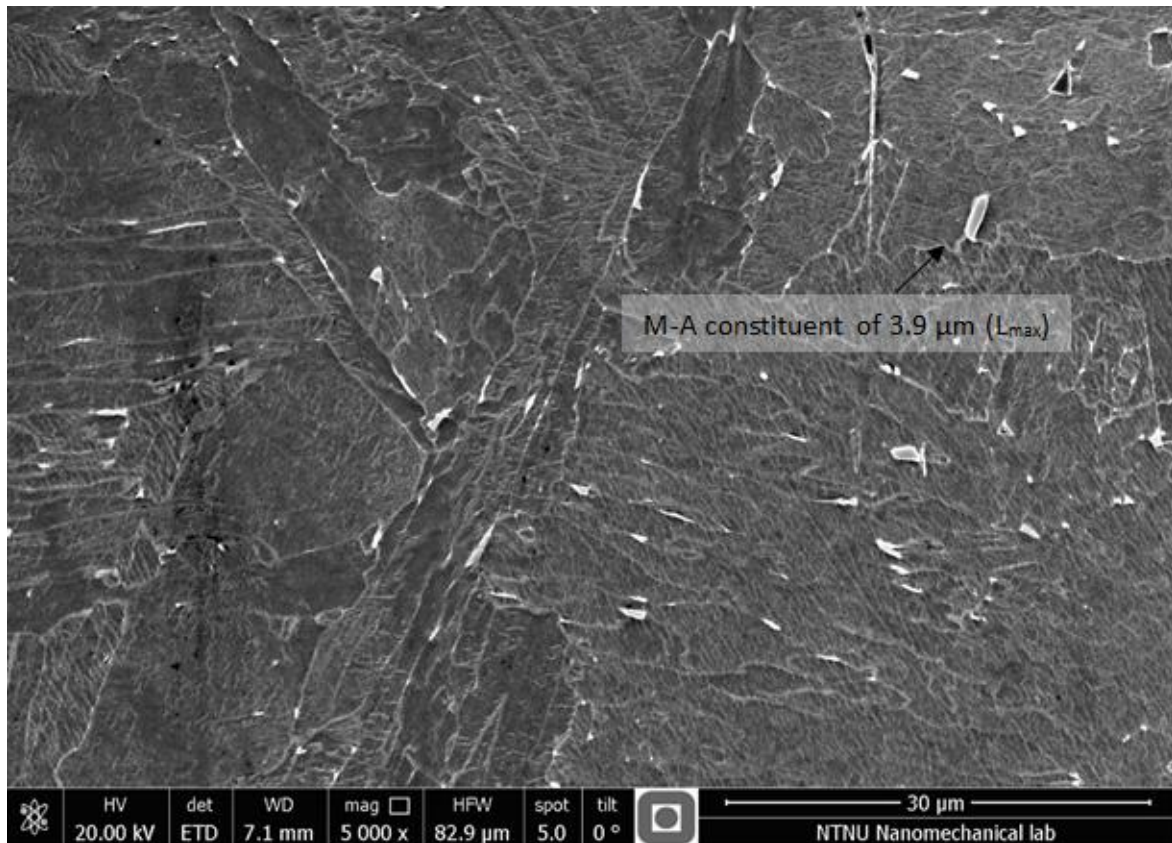


Figure 40 - SEM micrograph LePera etched for approx. 20 sec - Test no. 12 1cyc15sec

6.1.2 Hardness

Overview of the average hardness values R50A 420 s

All the data can be found in the appendix, chapter 12.11. Standard Deviation is calculated in Microsoft.

Vickers Hardness			
Specimen	Line number	HV	Standard Deviation
31-1cyc 5sec	1	231.4HV0.1	12.92
31-1cyc 5sec	2	191.0HV0.1	21.10
17-1cyc 10sec	1	232.0HV0.1	10.35
17-1cyc 10sec	2*	193.7HV0.1	12.13
18- 1cyc 10sec	1	231.2HV0.1	18.78
18- 1cyc 10sec	2	186.9HV0.1	10.22
7-1cyc 15sec	1	234.4HV0.1	20.03
7-1cyc 15sec	2	195.2HV0.1	17.24
36-2cyc 5sec	1	228.1HV0.1	14.05
36-2cyc 5sec	2	199.2HV0.1	14.37
24-2cyc 10sec	1	264.1HV0.1	43.51
24-2cyc 10sec	2	191.9HV0.1	10.42
12-2cyc 15sec	1	225.8HV0.1	11.58
12-2cyc 15sec	2	200.7HV0.1	10.62

Table 6-1 - Vickers Hardness R50A 420

*This is defined as line number 3 in the appendix but is equivalent to line number 2 on the other specimens.

6.2 Tests run to complete fracture

The tests which were run to final fracture can be described with three different zones after the pre-fatigue. The first event/zone to appear is called “stretching zone”, then followed by a ductile zone before the brittle cleavage facet appear. As can be seen in Figure 43 are the cleavage facets continuous and there are difficult to identify both crack initiation and crack arrest. It is especially difficult to link a cleavage facet to an AE signal.

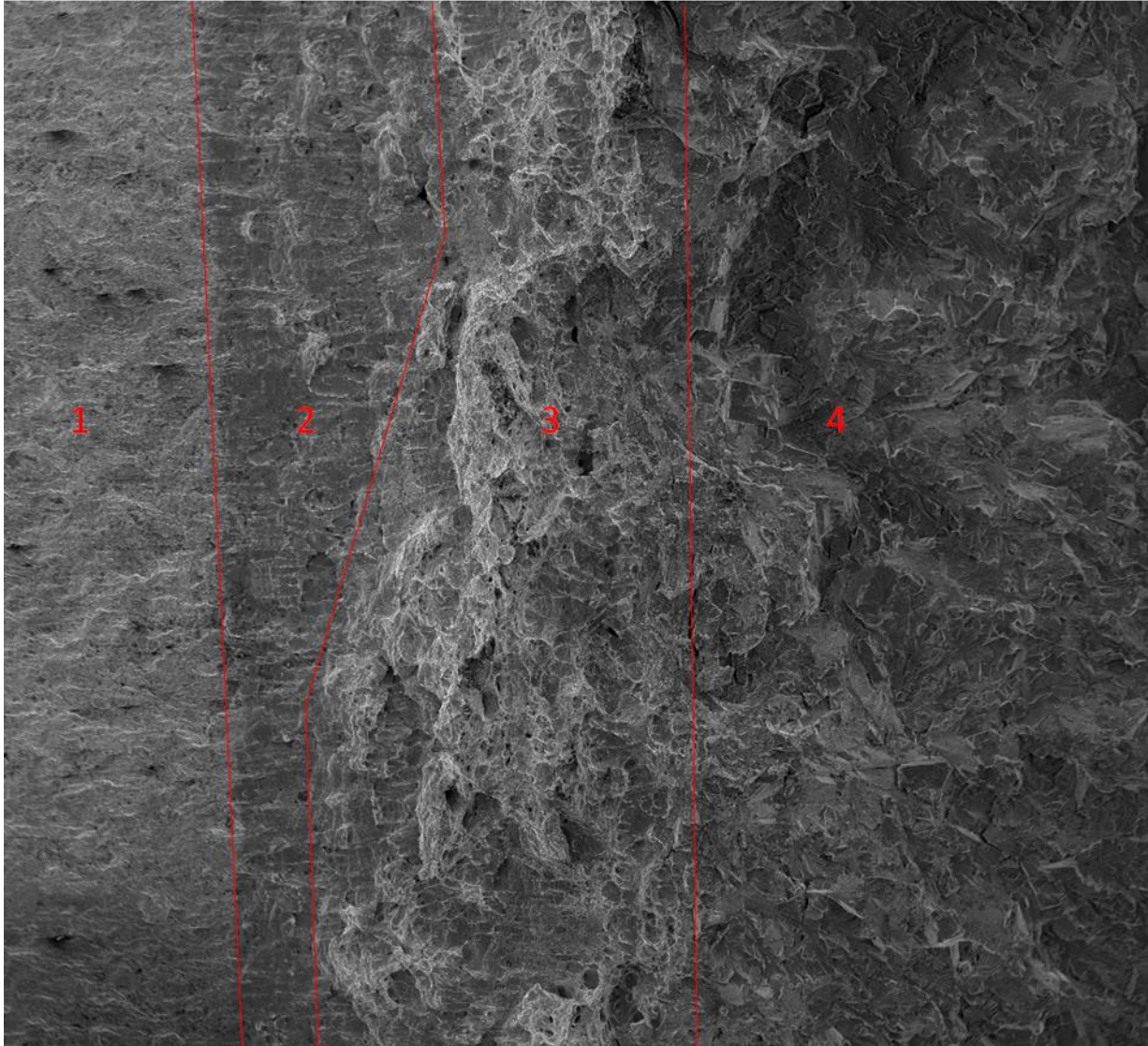


Figure 41 - Test no. 24 (2cyc 10sec -60 °C) – 110X - fracture zones in ductile specimen

1. Pre-fatigue zone, 2. Stretching zone, 3. Ductile zone, 4. Cleavage zone.

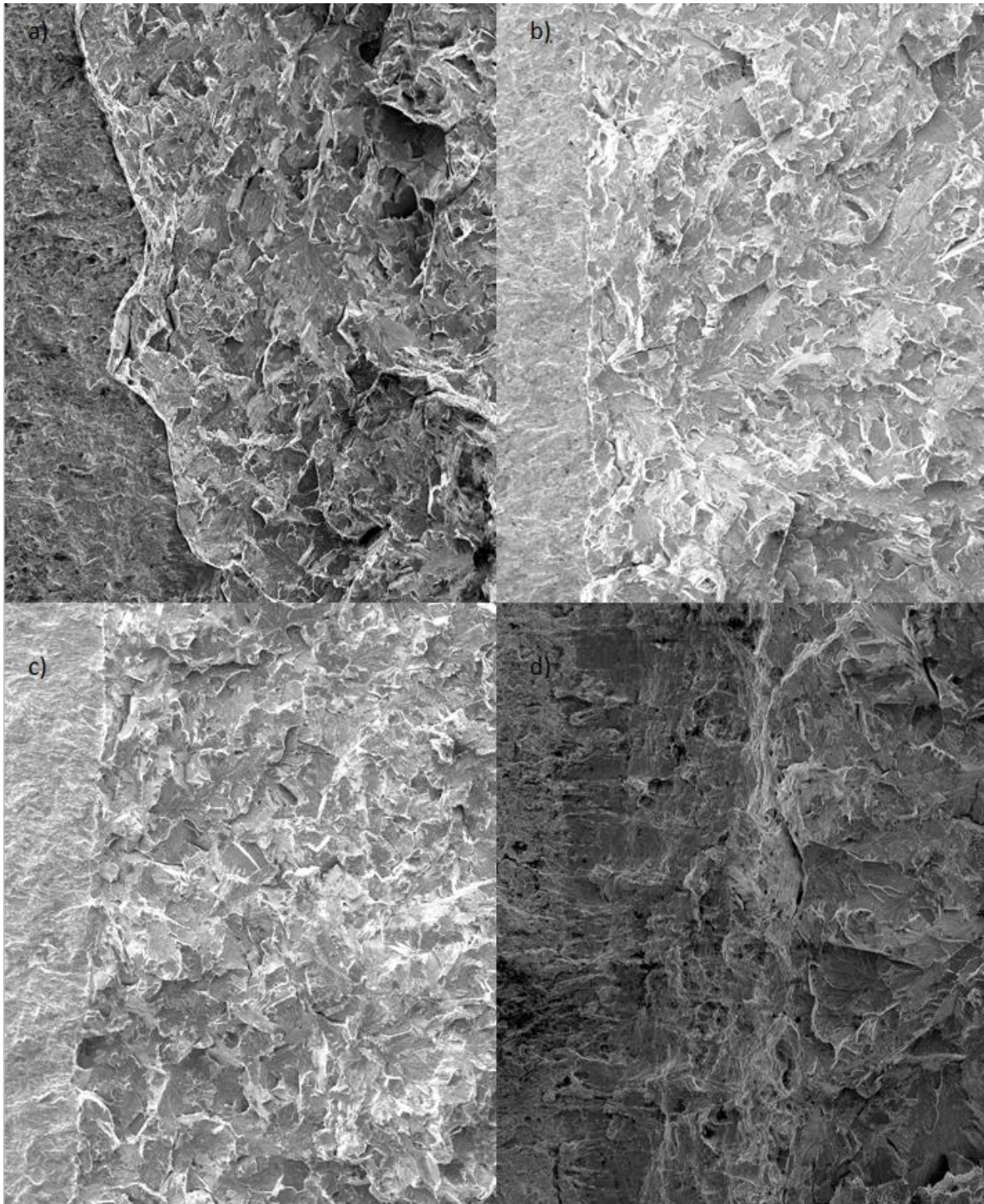


Figure 42 - Pre-fatigue to SENB surface

a) Test no. 18 (1cyc10sec -60 °C) 200X, b) Test no. 12 (2cyc 15sec -60 °C) 100X, c) Test no. 91 (1syc15sec 0 °C) 100X, d) Test no. 7 (1cyc 15sec -60 °C) 200X.

One of the challenging aspects with this material is displayed in this chapter. The behavior of the material is not consistent as it can be completely brittle at 0 °C and ductile at -60 °C, see Figure 41, frame c) and d).

The ductile zone can be identified with large dimples and no plane surfaces with rivermarks.

6.2.1 Cleavage zone and possible initiation points

The red dots indicate possible initiation points. As can be seen is it more or less impossible to give a clear definition of where the fracture is arrested and which of the initiation points that are a the original initiation and which are re-initiation caused by the original fracture.

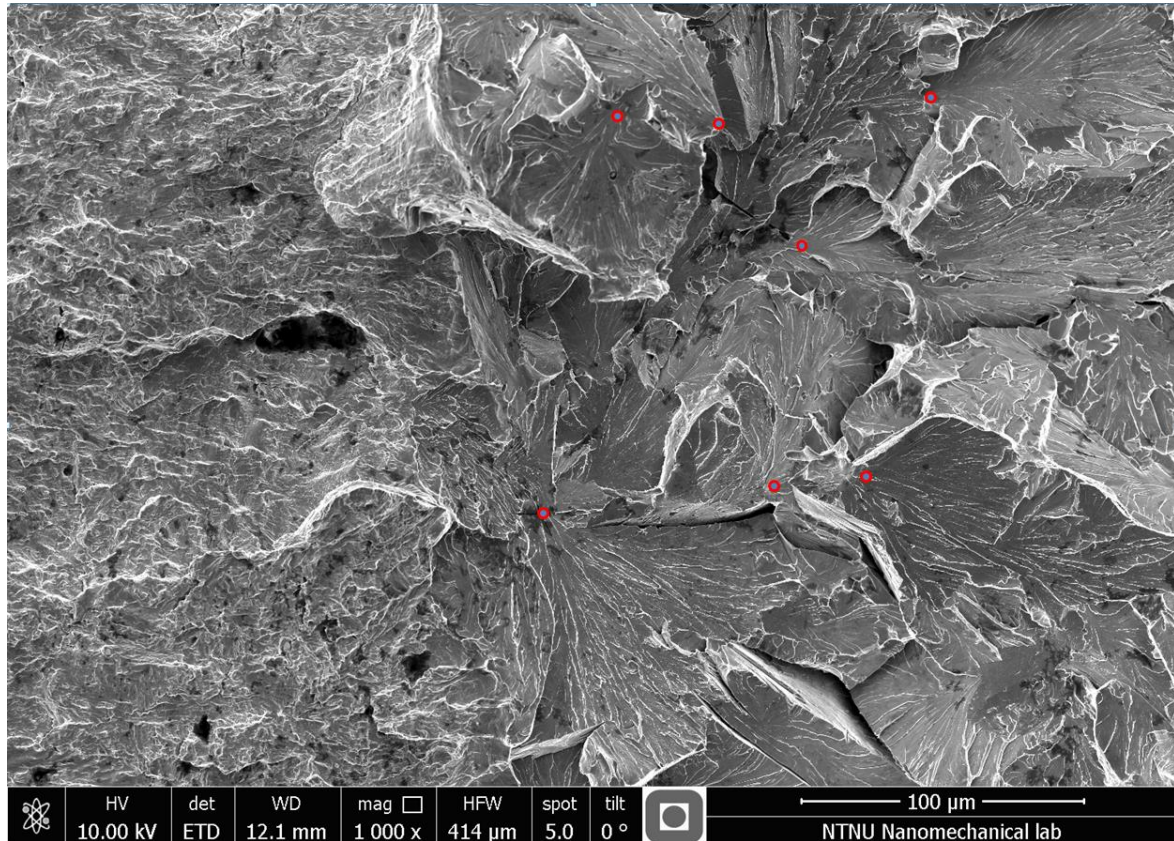


Figure 43 – Possible initiation sites - Test no. 12 (2cyc 15sec -60 °C)

In other samples investigated could crack initiation be identified as shown in Figure 44 and Figure 45 where the pre-fatigue and stretching zone can be seen on the right side of the picture. It initiates at or close to a inclusion and propagates back, towards the pre-created crack. The CTOD calculated for specimen 7 gives a CTOD at final fracture of 0.54 mm while the distance from the start of stretching zone to the initiation point is calculated to be 1.15mm which makes it impossible to be a source of AE signal.

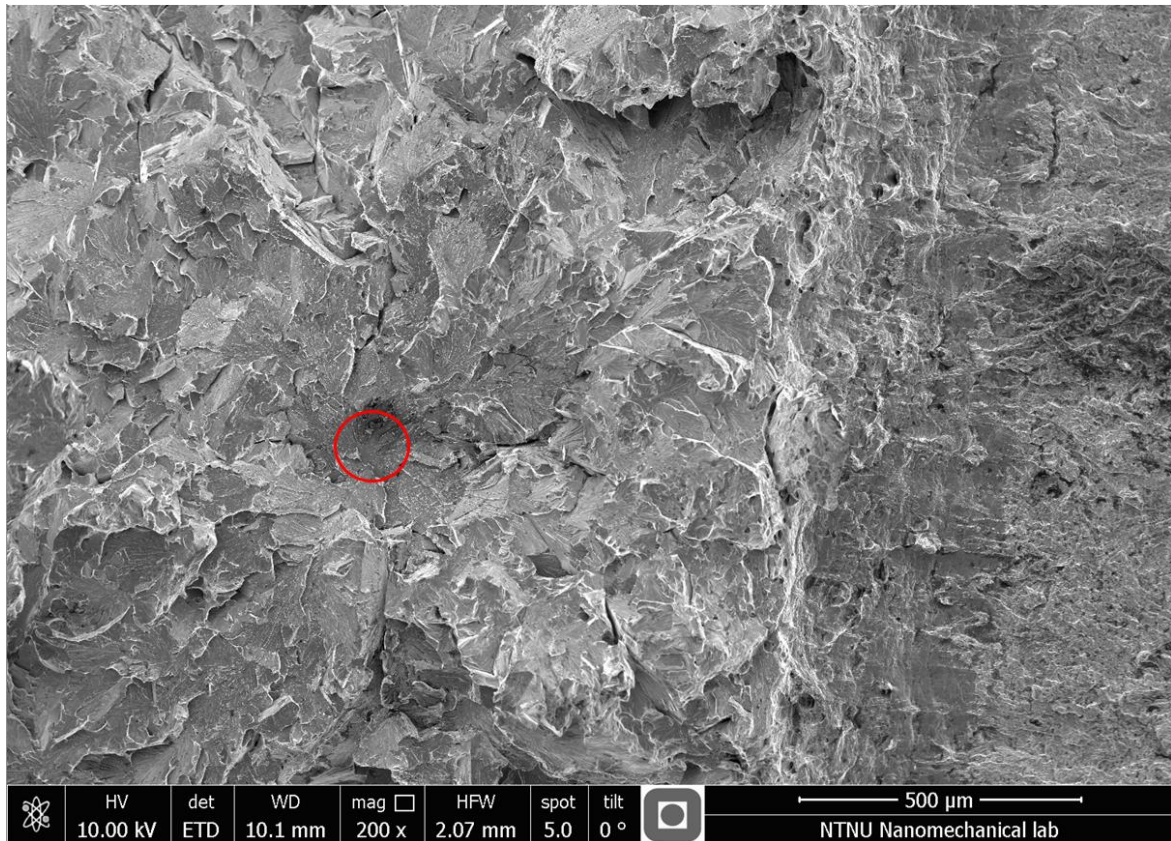


Figure 44 - Crack initiation overview, test no 7 - 1cyc 15sec -60c

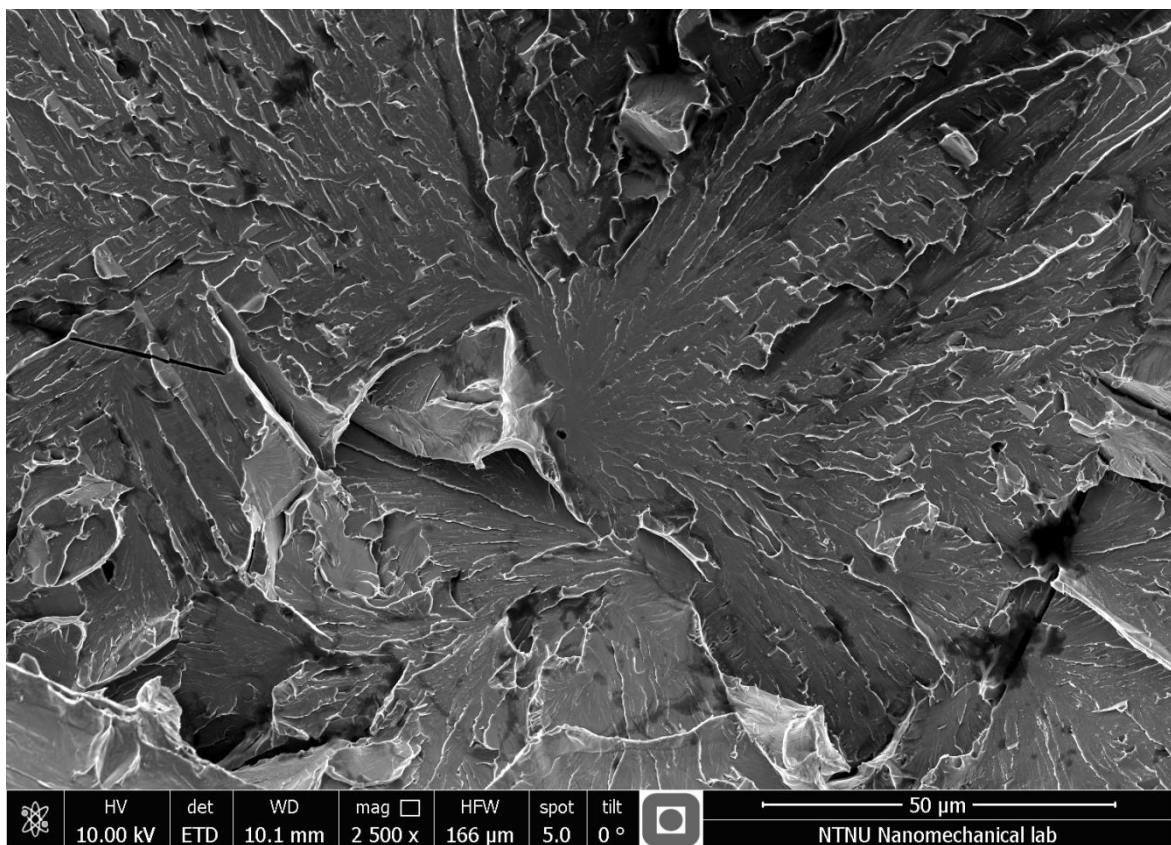


Figure 45 - Crack initiation magnified - Test no. 7 - 1cyc 15sec -60c

6.3 Test stopped after first signal

Tests were stopped after the first signal to make it easier to locate the fracture which emitted the signal. Unfortunately, only one fracture surface were possible to identify.

6.3.1 Cleavage facet

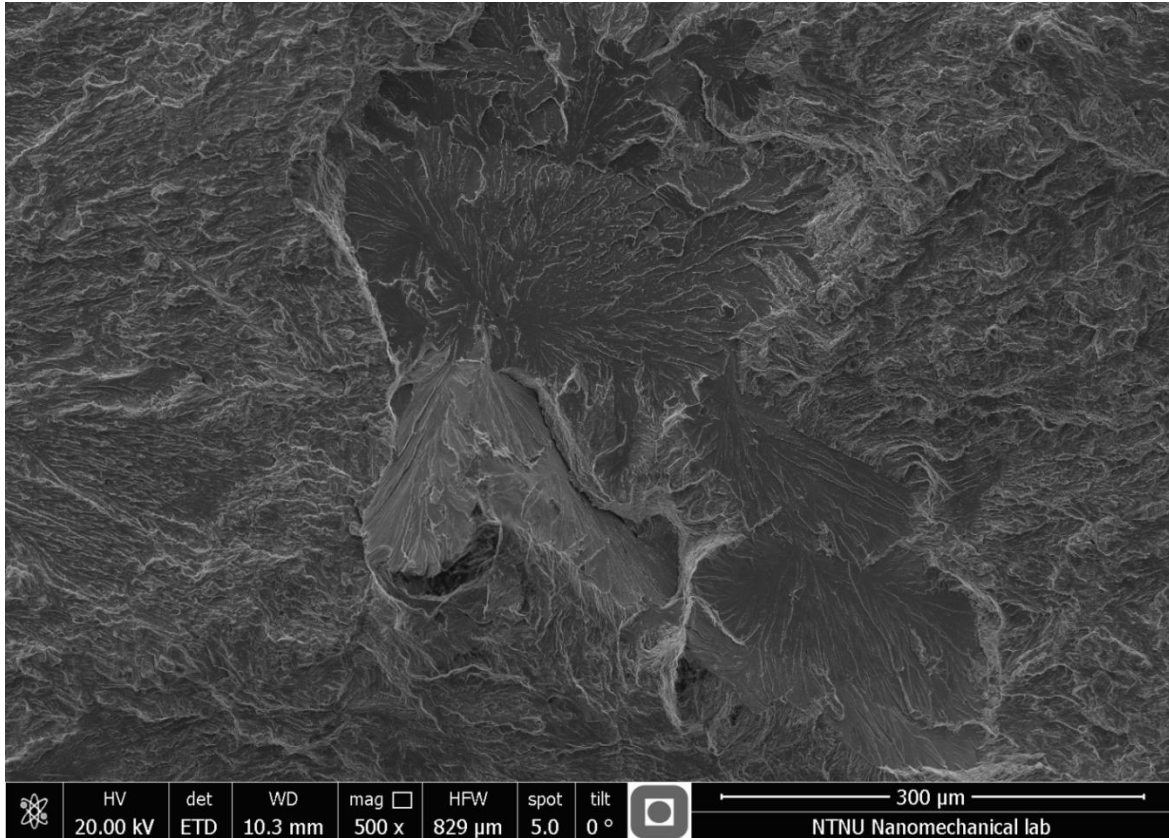


Figure 46 - Cleavage facet - Test no. 167 - 5sec1cyc-30c

Figure 46 shows a fracture facet with clear rivermarks. Two inclusions were found, see Figure 47 and Figure 48. In addition were the inclusions investigated with EDS, Figure 49.

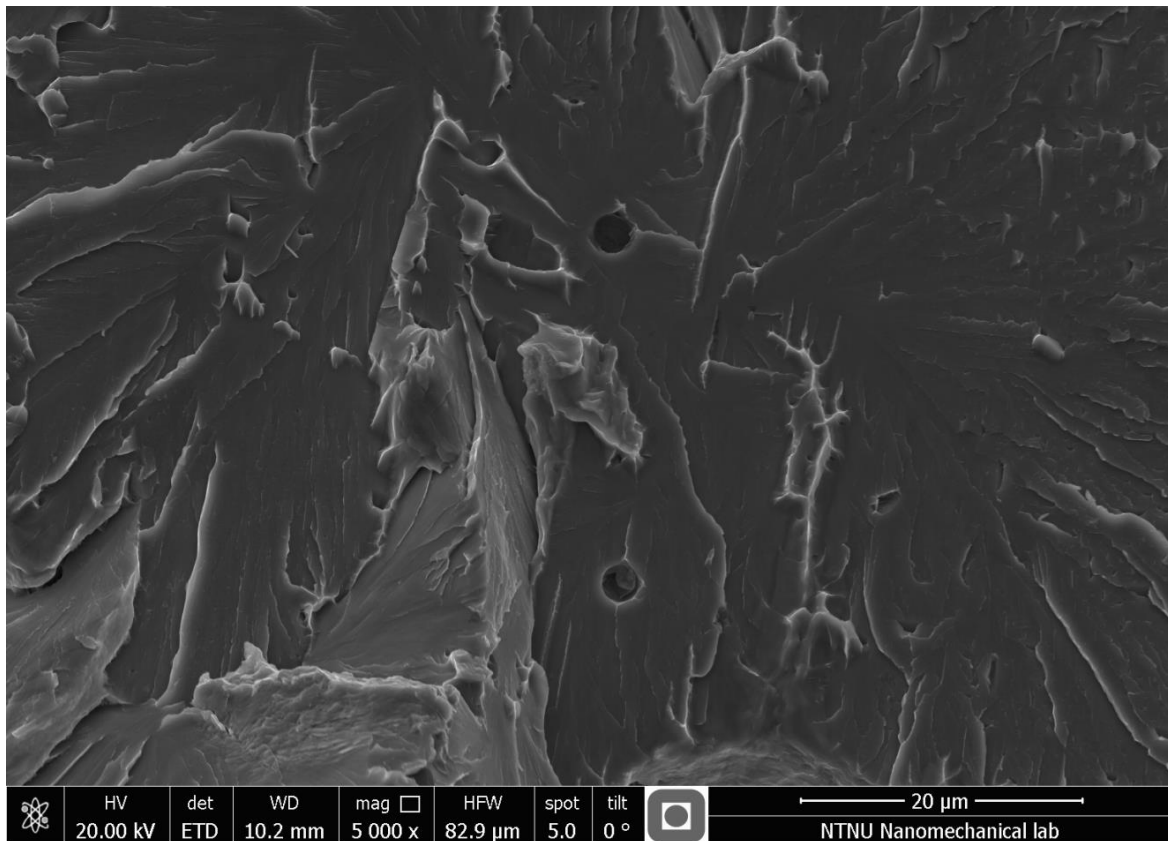


Figure 47 - Magnification on inclusions, cleavage facet

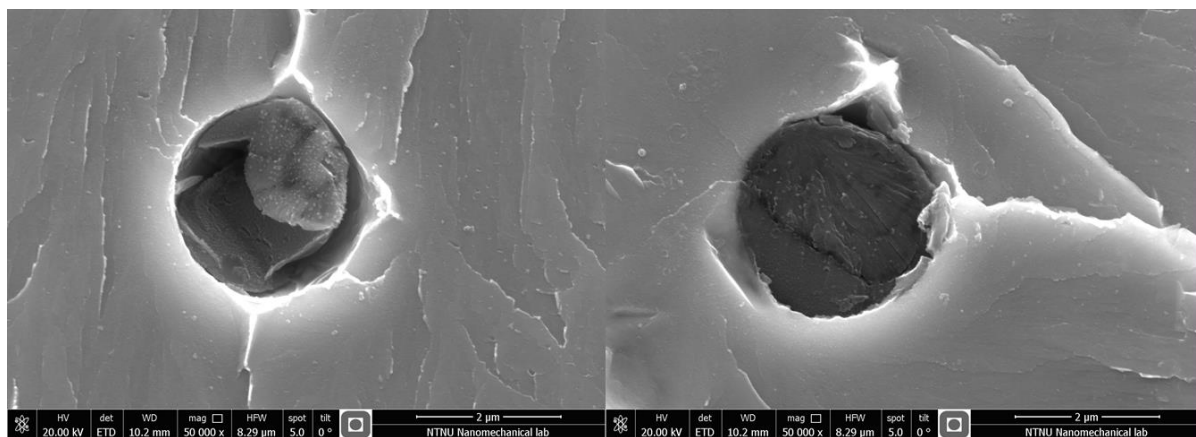


Figure 48 - Inclusions at cleavage facet – Test no. 167 – 5 sec1cyc-30c

The left picture is a magnification of the lower inclusion in Figure 47 and the right picture is and magnification of the upper inclusion.

The shape of the fractured inclusion has the form of an inclusion exposed to the both compression and bending as 2/3 of the fracture is parallel to the fracture plane (due to bending) and the last 1/3 with an angular plane (due to compression). The inclusions are both approximately 2 μ m. An EDS analysis, see Figure 49 and appendix 12.13 , were executed on both inclusions and on both fracture surfaces, four in total.

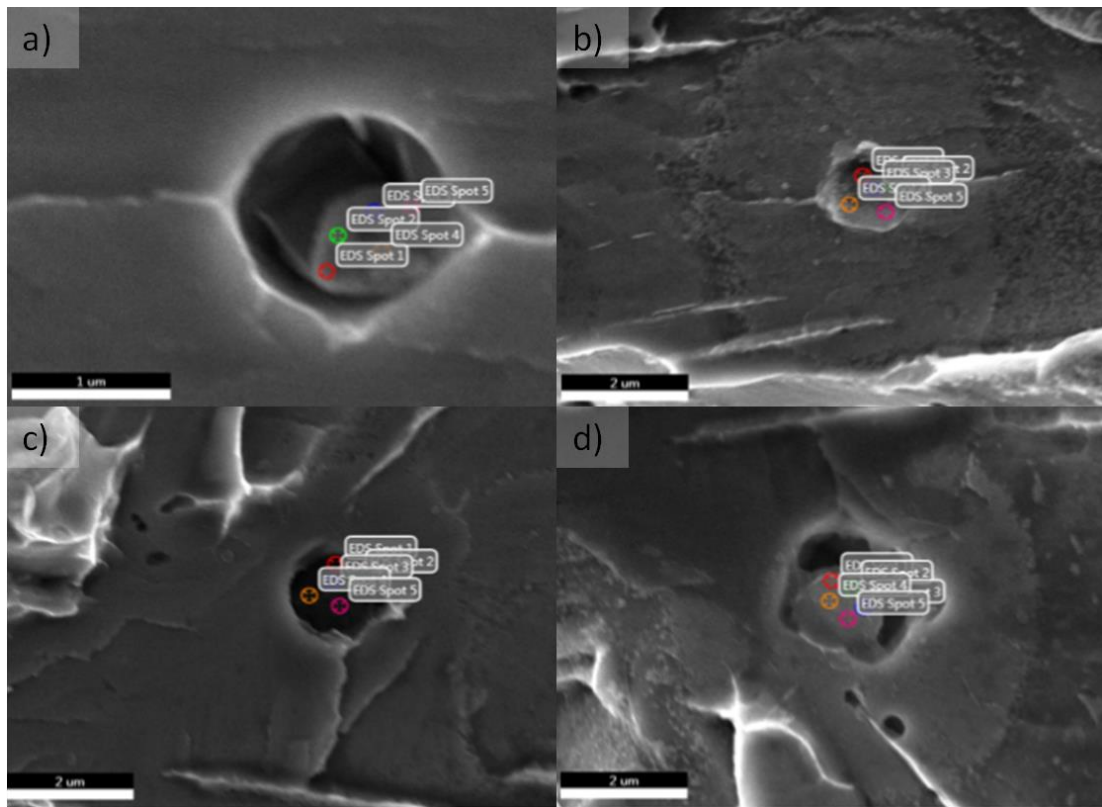


Figure 49 - Inclusion on cleavage facet - test no 167

a) and b) are each side of the lower inclusion while c) and d) are each side of the upper inclusion. See Figure 47 for overview.

The EDS show that the upper inclusion has a higher amount of Oxygen (8.2wt %/6.1wt %), Aluminum (7.0wt %/2.6wt %) in addition to an increased amount of Sulfur (3.98wt %/1.56wt %) and Calcium (6.3wt %/1.56wt %). The lower inclusion shows a larger scatter between the two sides. The reason is most likely the inclusion fractured inside the matrix so that one of the fracture facets are “hidden” deep in the hole, see picture a). Oxygen (8.2wt %/4.0wt %), Aluminum (8.0wt %/1.74wt %), Sulfur (6.3wt %/15.1wt %) and Calcium (22.2wt %/20.3wt %) are the four elements which stands out, see appendix 12.12 for all EDS data.

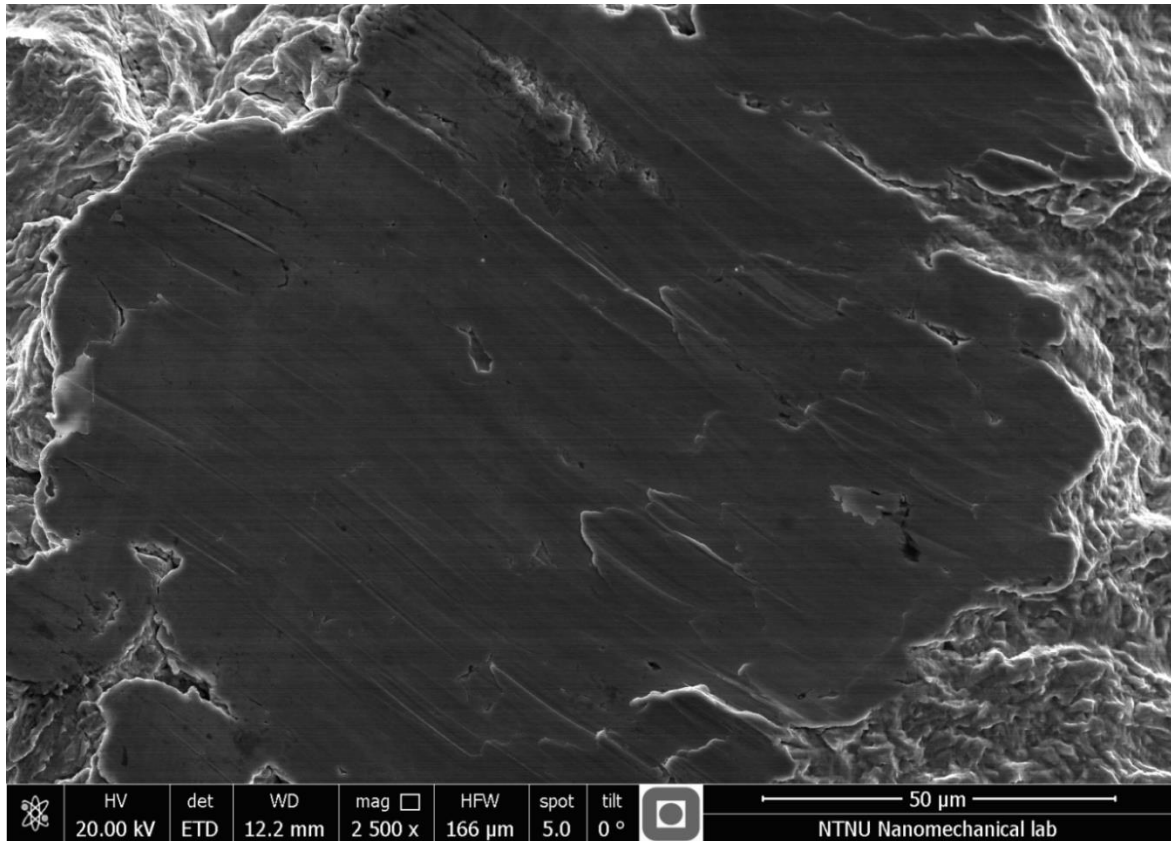


Figure 50- Test no. 217 – 2cyc5sec -60c

Figure 50 is placed in this chapter as it is the feature that reminds the most of a cleavage facet, but needs to get its own definition. It lacks rivermarks, no identical mark was found on the other half of the specimen and the area is too large to fit the AE signal. On the other hand it is placed on the “fatigue line”, see Figure 52 and chapter 6.3.2. This means that it was created during the SENB test and not during pre or post fatigue. It stands out from the other smooth surfaces as it looks like a plateau while the other smooth surfaces “blends in” with the rest of the surface. When zooming in on the surface one can see clear straight marks and it looks as someone cut it with a blunt knife or smeared it out, see picture of deformed edge, appendix chapter 12.16.2. Even though no identical print can be seen on the other side, a trace can be found.

Further on were EDS used in an attempt to identify the surface by comparing it to the nearby area, see appendix 12.14. No large differences were observed except for carbon where the unidentified surface had more carbon than the surrounding, 4.98 wt% vs 2.75 wt%.

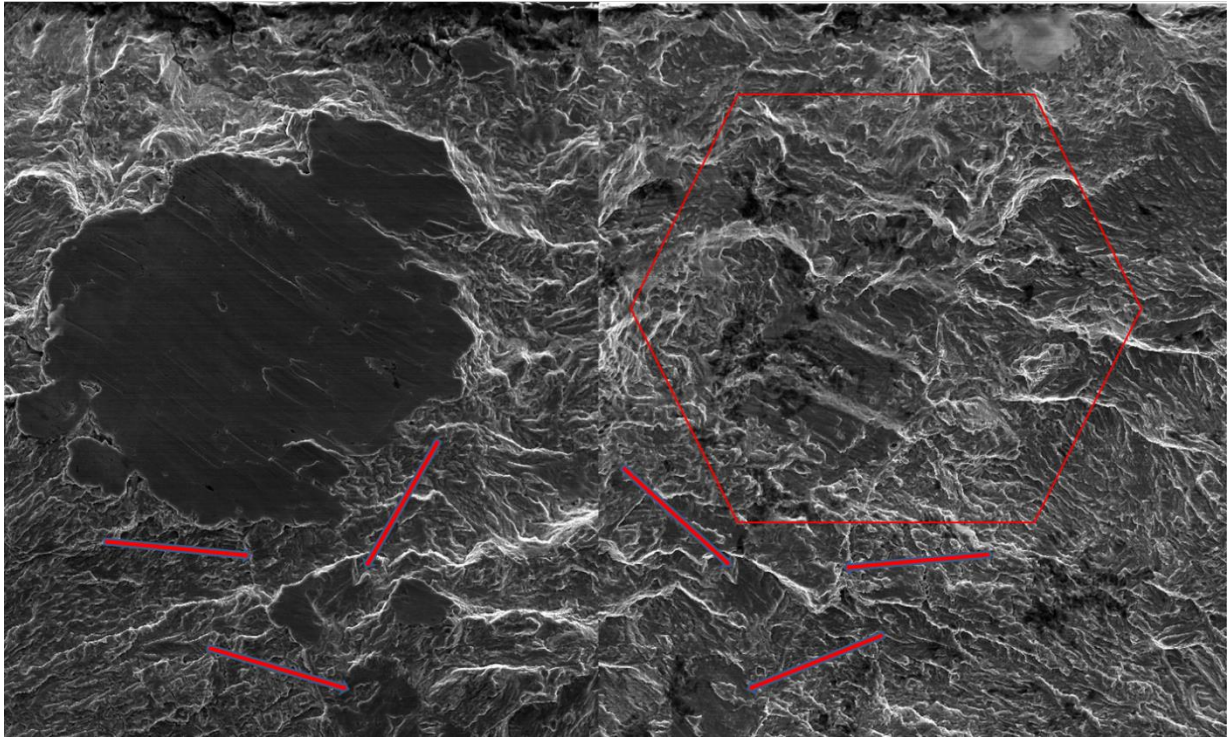


Figure 51 - Test no. 217 - 2cyc5sec -60c

6.3.2 Fatigue line

The “fatigue line” is created at the intersection between the pre- and post-fatigue. It is especially useful for location of cleave facet in samples which were stopped after the first signal.

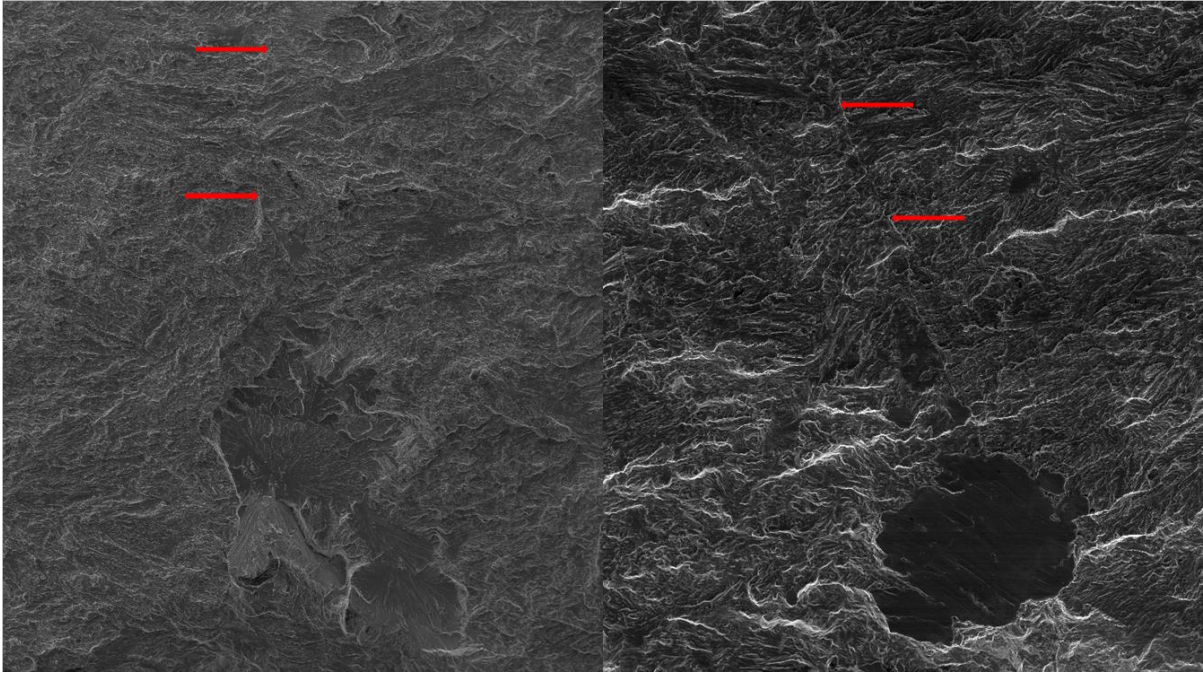


Figure 52 - Fatigue line from cleavage facet

To the left: Test no. 167 – 200X. To the right: Test no. 217 – 500X.
Arrows show both fatigue line and direction of fatigue.

Figure 52 shows the fatigue line, shown with red arrows. The line to the left can be seen clearly while the one to the right is more unclear and visibility varied greatly with magnification.

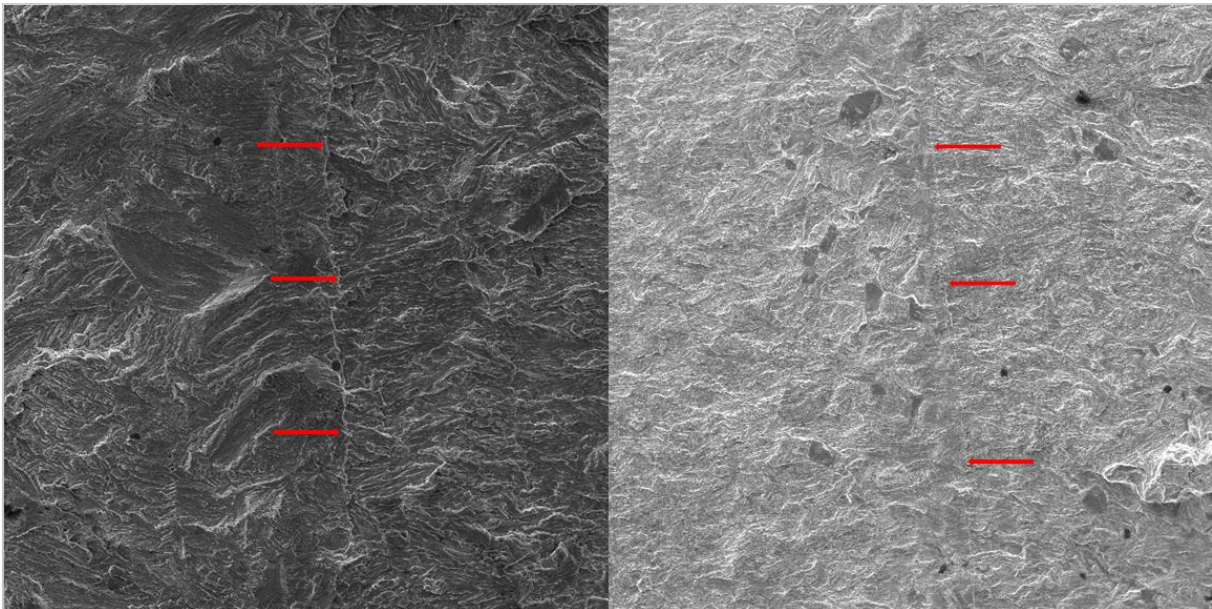


Figure 53 - Fatigue line from cleavage facet

To the left: Test no. 339 – 500X. To the right: Test no. 339 – 200X.
Arrows show both fatigue line and direction of fatigue.

6.4 Inclusions

Several inclusions were found but two were of special interest.

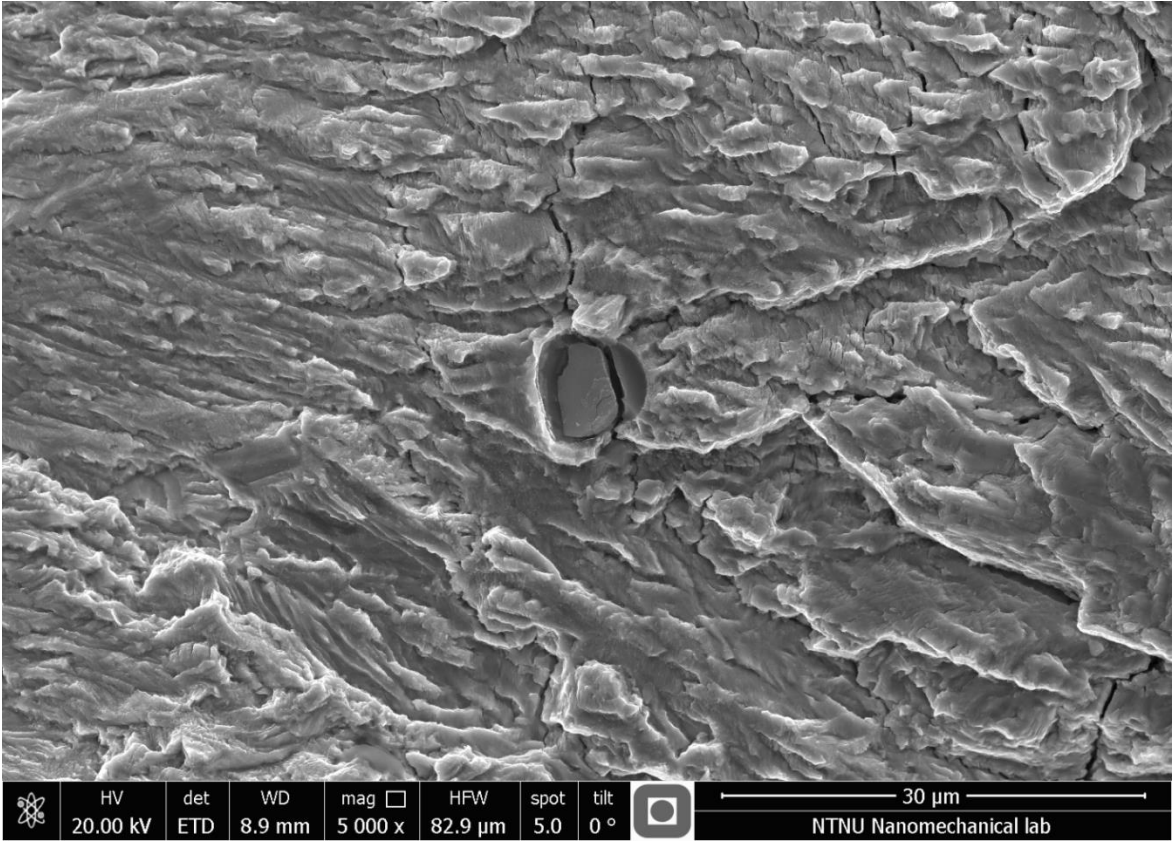


Figure 54 – Crack through inclusion. Test no. 167 - 5sec1cyc-30c

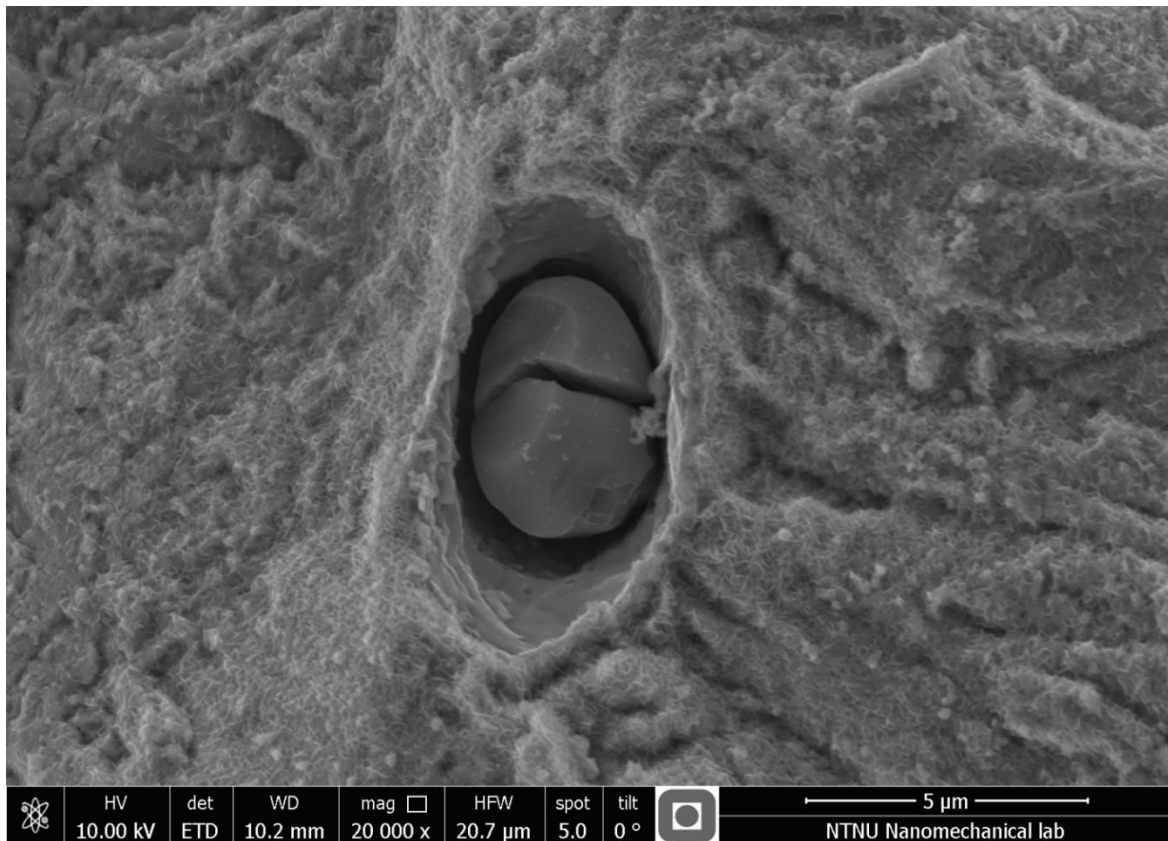


Figure 55 – Crack trough inclusion. Test no. 180 - 15sec1cyc-60c

Figure 54 and Figure 55 show inclusions which have both fractured. It is assumed that the fracture was initiated in the second phase particle, which is the only possibility for Figure 55, and while the fracture in Figure 54 have propagated in to the material the fracture in Figure 55 have been arrested at the particle/matrix interface. This can be seen in context with the MBM, see chapter 2.5. The inclusion in Figure 54 was investigated with EDS which showed a high value of Sulfur (22.13 wt%) and Calcium (38.39 wt%) at a low error percentage, see appendix 12.13 for complete analyze. It was intended to run EDS on the inclusion in Figure 55 but it were missing, see appendix 12.16.1. Inclusion in Figure 54 is estimated to be 7.5µm and Figure 55 is estimated to be 4µm in the shortest direction.

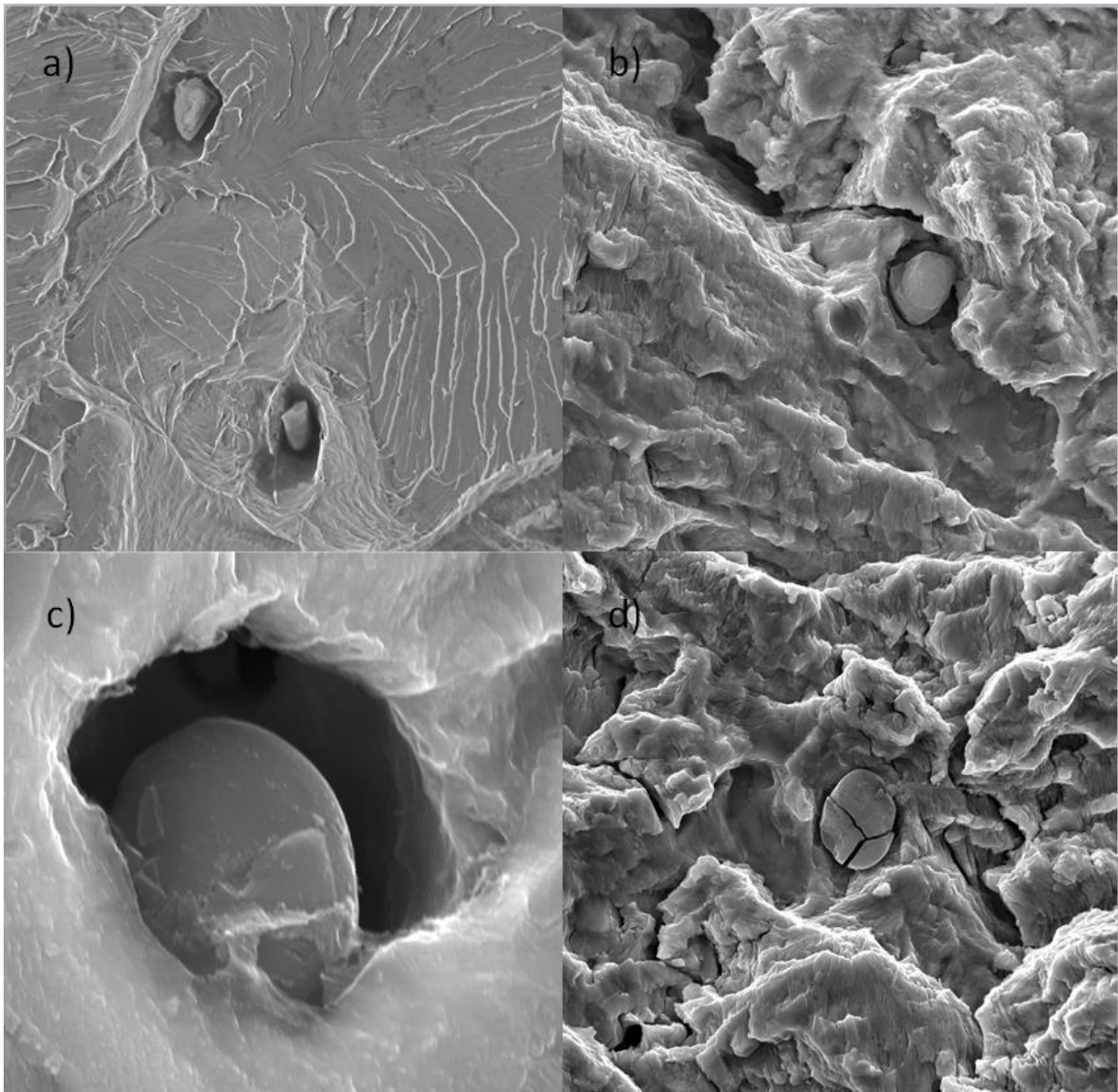


Figure 56 - Different inclusions

a) Test no. 138 - 25sec 1cyc -75c, 5000X. b) Test no. 167 - 15sec1cyc-30c, 10000X. c) Test no. 167 - 15sec1cyc-30c, 50000X. d) Test no. 167 - 15sec1cyc-30c, 10000X.

A wide range of different inclusions were found and some were analyzed with EDS, see the section below. The pictures in this chapter show that the inclusions appear in different sizes and locations. They have been found at smooth surfaces, at fracture facets, in the ductile zone after pre-fatigue and the main surface. It is observed that some are whole, while some have fractured in the cleavage plane while other have only fractured parallel to the cleavage plane.

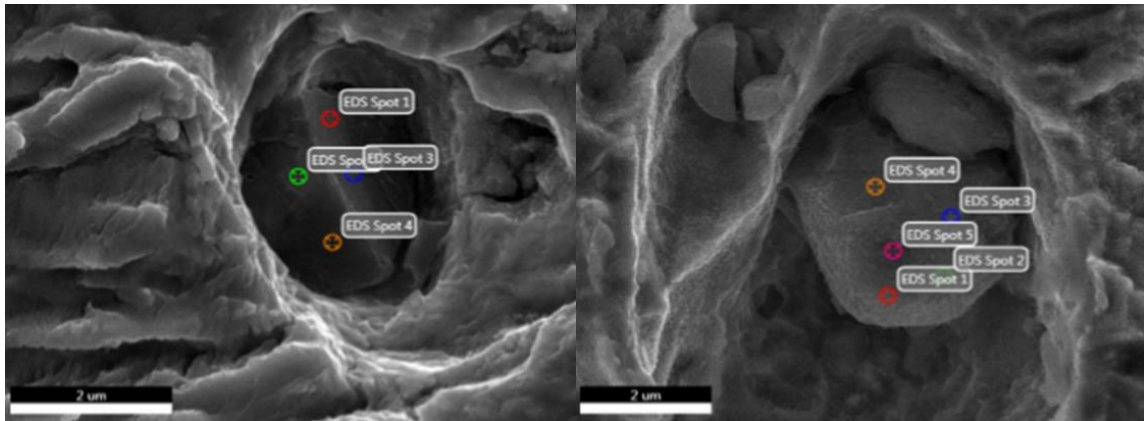


Figure 57 - EDS on inclusions

Left picture: Test no 217 2cyc5sec-60c - . Right picture: Test no. 180 – 15sec1cyc-60c

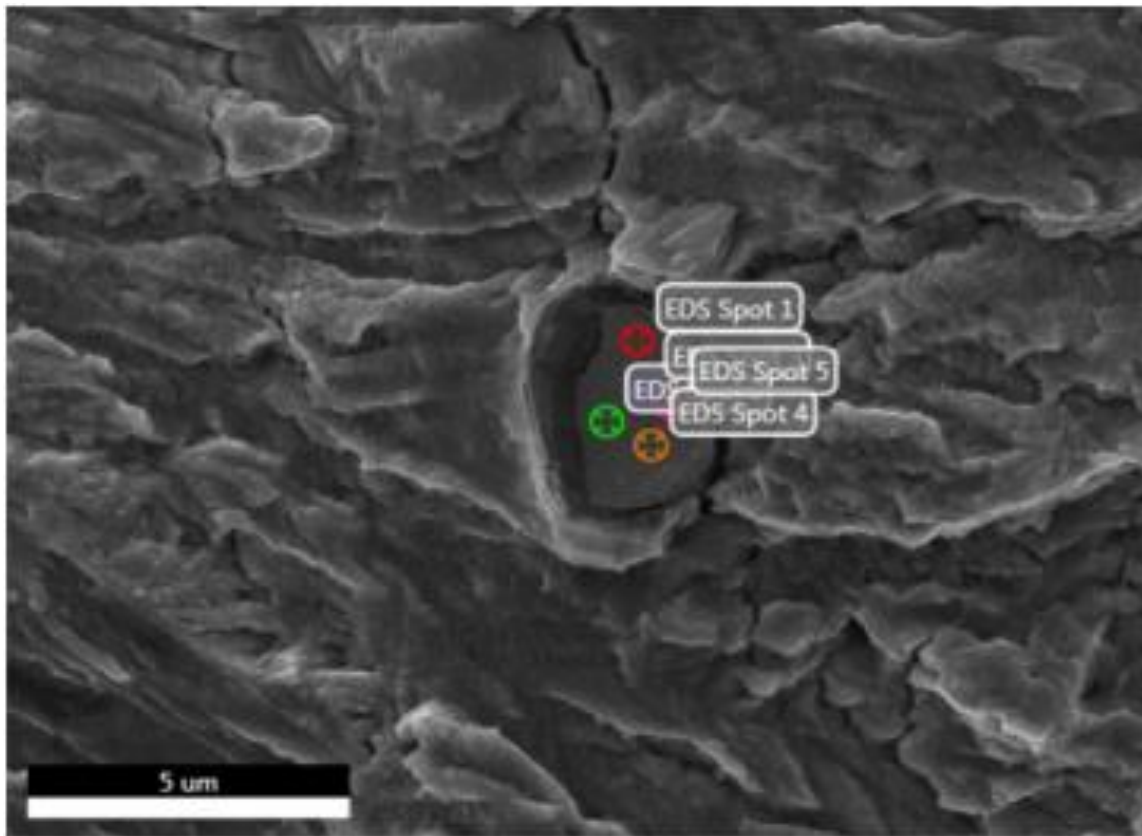


Figure 58 - EDS on "Crack through inclusion". Test no. 167 - 5sec1cyc-30c

6.5 Bridge

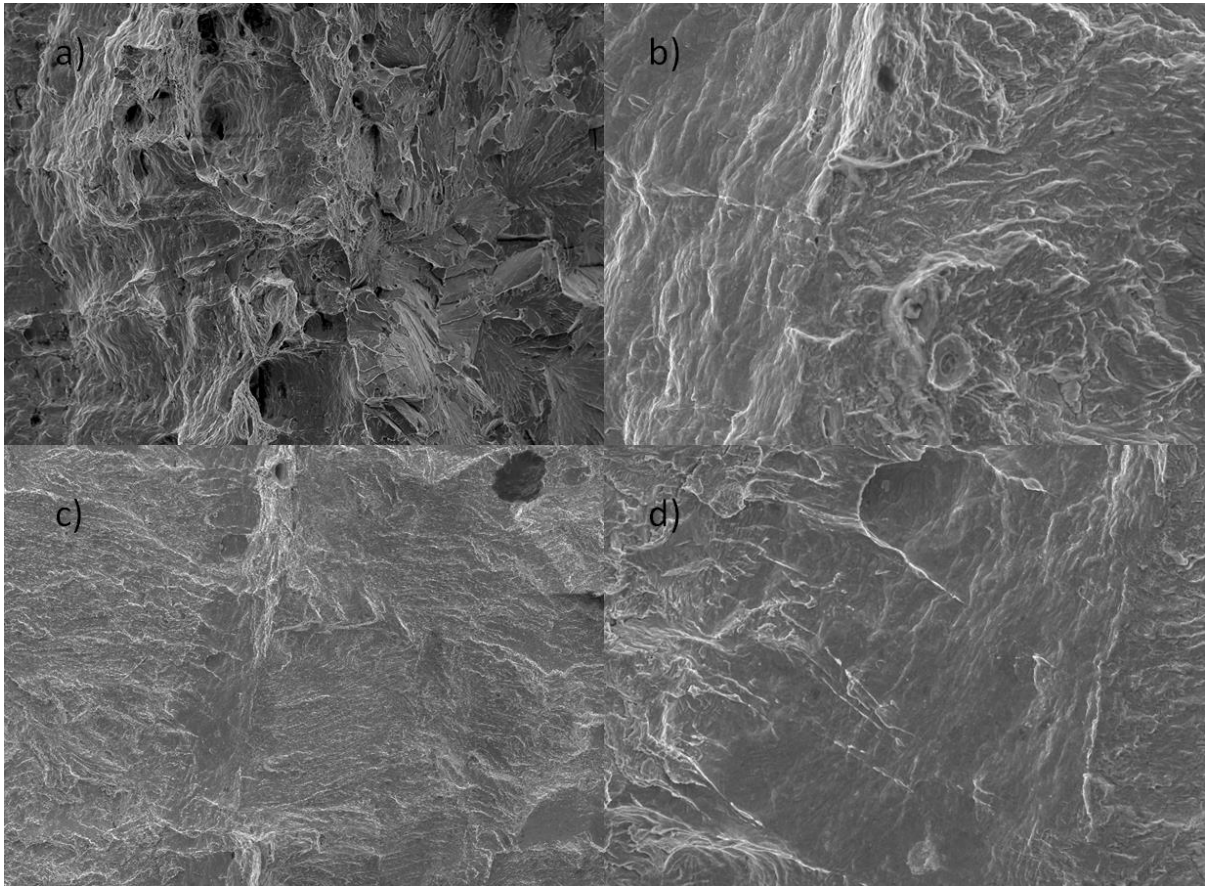


Figure 59 - Bridge

a) Test no. 7 -776X. b) Test no. 180 – 2500X. c) 180 – 500X. d) 180 - 2500X.

At several occasions was a phenomenon, in this thesis called bridge, where a gap in the ductile deformation observed. Some plastically deformation can be seen perpendicular to the plastic zone. This was seen in both specimens whom was run to final fracture and stopped after the first signal. Even though this is not discussed or devoted attention previous in this thesis it is shown here to show inhomogeneous behavior which were stated in chapter 6.1.

6.6 Dimples in ductile zone

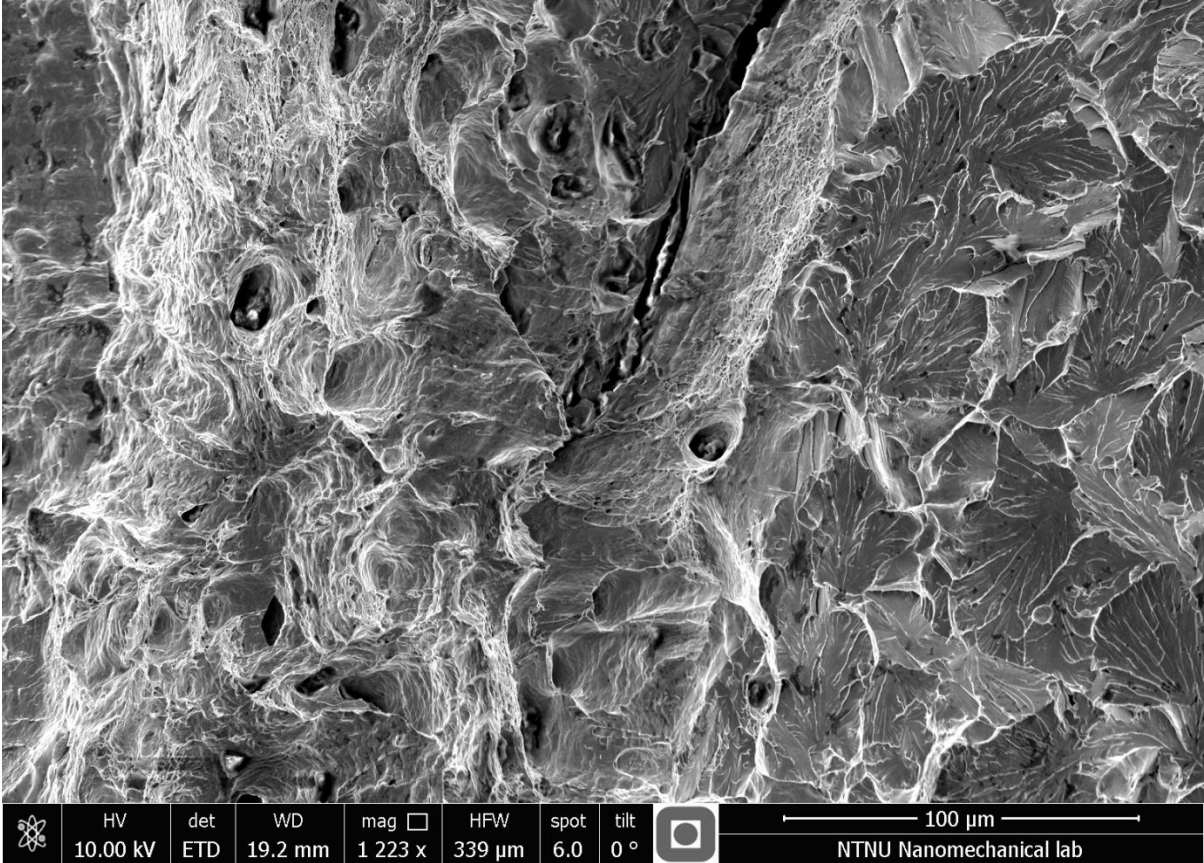


Figure 60 - Test no. 7 - ductile zone

6.7 Smooth surfaces

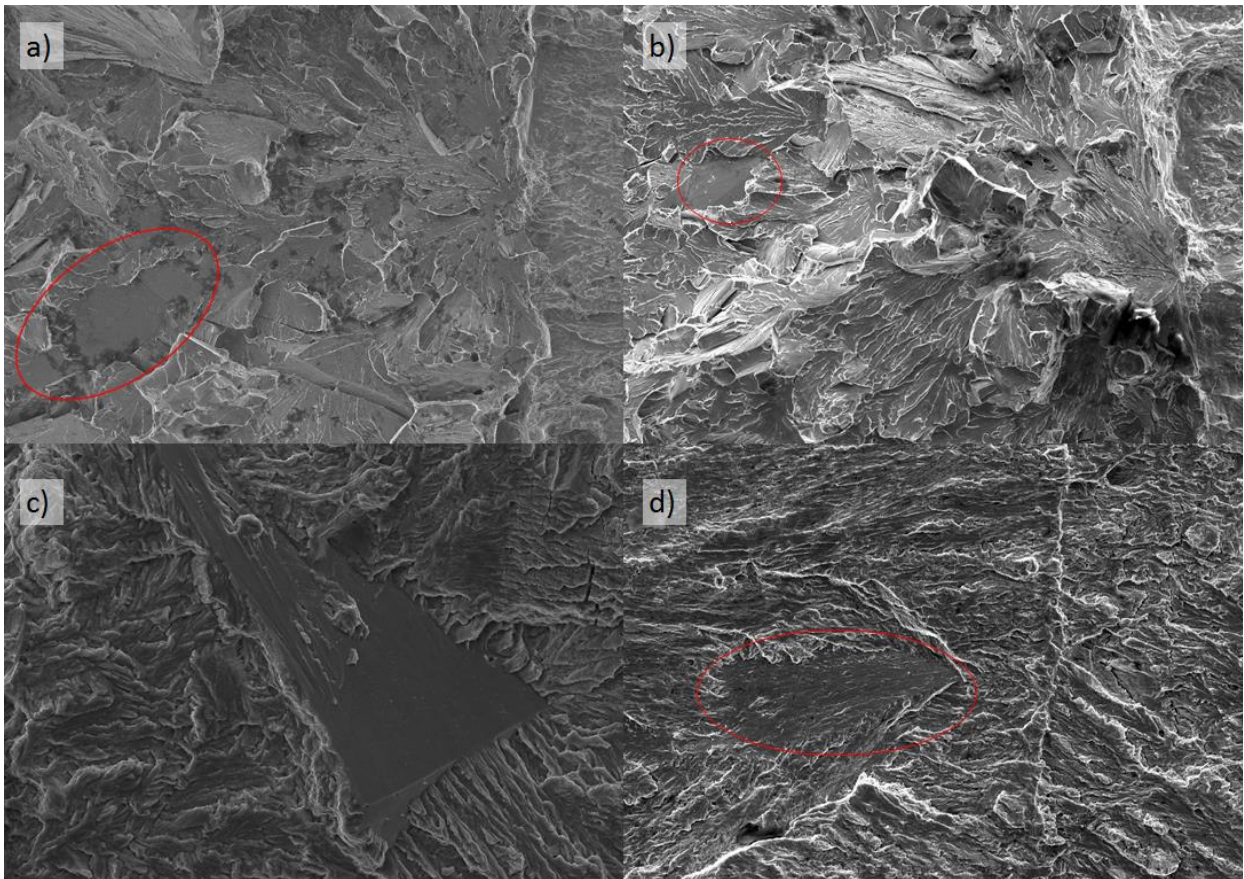


Figure 61 - Smooth surfaces

a) 138 – 1000X. b) 139 – 500X. c) 167 – 2500X. d) 217 – 1000X.

Smooth surfaces are discovered in many different shapes and places. Picture a) and b) shows the smooth surface placed among cleavage facets in tests which are run all the way. The most distinguishing difference from the surroundings is the lack of “river patterns”. Picture c) and d) are both taken on specimens who were stopped after the first signal and show the two extremes, c) with a large smooth surface and straight edge and d) which blends in and the large smooth surface consists of a fragmented parts, see appendix 12.16.3.

The smooth surfaces are found in the both pre – and post – fatigue, on the fatigue line and in the cleavage area. The size varies between 10 μm and 150 μm . Inclusions, pits and elevations are seen on the surface and they have been observed alone and loosely connected in pairs or on larger groups, see Figure 66.

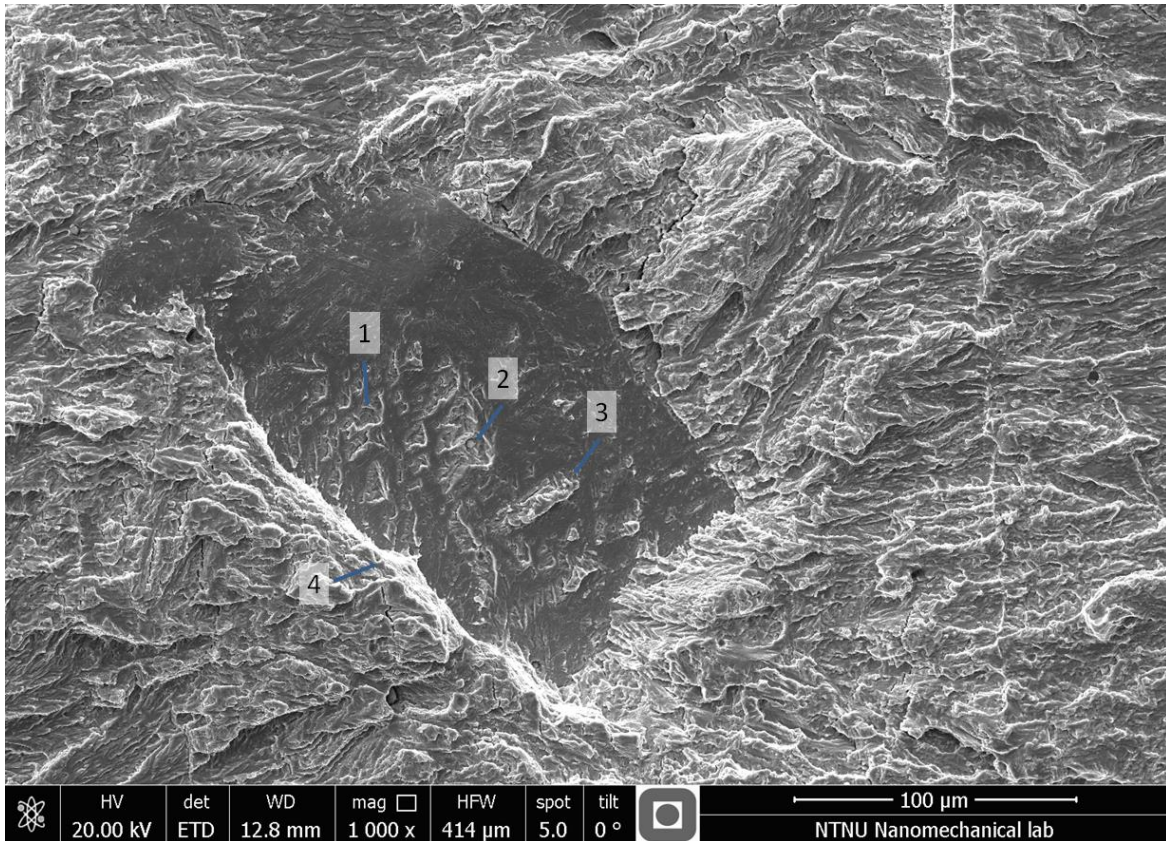


Figure 62 - 217 - Smooth surface with pits, inclusion, elevations and plastic deformation

Point 1: Pit. Point 2: Inclusion. Point 3: Elevation. Point 4: Plastic deformation.

6.7.1 Smooth surface and AE correlation

One theory has been that the smooth surfaces can be the source for AE signals. Some effort has therefore been put into locating smooth surfaces located in the post-fatigue zone in the proximity of the fatigue line or maximum 2CTOD away. Only the tests which were stopped after the first signal were investigated. Test no 167 is left out as it is clear that the signal is connected to the cleavage facet. The a_{micro} is an approximation from the graph and table in Østby et al. (2012).

Test no. 126

Measured amplitude is 87dB which equals an approximate a_{micro} of $82\mu\text{m}$ ($6724\mu\text{m}^2$). Several possible smooth surfaces were detected, but a surface with distance $500\mu\text{m}$ were chosen due to location, see Figure 63. An approximation of the area is measured to $2585\mu\text{m}^2$ which fits poorly.

Test no. 180

Measured amplitude is 64dB which equals an approximate a_{micro} of $32\mu\text{m}$ ($1024\mu\text{m}^2$). It has a large number of smooth areas, where many of them lies in the right distance from the fatigue line. There is in other words a large amount of uncertainty involved here. The chosen smooth surface, see Figure 64, fits roughly with an area of $1000\mu\text{m}^2$. It lays approximately $120\mu\text{m}$ from the fatigue line.

Test no. 217

Measured amplitude is 66dB which equals an approximate a_{micro} of $38 \mu\text{m}$ ($1444 \mu\text{m}^2$). A smooth surface spotted on the fatigue line was chosen, see Figure 65. Several other smooth surfaces were spotted at the fatigue line, but this was chosen due to its size, approximately $1500 \mu\text{m}^2$.

Test no. 339

Measured amplitude is 64dB which equals an approximate a_{micro} of $32 \mu\text{m}$ ($6724 \mu\text{m}^2$). Several smooth surfaces were observed on the fatigue line or just inside the post – fatigue zone, see Figure 66. The smooth surface chosen is marked and has an approximate area of $400 \mu\text{m}^2$ which is too small. The other surfaces seen below the marked are too large.

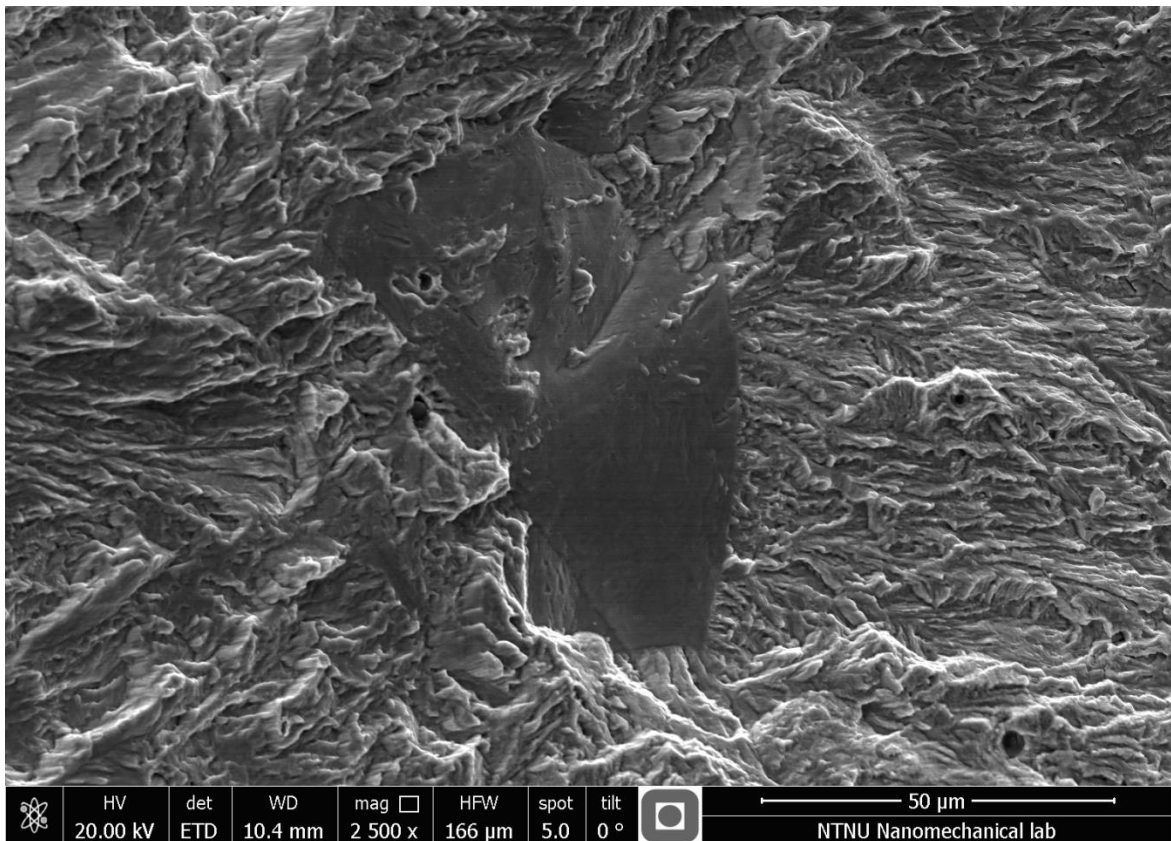


Figure 63 - Smooth surface - Test no. 126

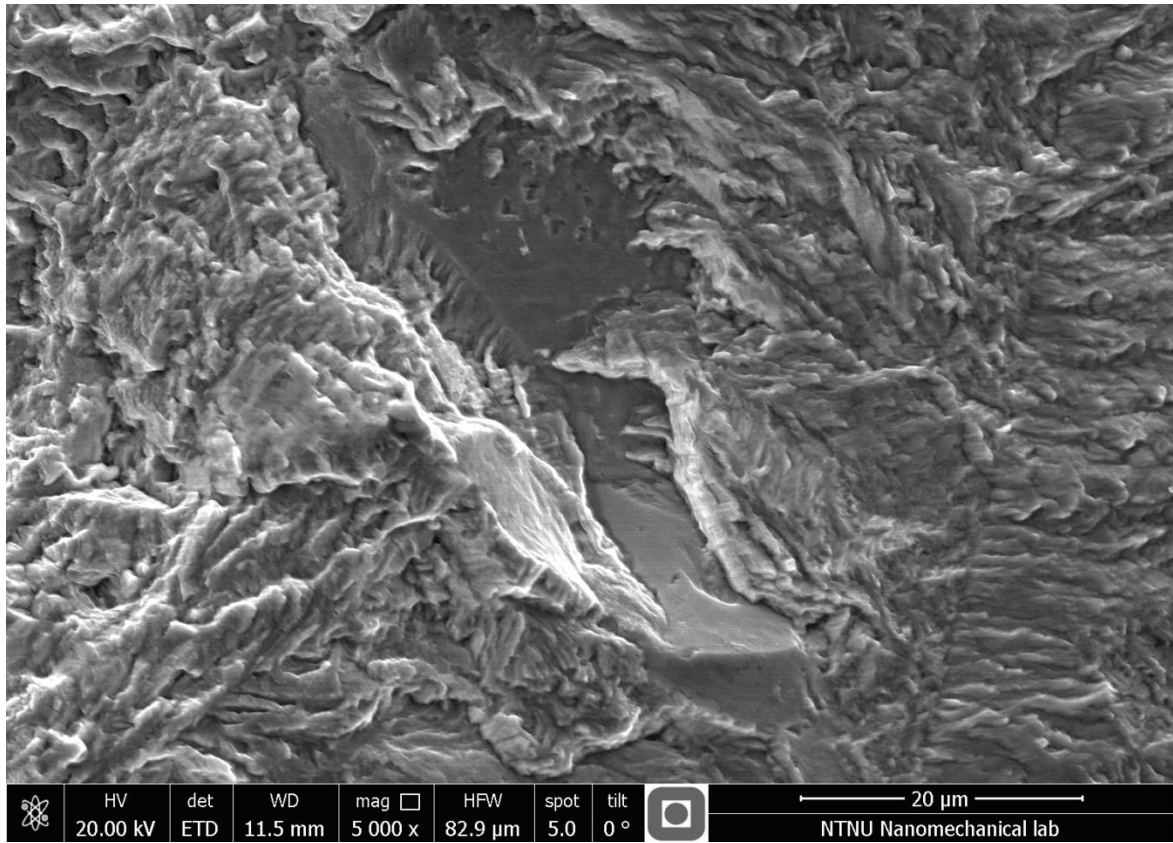


Figure 64 - First smooth surface - Test no. 180

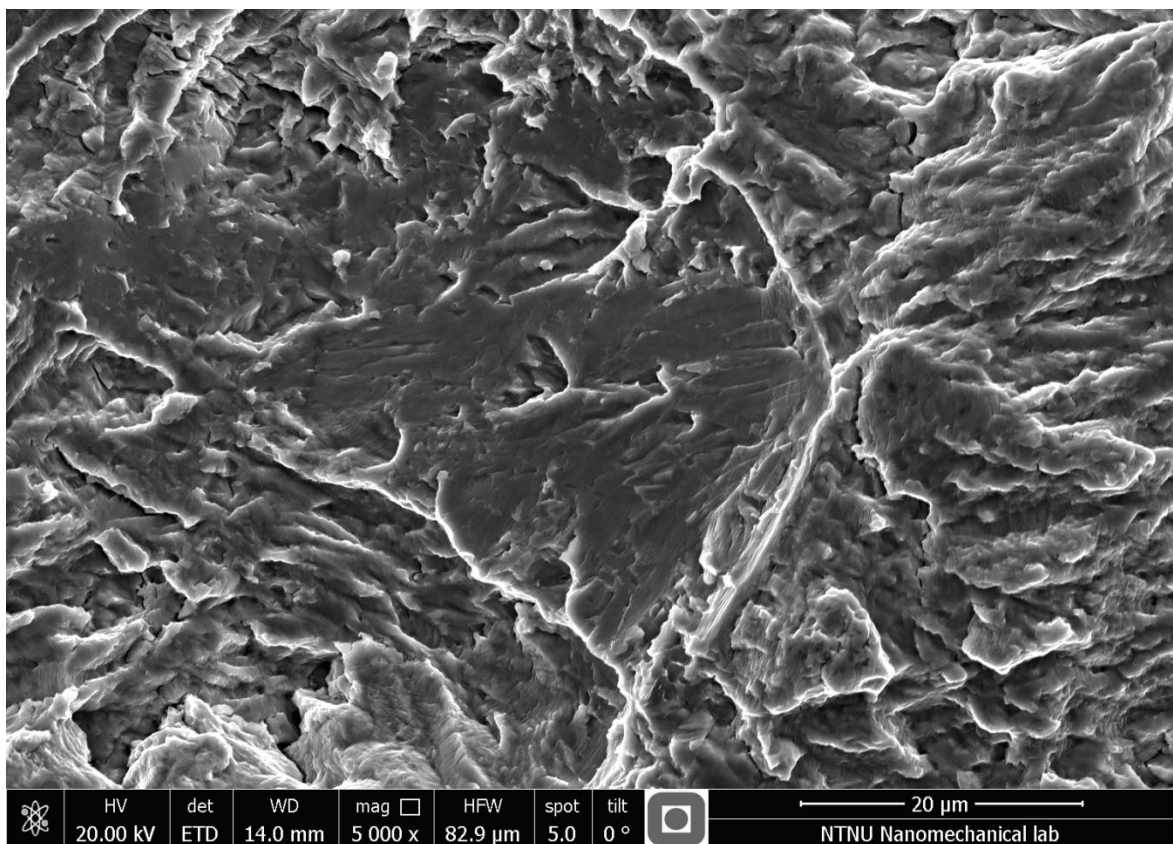


Figure 65 - Firs smooth surface - Test no. 217

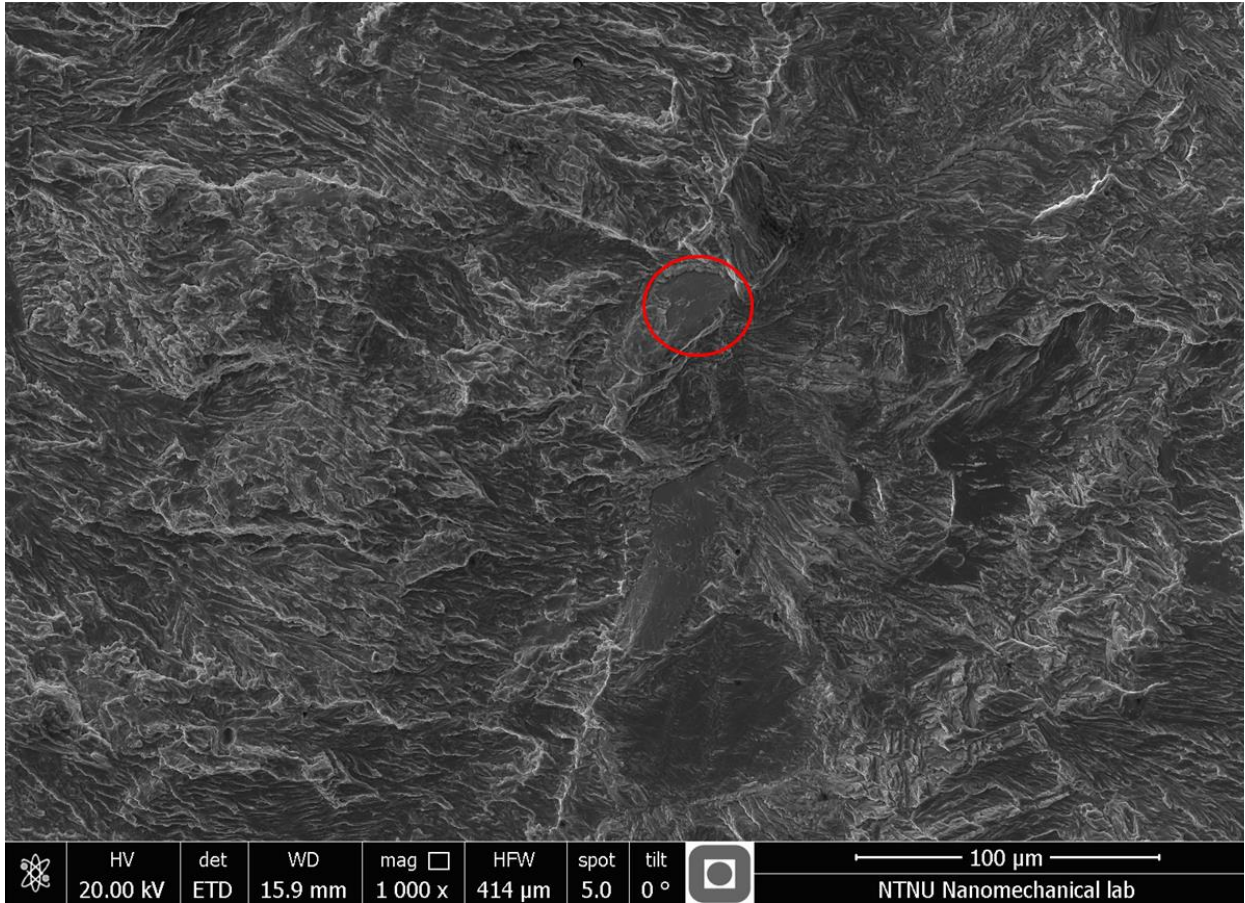


Figure 66 - First smooth surface - Test no. 339

Backscatter

An attempt to use backscatter to identify the smooth surfaces were done, but the result is questionable as no contrast is detected which means that this area is completely homogenous. It is possible that some kind of surface treatment is needed. See Figure 67.

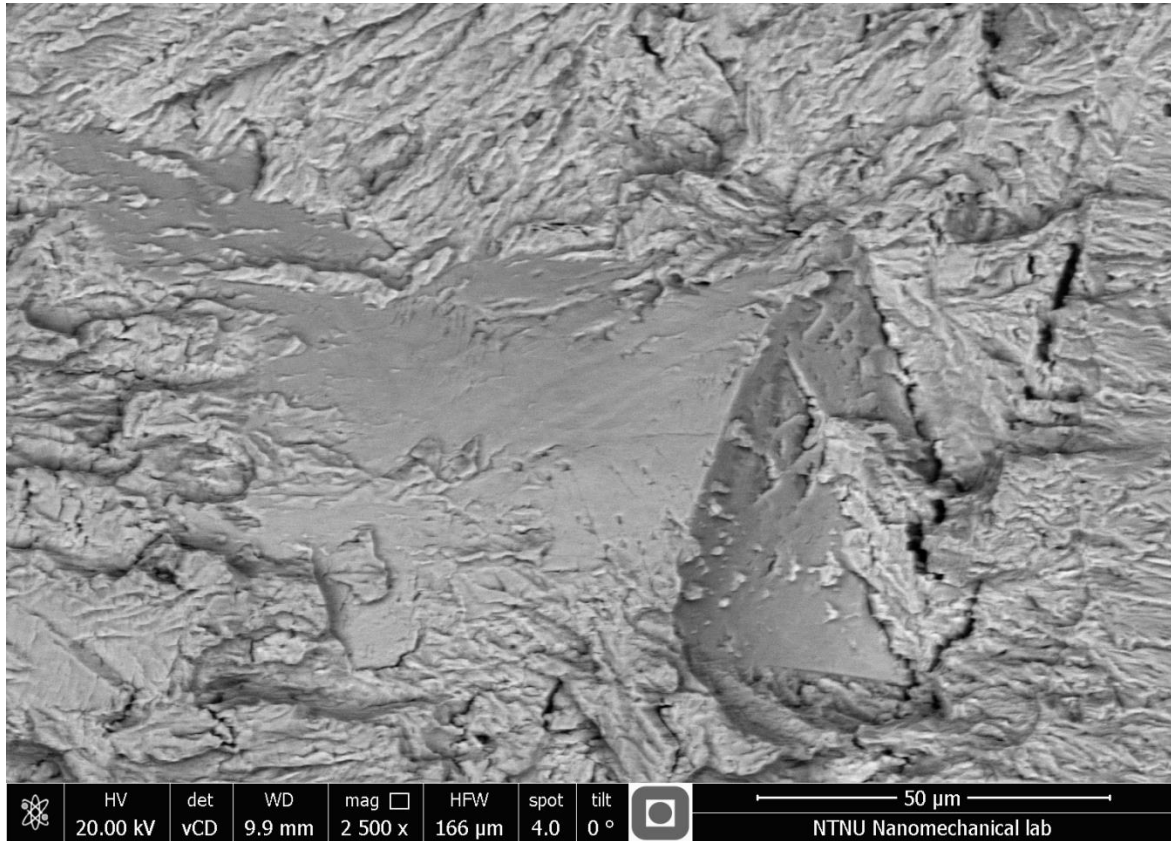


Figure 67 - Backscatter on smooth surface - Test no. 167

Etching of smooth surfaces

The smooth surfaces were etched with 2% Nital for approximately 10 seconds and then examined in SEM, see Figure 68. The result indicates that the smooth surface consists of bainite.

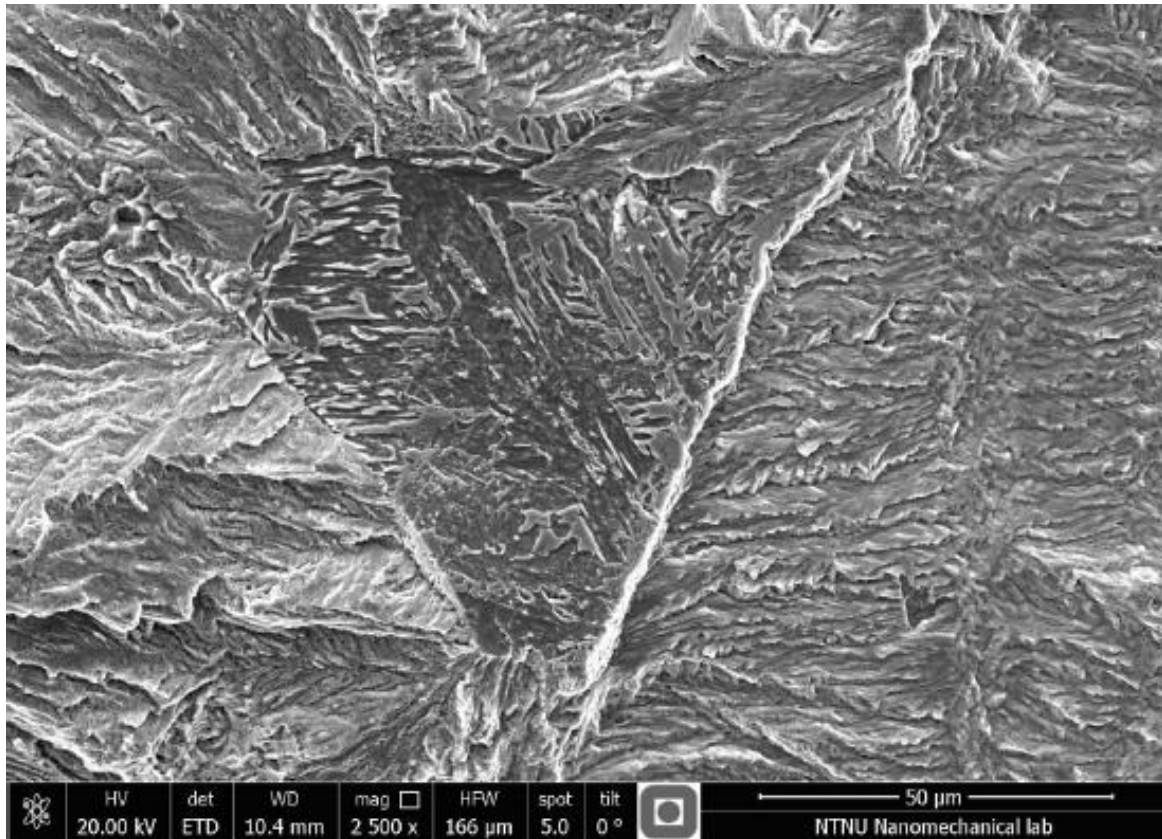


Figure 68 - Etched smooth surface - Test no. 180

EDS on smooth surfaces

EDS was applied on the smooth surfaces in addition to the accompanying rough surfaces around which were used as reference. The scanning time were set to 30 seconds, except for test no. 339 which had a scanning time of 100 sec without any notable difference. Several points were picked at each scan and several smooth and rough surfaces were scanned at each specimen. The average from each specimen is compared with the material data given by Ruukki. Due to a large percentage of error, most likely due to the topography, and large values compared to the datasheet provided by Ruukki are the results of limited value. Some trends were nevertheless discovered.

There were not discovered any significant difference in amount of oxygen between the rough and smooth surface and the amount varied some at both the rough surface and the smooth surface. Further on were a large amount of the following elements observed at every test: Carbon, Aluminum, Phosphorus, Sulfur, Molybdenum, Chromium, Niobium and Manganese, see appendix 12.10.

6.8 Straight cracks

In earlier stages was it speculated that the smooth surfaces and straight cracks were connected in some way, but this theory has later been thought of as less likely. The reason is the large amount of smooth surfaces compared to straight cracks and that many of them seem to have curves instead of being flat. They were devoted attention since they had not been observed before and were thought to be special for this material. As can be seen in both Figure 69 and Figure 70 are straight cracks present in both in front of a possible crack initiation and behind, the crack initiation marked with a circle. They also appear parallel and perpendicular to the crack growth direction.

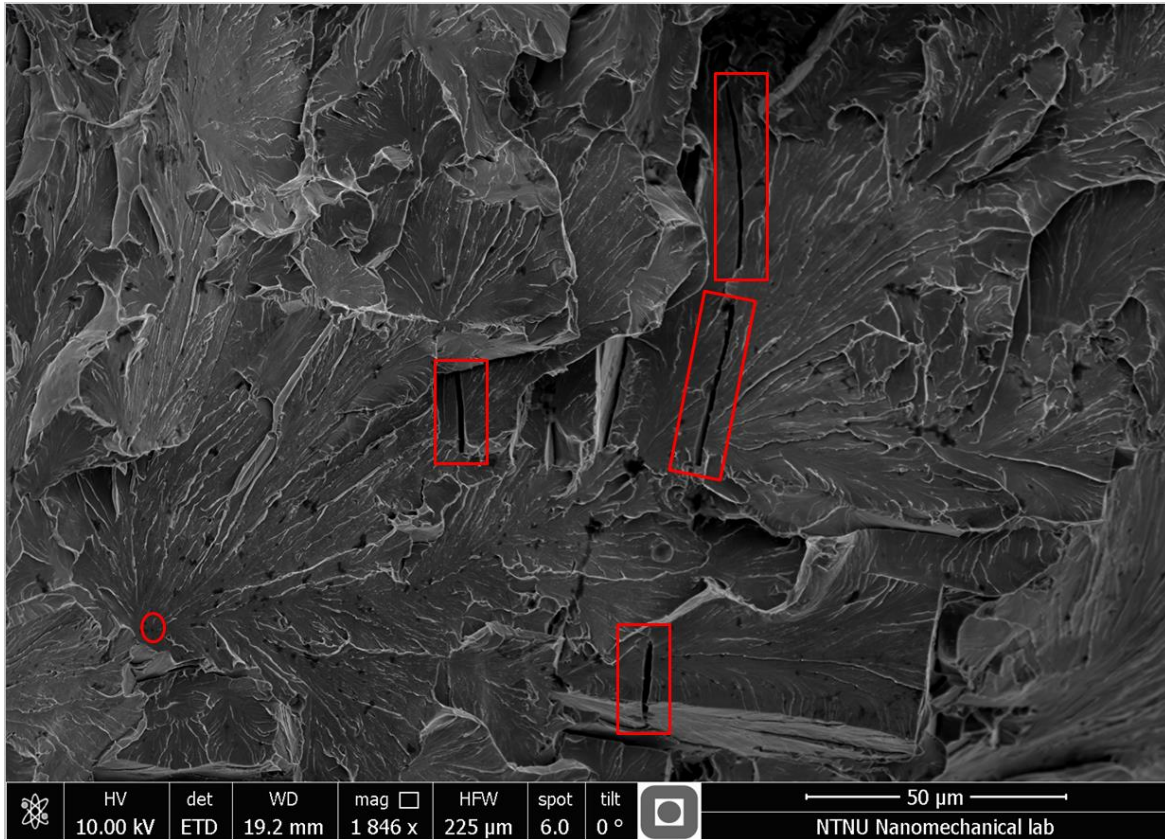


Figure 69 - Straight secondary cracks - Test no. 7

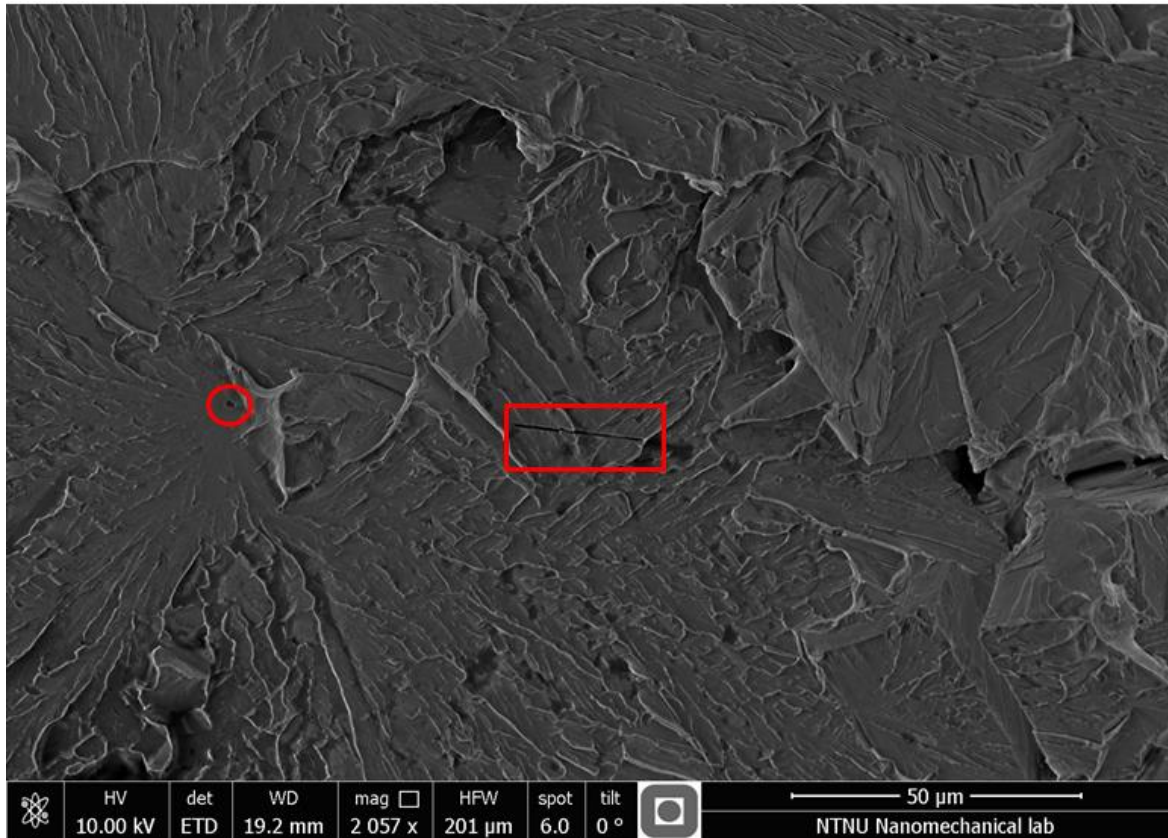


Figure 70 - Straight secondary crack - Test no. 7

Straight cracks were also found by (Jr et al., 2013) when investigating cleavage in lath martensitic steel (9 wt% Ni), see Figure 71. The material is annealed to have a large prior austenite grain size ($>100 \mu\text{m}$) and is tested in the as-quenched condition to produce relative coarse lath martensite. The cleavage is created by breaking a fatigue pre-cracked Charpy specimen at 77K.

The straight crack observed is parallel to the fracture surface. In the paper it is assumed that straight cracks are associated with the cleavage of single blocks which makes it tempting to assume that the crack is associated with a single large block.

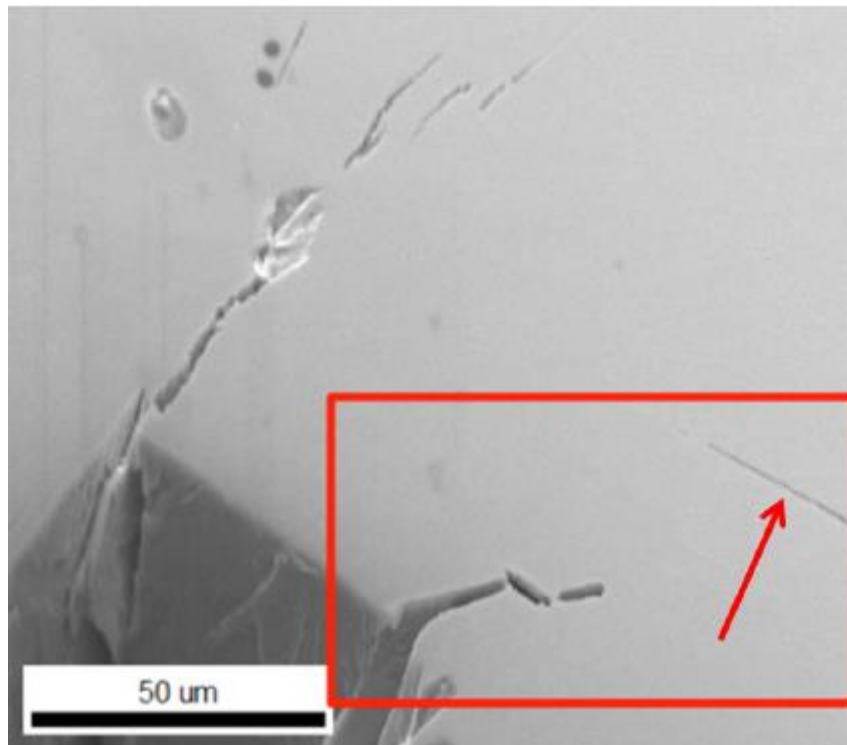


Figure 71 - Straight crack, from Jr et al. (2013)

The upper map in Figure 72 shows that this is not the case as the crack plow through three blocky features and remains straight. The explanation is given in the lower map. The three blocky features are identified as blocks that have the same bainite variant, but are crystallographically distinct since they are contained in three different packets. Blocks from different packets that have the same bainite variant have nearly parallel $\{100\}$ cleavage planes and the cleavage crack can easily propagate across the boundaries between them. The crack trace lies along a $\langle 100 \rangle$ direction as shown by the oriented $\langle 100 \rangle$ axes plotted in the upper map. The light blue areas in the map are laths of different bainite variants. The crack is assumed to be propagating from right to left which makes it appear as it bypasses the first set of those laths but is stopped at the second set. The long line intersecting is thought to be a slip line.

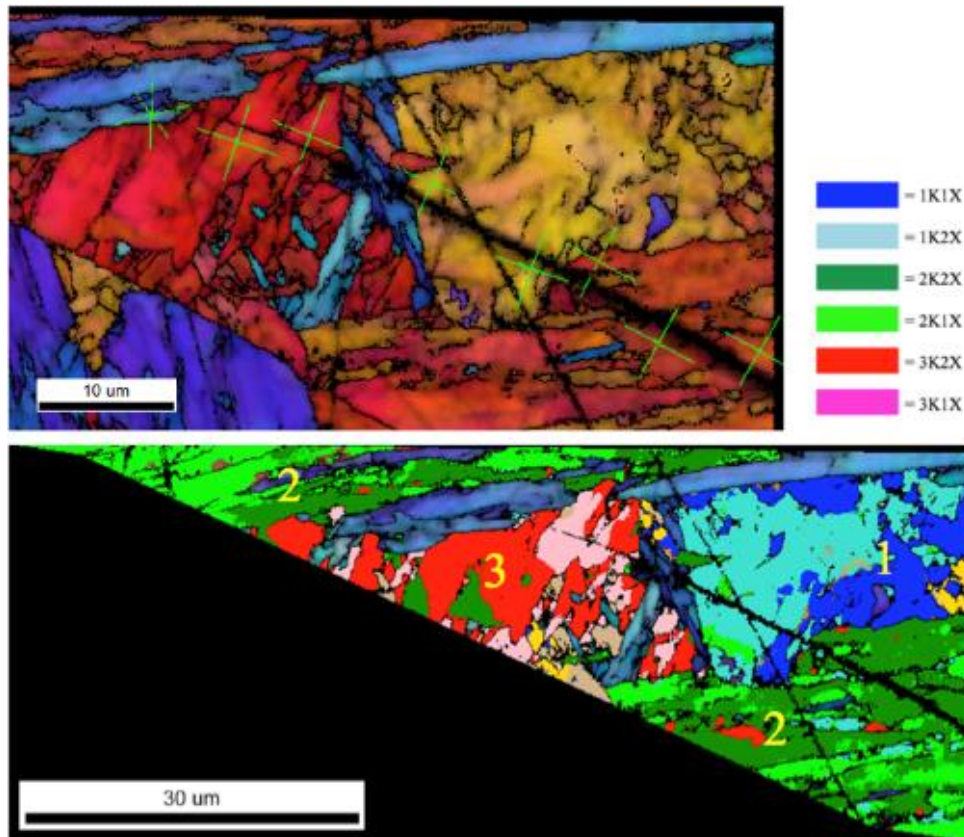


Figure 72 - Straight crack – EBSD map - Jr et al. (2013)

7 Results AE

An overview over all the signals with comments is presented in appendix 12.9. Only SENB05 is presented, although tests on SENB02 as well. These signals have been sorted as well and the test produced, due to higher stress at the notch, more signals than the SENB02. Again is the reader

7.1 Amplitude vs CMOD

Tests run to final fracture

In this case are signal with amplitude of 113dB or more excluded. The tests have been aborted when the CMOD is equal to 4mm. Only graphs for -30°C and -60°C will be showed due to large number of signals.

In Figure 73 can it be seen that there is a large scatter in the relation between CMOD and Amplitude. Three parallels were tested for each microstructure. For 5sec did two go straight to fracture, for 10sec went one straight to fracture and none tests went to macroscopic fracture for 25sec.

With two specimens going straight to macroscopic fracture and with all points recorded at more or less the same CMOD is it clear that 5sec is a highly brittle microstructure. Based on the number of specimens that went to macroscopic fracture and the number of AE signals is it clear that ductility and fracture toughness increases with increased cooling time. This is as expected.

For 15sec are most of the signal recorded around 2.5 mm while for 25sec are the largest part of the signals recorded at two stages, around 0.35 mm and 2.25mm. In the datasheet is the first signal with the highest amplitude on 73dB emitted from a 25sec specimen.

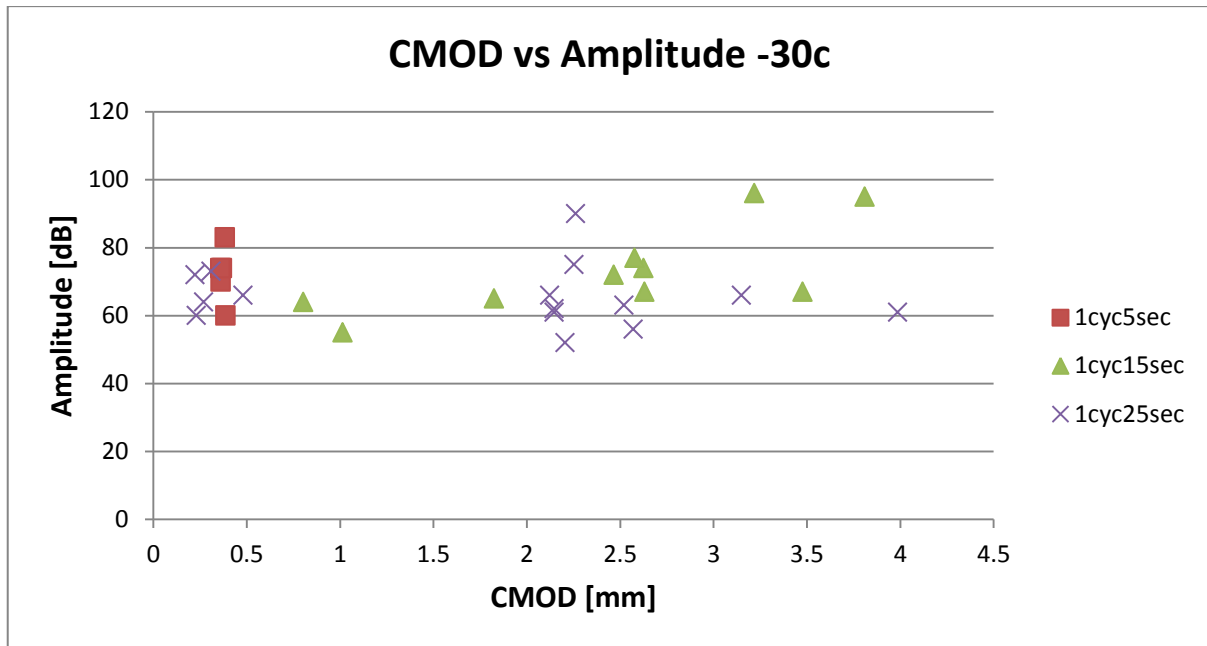


Figure 73 - CMOD vs Amplitude -30c

For Figure 74 is there a larger scatter. Note that no signals are plotted for 1cyc5sec and 2cyc5sec as they did not record any approved signals before macroscopic fracture. This, in addition to the signals recorded at 2cyc15sec shows that brittleness is present for some parallels and is more brittle than what seen at -30°C. On the other side are the rest of the signals recorded at a high CMOD compared with -30°C which imply a higher toughness. . In the datasheet is the first signal with the highest amplitude on 79dB emitted from a 1cyc15sec specimen.

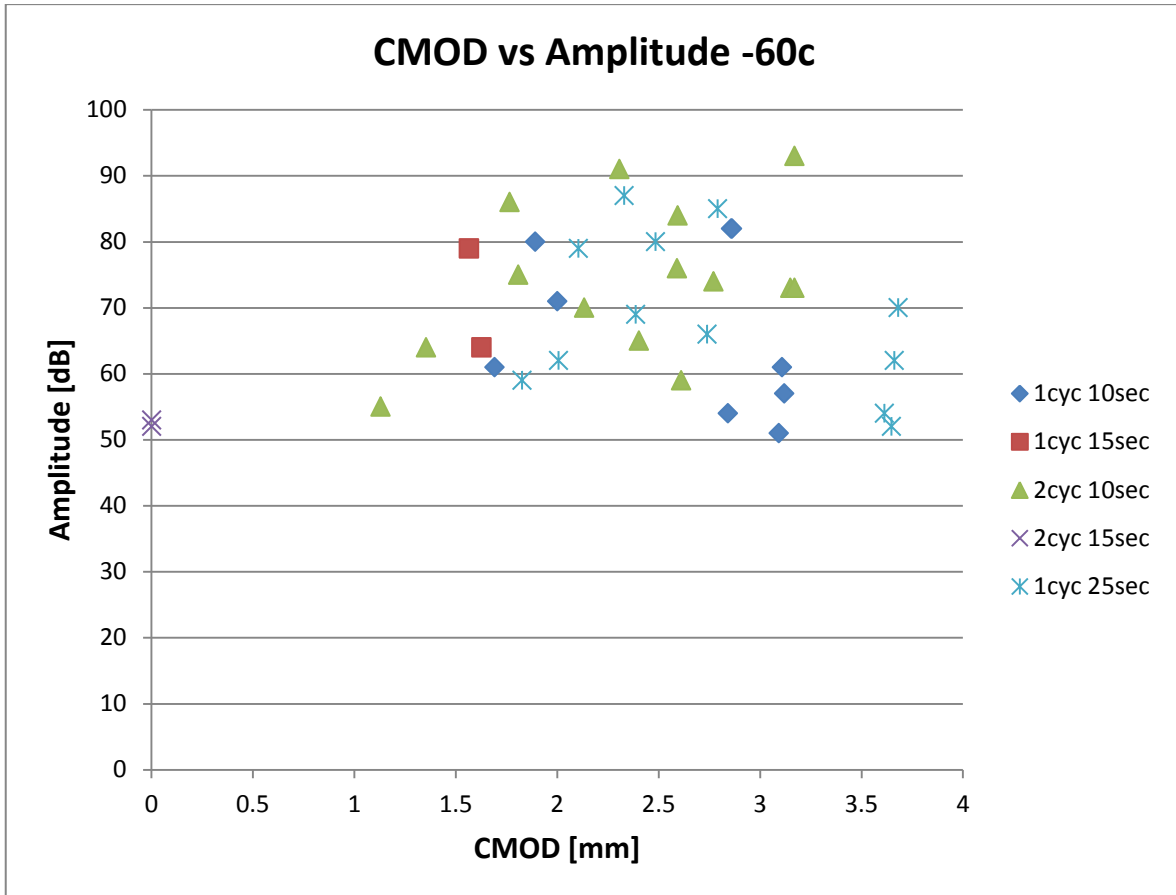


Figure 74 - CMOD vs Amplitude -60c

Interrupted tests

Several of the test experienced several signals before they were stopped. This can be due to both late reaction by the operator and that several initiations were initiated at the same time. In this graph only the first signal are taken. Tests which went to immediate fracture are also displayed as to show inhomogeneous of the material and to indicate which microstructure that is most appropriate for later testing. An amplitude equal to 113 dB or higher equals macroscopic fracture.

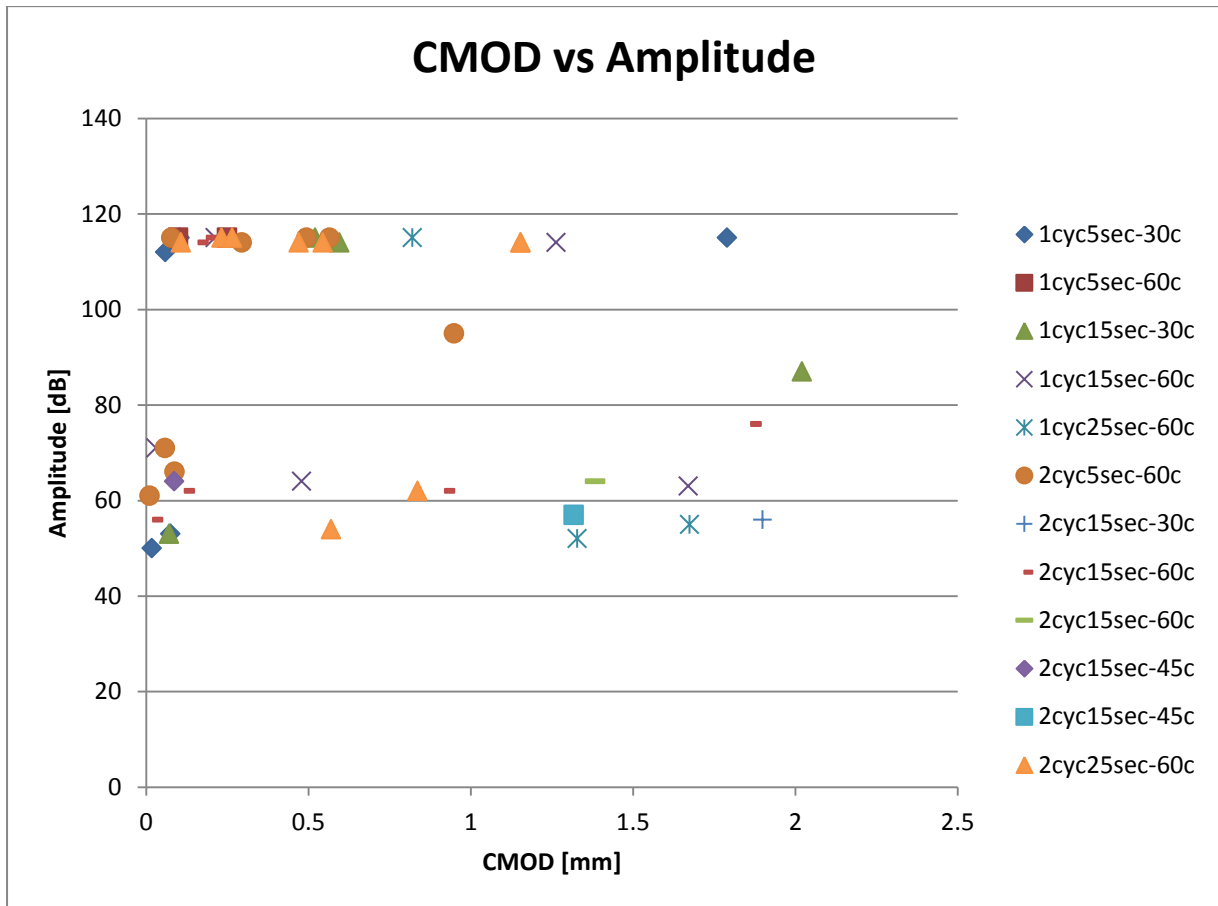


Figure 75 - CMOD vs Temperature - interrupted tests

Some parallels consisted only of one or two specimens and it is therefore hard to conclude with anything. What can be stated from the graph is that there are a large scatter, but that about 2/3 of the specimens received their signal or went to fracture at a CMOD equal or less than 0.6mm. In addition is there an overweight of the specimens which goes to macroscopic fracture before they receive a signal. It is clear that this material is not ideal for running interrupted test in that way that the specimens either go to instant fracture or get low Amplitude.

As mentioned earlier consists some of the parallels of too few specimens for any conclusions to be made, but 2cyc5sec-60c seem to be the best combination for achieving signals in addition to 1cyc5sec-30 which are the parallel where the microcrack was found. The reason is that it in average had the highest amplitude at low CMOD, one signal at 96 dB and about 50% chance of getting a signal before final fracture. On the other side should 1cyc5sec-60c, 2cyc25sec-60c be avoided.

7.2 Deformation

The specimens which were run until macroscopic fracture, have been investigated.

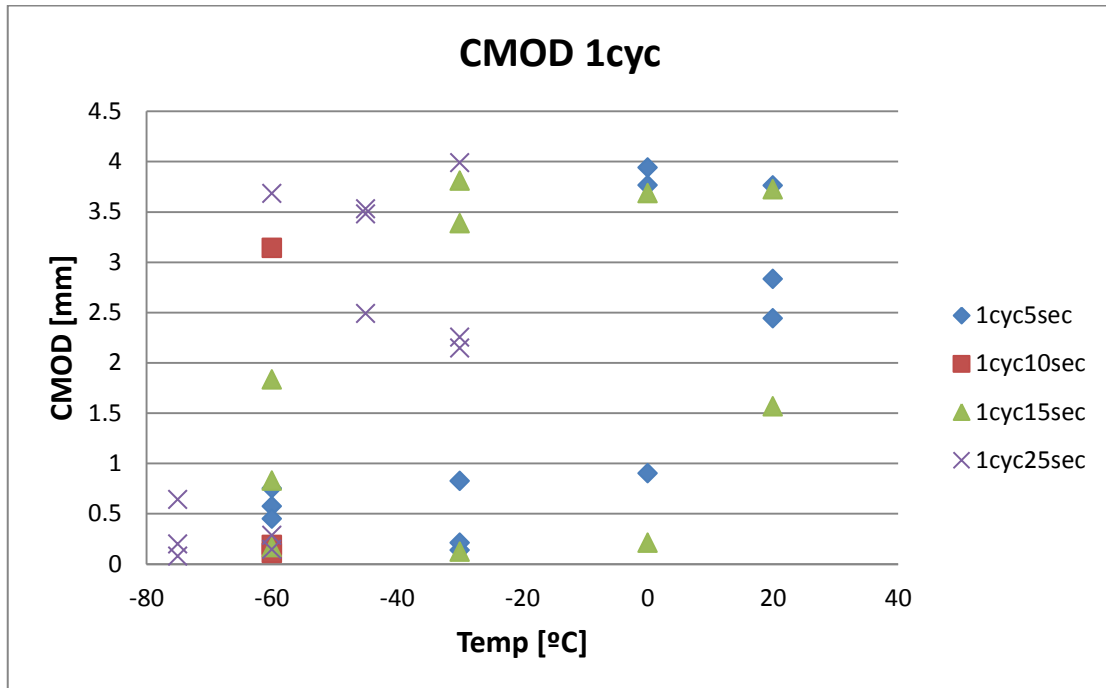


Figure 76 - Fracture toughness 1cyc

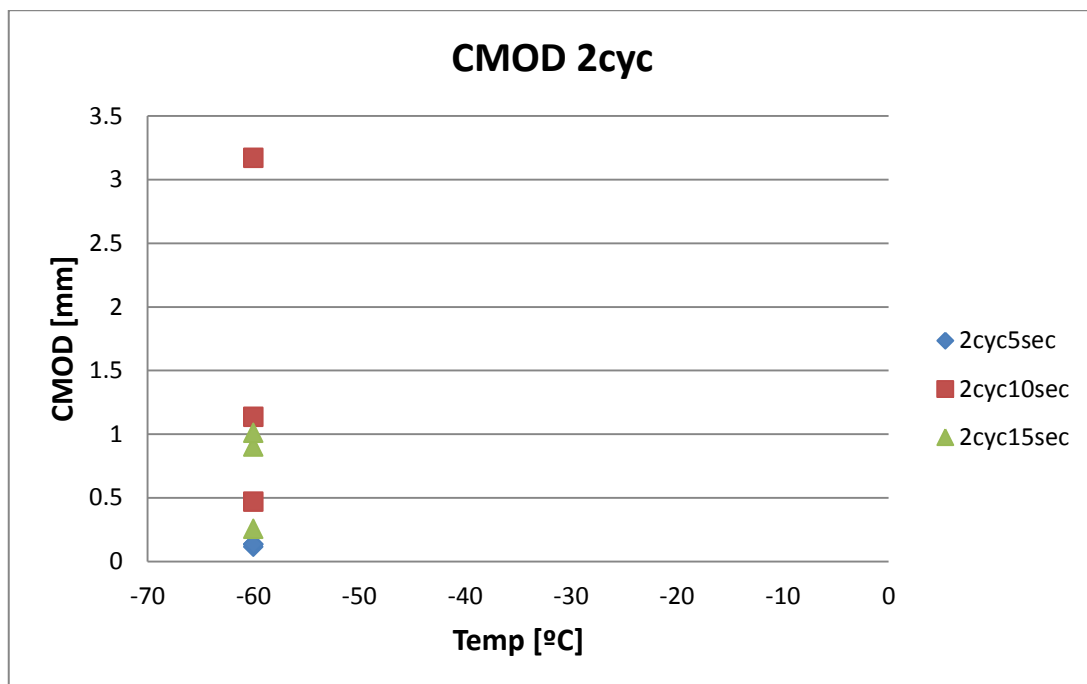


Figure 77 - Fracture toughness 2cyc

For the 1cycle specimens is there a large scatter but so the trends will be discussed. Not surprisingly are the lowest CMOD experienced at -75c and -60c with only a few deviation

and the largest minimum CMOD when testing at 20c. When 1cyc25sec is tested at higher temperatures than -75c are they the microstructure with highest fracture toughness. For the other microstructures are there a large scatter when the temperature increases to -30°C or higher.

For the 2cyc specimens are there less deviation and in general a much lower fracture toughness than for the 1cyc. 10 seconds cooling time seems to be what gives the highest toughness.

7.3 Further observations

Further on is it observed a strong correlation between the macroscopic fracture and the location was the signal is located between the sensors. Most of the signals with amplitude of 113 dB and more are located at GP = 12.5 or very close.

It is also observed that signals connected to macroscopic fracture has higher DURATION than microscopic ones.

7.4 Calculation of CTOD

During calculation of CTOD after BS7448:1991, see chapter 2.6, was it discovered that it did not correlate with CTOD data provided from SINTEF. It was discovered when comparing CTOD at final fracture based on the CMOD and load from the AEwin software. As E-modulus, tensile strength and Poisson number have little significance, as long as reasonable values are used, were these possible errors of little interest. It was believed that difference in used depth of pre-crack were the reason as SINTEF used a measured pre-crack instead of 5mm. This were tested but did not give any significant difference.

Table over calculated CTOD				
Method	Test	Measured crack depth	CTOD	Difference [%]
BS 7448:1991	7 1cyc 15sec -60c	5.03	0.5395	
SINTEF spreadsheet	7 1cyc 15sec -60c	5.03/5.27*	**	
BS 7448:1991	31 1cyc 5sec -60c	5.00	0.2345	
SINTEF spreadsheet	31 1cyc 5sec -60c	5.00/5.69*	**	
BS 7448:1991	36 2cyc 5sec -60c	4.92	0.0511	
SINTEF spreadsheet	36 2cyc 5sec -60c	4.92	**	
BS 7448:1991	49 5sec 1cyc -30c	4.90	0.2619	
SINTEF spreadsheet	49 5sec 1cyc -30c	4.90	0.1105	200.4%
BS 7448:1991	91 15sec 1cyc 0c	4.83	0.0727	
SINTEF spreadsheet	91 15sec 1cyc 0c	4.83	0.0602	74.1%
BS 7448:1991	126 15sec1cyc-30c	5.05	0.5872	

SINTEF spreadsheet	126 15sec1cyc-30c	5.05/5.37*	0.5757	98.9%
BS 7448:1991	129 25sec 1cyc - 30c	4.87	0.6860	
SINTEF spreadsheet	129 25sec 1cyc - 30c	4.87/5.29*	0.7316	88.4%
BS 7448:1991	138 25sec 1cyc - 75c	4.87	0.0709	
SINTEF spreadsheet	138 25sec 1cyc - 75c	4.87	0.0379	49.5%
BS 7448:1991	139 25sec 1cyc - 75c	4.88	0.2066	
SINTEF spreadsheet	139 25sec 1cyc - 75c	4.88	0.1399	67.9%
BS 7448:1991	167 15sec1cyc-30c	5.16	0.0202	
SINTEF spreadsheet	167 15sec1cyc-30c	5.16	0.0097	84.5%
BS 7448:1991	180 15sec1cyc-60c	4.89	0.1580	
SINTEF spreadsheet	180 15sec1cyc-60c	4.89	0.1361	96.6%
BS 7448:1991	217 2cyc5sec-60c	4.73	0.0314	
SINTEF spreadsheet	217 2cyc5sec-60c	4.73	0.0135	84.4%
BS 7448:1991	339 2cyc15sec-45c	5.00	0.0322	
SINTEF spreadsheet	339 2cyc15sec-45c	5.00	0.0155	90.7%

Table 7-1 - Table over calculated CTOD

*At large plastic deformation are two parameters used.

** Input data not available.

As can be seen from the calculated difference in % is the CTOD calculated in the SINTEF spreadsheet, in nine of the ten cases, larger. There is also a large spread in the results. A closer investigation of the input data shows that the maximum CMOD in the input file for the SINTEF spreadsheet is different from the maximum CMOD recorded in the AEWin software. In many cases could this be explained by the fact that the last signal is not at the highest CMOD, see Figure 78 - frame b) and c), while the load-displacement curve used in the SINTEF spreadsheet record the whole time and therefore will contain a higher CMOD. Investigation of the aborted tests shows that the major differences exist there as well, see Table 7-1, where test no 167, 180, 217 and 339 shows clear differences.

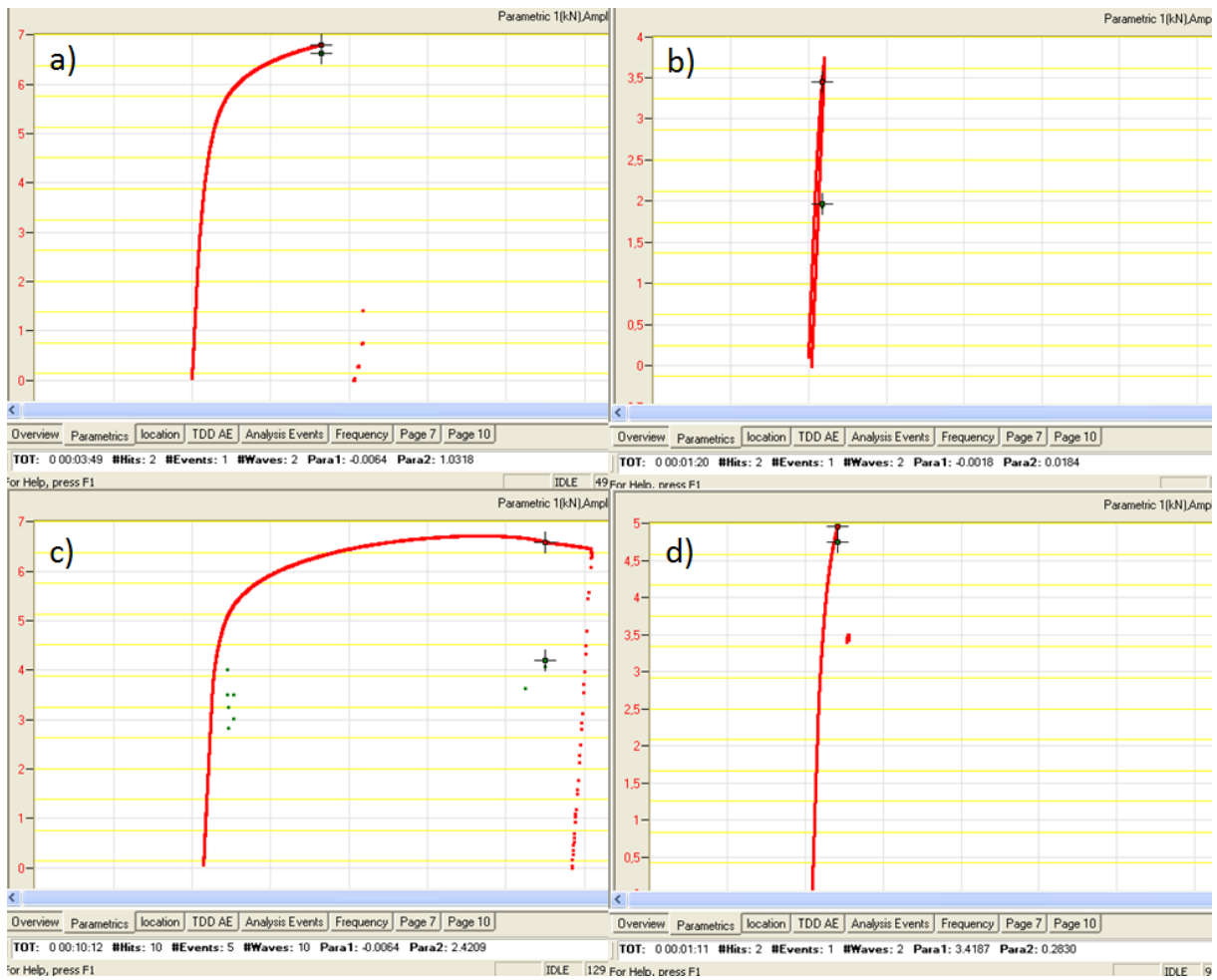


Figure 78 - Load deformation curve from AEwin

a) Test no. 49 5sec1cyc-30c. b) Test no. 217 2cyc5sec -60c. c) Test no. 129 1cyc5sec -30c. d) Test no. 91 1cyc15sec.

7.5 Relation between AE signal amplitude and arrested micro crack size

This chapter is connected with the theory presented in chapter 3.2.

7.5.1 How to measure area?

According to (Østby et al., 2012) the area is measured with the geometrical shape of a rectangle. The way the area is measured greatly affects the result and who measures the area will affect the results. The arrested microcrack was measured by dividing it into three different areas, one for each part of the microcrack, see Figure 79.

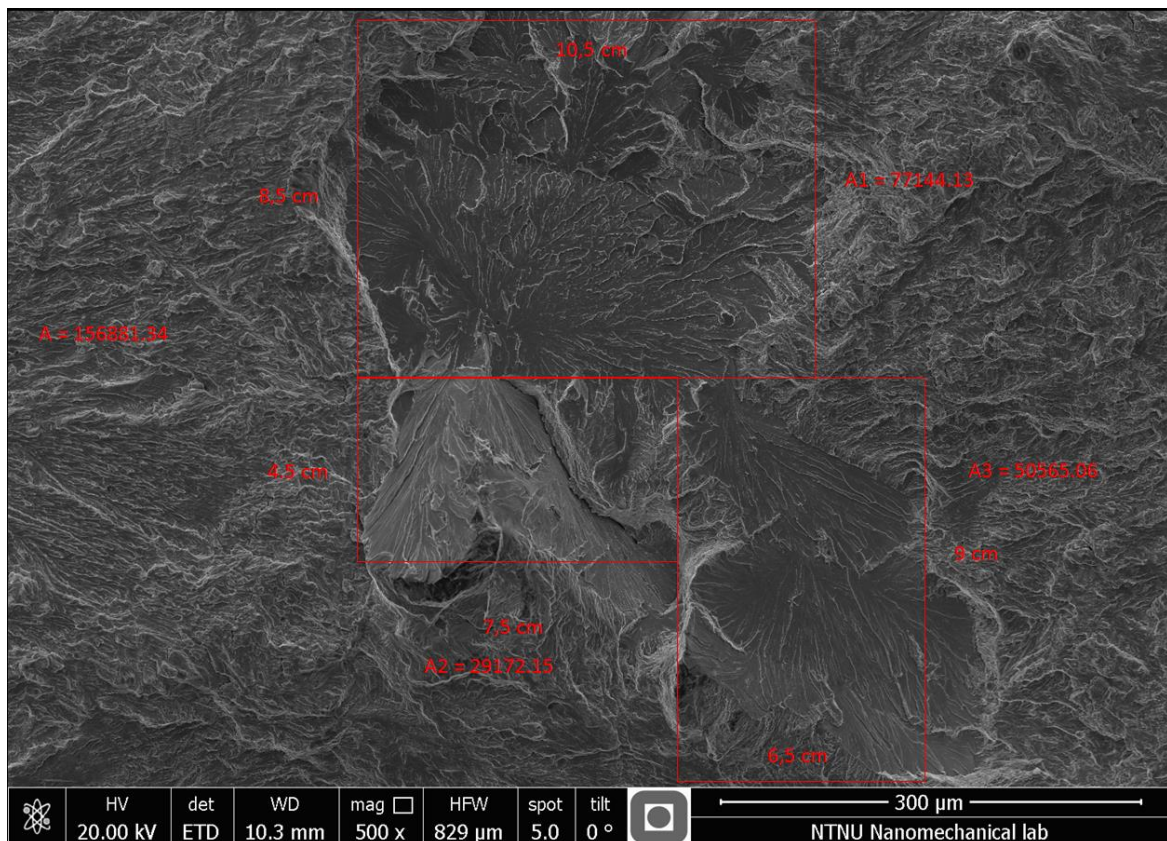


Figure 79 - Measurement of arrested microcrack - Test no. 167

The measured area was then squared and inserted in the table presented in Østby et al. (2012), see Table 7-2 and plotted into the graph, see Figure 80. The area is considerably larger than the area linked to the signal in Østby et al. but as seen in Table 7-2 are large variations occurring, reference to amplitude 78/79 dB and 111/112 dB.

Material	Test No.	A_AE	a_micro
420	6	64	32
420	4	78	35
420	7	79	55
420	3	90	87
420	5	93	89
X65	2	97	125
420	2	109	232
X65	1	111	260
420	1	112	354
R50A - 420	167	112	396

Table 7-2 – AE amplitude VS a_micro.

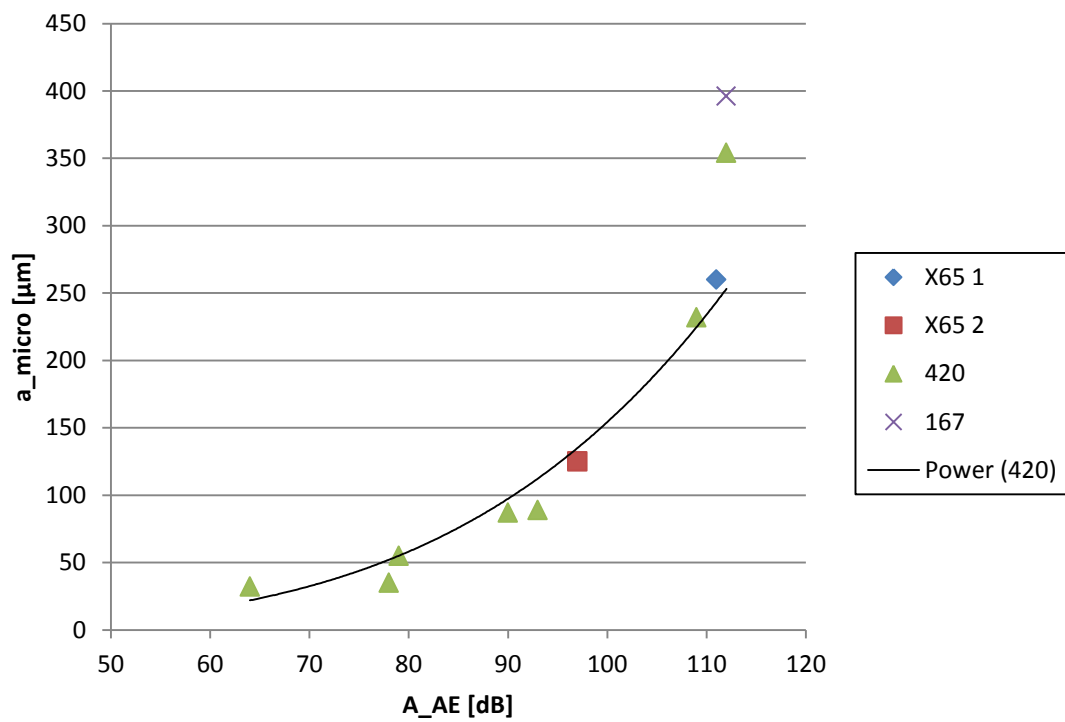


Figure 80 - Relation between the microcrack size and the AE signal amplitude

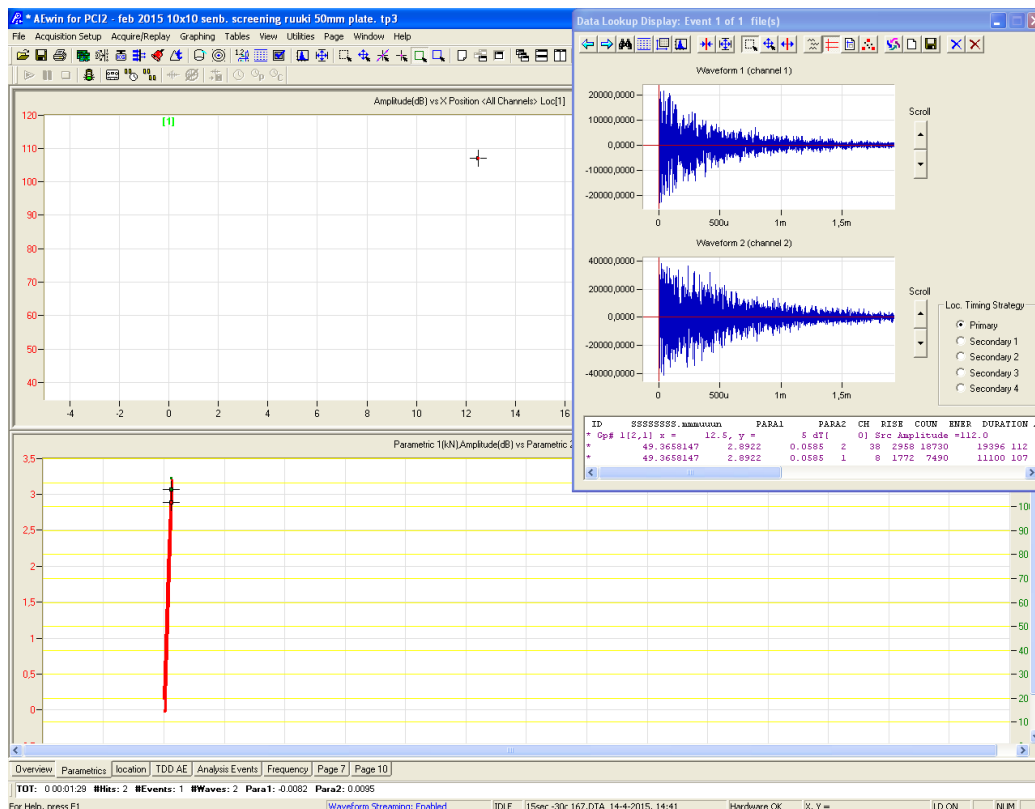


Figure 81 - AE amplitude linked to creation of microcrack - Test no 167

7.5.2 The constant “k” and power law

It were discovered during work with linking the AE signal to the area of the crack surface that the constant K were not consistent, see chapter 3.2 and appendix 12.8, where this is proved. According to Erling Østby, the author of (Østby et al., 2012), have there never been done any attempts of defining “k” in detail.

An attempt to create a power law which describes the curve from Østby et al. (2012) was made. This was done in excel, starting with the basic power law $y = A + Bx^n$ where A, B and n are constants. Y denotes the value on the y – axis, in this case the square root of the cleavage facet, a_micro. X denotes the values on the x – axis, AE amplitude.

Five attempts was made to acquire he constants, were the first consisted of all the points while the last only consisted of two, the lowest and the highest amplitude. This was done because of poor results were the calculated y, called y_model, deviated largely from the measured y. The reason for these bad results can be linked to large variations in measured area relative to the measured amplitude, as can be seen in Table 7-2. In particular have test 4 [78dB] an a_micro which are closer to test 6 [64dB] than test 7 [79dB]. There is no basis for stating that the reason is due to different base material since the basis is relative small and the fact that the largest variation in measured area vs AE is done in the same material.

The following power law is based on all the points in Østby et al (2012).

$$y = A + Bx^n$$

$$A = 0, B = 7,53 \times 10^{-7}, n = 4,18$$

$$y = 7,53 \times 10^{-7} \times x^{4,18}$$

8 Discussion

This chapter will discuss the objectives stated in the start and refer to different experiences

8.1 Relationship between arrested microcrack and AE amplitude

8.1.1 Cleavage facet

The further investigation of the theory from Østby et al. (2012) which are based on Lysak (1996) by obtaining quantitative data was the main objective when the work on this thesis started. One arrested microcrack was found and placed inside the graph with the data from Østby et al. (2012). At first the whole area were measured and plotted, see Figure 80 and Figure 79 which gave a_{micro} of 396 µm. This is higher than the a_{micro} (354 µm) found in by Østby at the same amplitude, see Table 7-2, but could still be valid due to natural deviation. The cleavage microcrack has a form that may indicate that the propagation occurred in two or three steps with a creation of the large surface (A1) first before A2 and A3 follows in that order or simultaneously.

What might be the strongest argument against this course of events is the AE signal, see Figure 81. For the first is only one event recorded and for the second is no signs of double signal spotted, see Figure 19.

8.1.2 Smooth surfaces and straight secondary cracks

It has not been possible to link the smooth surfaces to any AE signal. For the first are there too many and they are often several possible smooth surfaces at the CTOD linked to the signal. In addition do they have a low toughness as they are created during both pre – and post- fatigue. This means that the energy released most likely would not be enough to create a AE amplitude higher than the threshold value.

If the straight cracks are secondary cracks they will be formed after the test is stopped, most likely during post- fatigue. They will therefore not be recorded. If they nevertheless are created during the SENB testing will their orientation, which is parallel to the fracture surface, make it impossible to measure the area.

8.2 The Multiple Barrier Model

Cleavage area in sample 167

The microcrack in sample 167, see Figure 48 and Figure 49, which has a CGHAZ 15 sec microstructure is most likely initiated at or close to the two inclusions. It is clear that they are not M-A particles from the EDS analysis as they both contain elevated amounts of Oxygen, Aluminum, Sulfur and Calcium, see chapter 6.3.1. There are two possible theories to what initiated the fracture and the inclusions plays a role in both of them.

1. The inclusions have lower fracture toughness than the matrix around which makes one or both of them fracture and initiate the fracture.

2. The particles have a higher toughness than the matrix around and act as stress raisers. The inclusions can be described as two beacons emitting a 360 degree stress field and in the middle two fields meet and create enough stress for initiation.

The result from the EDS can be compared with the results found in (Brandt et al., 2012) were an inclusion defined to be a oxide and sulphide slag particle initiated the fracture. In addition can a cavity be observed around one of the inclusions which also indicated that it is a sulphide particle (Agboola, 2010), see Figure 49. Without any more evidence the reason for initiation is hard to define but

The reason that the fracture initiated at these two particles might be a coincident and they might not have fractured if the pre-fatigue zone had been shorter. Because they are located close to the fatigue line they will most likely have been affected by the increased stress created by the notch.

It is difficult to link this directly to the MBM.

Independent inclusions

Several independent inclusions were found in the specimens, but the two shown in Figure 54 (test no. 167) and Figure 55 (test no. 180) is chosen. Both inclusions are found in a CGHAZ 15 sec microstructure but specimen 167 is tested at -30 c while specimen 180 is tested at -60. In both cases it is assumed that the crack initiated inside the particle. While the crack in 180 were arrested at the particle/matrix border propagated the crack in 167 into the matrix before getting arrested. One of the principles in the MBM model is that the crack arrest toughness is reduced with lower temperature, which are not the case here. Tests of the base material has shown that the strength is increased as the temperature is reduced to -60c (Akselsen, 2014) and the same effect might occur for the CGHAZ as well.

Another explanation is the microstructure which has been defined to be a mix of upper bainite with a mix of auto-tempering. The arrest toughness will most likely be affected by the microstructure (Zhang and Knott, 1999) and can explain the different behavior. Location relative to the pre-fatigued crack is also of significance as it acts as a stress raiser. What can be said is that there was not enough energy to drive neither of them to any kind of final fracture.

The material which the inclusion consists of plays a role as well. The particle in specimen number 167 consists of a large part of Sulfur (22.1 wt%) and Calcium (38.4 wt%) while the particle in specimen 180 had fallen out after the first examination. If a considerable amount of Manganese had been found could it help with concluding that the particle in 167 was the initiation site as fracture have been proven to initiate in manganese sulfide, (Rosenfield et al., 1983).

8.3 Different observation on fracture surface

Undefinable surface test no. 217

The facet observed in test no 217, cannot be the source of the AE signal as the amplitude is 66dB which means it should have an area of approximately $32\mu\text{m}$, or an area of $1024\mu\text{m}^2$. It is clear that it does not fit the signal. Based on what's mentioned in 6.3.1 it is more likely to be some part that is deformed somehow. The last thing that should be mentioned is that if it were elevated part of the surface before it was deformed, it should still be a mark on the other side.

Smooth surfaces and straight secondary cracks

One theory that may explain the smooth surfaces are delamination of some kind. In the beginning were only flat completely smooth surfaces observed, see Figure 61 picture c), but later have also more rough and curved smooth surfaces been observed, see Figure 65. As they appear at so many different locations and in so many different shapes are they hard to define. A more statistical analysis might show that they vary with certain conditions.

Several other theories have also been discussed/mentioned as brittle cracks along slip planes (which would have resulted in AE signals if they were large enough).

Some of the smooth surfaces can resemble smooth surfaces seen on the fracture surface in Aluminum. The EDS testing showed large values of Aluminum compared with the datasheet provided by Ruukki, but this have not been further investigated.

A theory during this work was that the smooth surfaces can be the result of delamination. No papers about delamination during SENB testing were found so the papers read are mainly addressing tensile testing and Charpy testing. What is clear is that delamination is clearly related to how the plates are manufactured, see chapter 2.3. Investigation in HSLA steels with a higher amount of carbon (0.065 wt%) were the control - rolled steel vulnerable for delamination in the rolling plane when exposed to transverse stress (Herø et al., 1975). Further have they found that the occurrence of delamination increased with decreasing finish temperature.

For the straight secondary cracks it is referred to chapter 6.8 where a possible solution was presented. There is proved to be a large amount of bainite present and it is unlikely that it have been propagating through blocks from different packets.

8.4 Arrested microcracks

Only at one of the five investigated specimens, which were interrupted after the first signal, were an arrested microcrack found. According to Erling Østby were cleavage facets seen in almost every test done in context with the paper from 2012. Of the twenty tests which were run did only one or two lack a cleavage facet. See also chapter 8.6.1.

Low plastically deformation (low CTOD) high amplitude (<85 dB) increases the chance for locating the fracture. As it can be seen from Table 12-4 few of the specimens tested fulfill

these requirements. According to Erling Østby is there a possibility that for high plastic deformation will fatigue crack grows around the cleavage facets so it don't appear on the fracture surface.

The results in this thesis should be used to decide both testing conditions with respect to temperature, but also the welding procedure if finding arrested microcracks are the goal. Based on the results, see chapter 7, is it 2cyc5sec -60c which have proved most promising even though the arrested microcrack were a 1cyc5sec tested at -30c. It seems as further testing on this material with respect to microcrack arrest should be done with specimens weld simulated with a cooling time of 5 seconds.

8.5 Welding effect and temperature effect on material toughness

Although a large scatter is observed is an increased cooling time beneficial for the materials toughness with respect to CGHAZ specimens, see Figure 75 where 25sec has the highest CMOD in most cases. For 1cyc15sec is there a large scatter at -30c and higher while 1cyc5sec experience large variation in toughness at 0c and higher. For ICCGAZ specimens, see Figure 77, is there little variation in the 5sec parallel and large for the 10sec parallel.

The microstructure for CGHAZ 25 were not investigated, but it is an trend that the amount of coarse upper bainite increases with increased cooling time. If it in addition have austenite grain size of 100µm as the other weld simulated specimens should it also have a fracture toughness lower than the others. Coarse bainite structures are thought to contribute to low fracture toughness and Lambert-Perlade (2004) proved that this microstructure have a low crack propagation resistance..

Further on were areas which may be fine - grained bainite and ferrite found, see arrows on Figure 34, which could possibly be a source for reduced fracture toughness. In addition would it provide an explanation to why the fracture toughness increases with increased cooling time. The amount of observed fine grained bainite and ferrite increase with reduction in cooling time and the increased amount could give rise to intense strain concentrations and combined with a high defect density initiate microcracks (Yokoyama and Nagumo, 1998)

8.6 Experience of theoretical relationship between AE amplitude and arrested microcrack

According to Lysak is it necessary that for the signal to correlate to the arrested microcrack it has to be initiated a distance in front of the macrocrack and grow back, see chapter 3.2.1. The difference in correlation when comparing a through crack and an internal crack makes the fomula presented in Østby et al (2012) somewhat dependent on both type of microstructure and geometry of the crack. It might be an idea to define who has the most benefit of this formula. Is it for scientific reasons and the user is well known with fracture mechanics or is it for use in NDT and the user is an engineer with basic knowledge of fracture

mechanics? Further development of the relation, in addition to more testing for validation of the curve, can be:

- Guidelines for measurement of the arrested microcrack
- Reintroducing crack orientation and other factors presented by Lysak (1996)
- Create a set of formulas which custom to different situations, especially internal and surface cracks.

8.6.1 Correlation to Arctic Materials 1 (AM1)

The graph presented in Østby et al. (2012) were developed in AM1 and was based on results from a 420MPa hot rolled steel plate with larger carbon content. The larger value of carbon gives an increased number of M-A constituents in the ICCGHAZ microstructure (Brandt et al., 2012). This could explain higher AE activity as M-A constituents initiate cleavage easily in addition to provide a explanation to why only one arrested microcrack were found.

9 Conclusion

This master thesis does not confirm or reject the theoretical relationship between the recorded AE amplitude and the arrested microcrack size. The behavior of the material has made it difficult to make specific conclusions, however conclusions to the other findings are presented as follows.

The low content of carbon reduces the formation of M-A particles. This leads to a reduction in possible locations for crack initiation and an increase in the fracture toughness. This conclusion is further strengthening due to the number of AE signals. The low number of AE signals compared with the 420 MPa tested in Østby et al. (2012), which had a higher carbon content, is the reason for the statement. Further can it be concluded that the steel is still vulnerable for loading in cold environments. No initiations has been linked directly to M-A phases, but different stages in the MBM were seen at larger inclusions. Furthermore, the microstructure is defined to be highly inhomogeneous and the presence of upper bainite and autotempered martensite increase the scatter in fracture toughness.

As only one arrested cleavage crack was found, it is evident that there must be other sources for AE. There is a high possibility that some of the sources originate from the ductile zone, possibly from dimples detaching from the matrix.

It is almost impossible to relate AE signals to cleavage facets, unless the test is topped after the first signal and post-fatigued. This is due to the large amount of cleavage facet on the fracture surface and that it is hard to define their size.

The constant, K , is not a constant and further investigation is needed to define it.

The scatter in measured area of arrested microcrack and AE amplitude can be explained by the different ways of measuring it, but also that the AE amplitude depends on several factors as crack orientation and if it is an internal crack or a surface crack.

10 Further work

Suggestions for further work are as follows:

- Interrupted testing to obtain more arrested microcracks and compare with the graph from Østby et al. (2012) should be continued.
- A standard for measuring the size of arrested microcracks should be created.
- A dilatometric analysis which measureS volumetric expansion of the steel during a thermal process should be performed. By doing this one can obtain the phase transformation from ferrite to austenite. This would be helpful to understand the phase transformation and the ductile to brittle transition.
- Preparation of specimens can be performed differently to minimize the amount of dirt and rust which is disturbing during the SEM analysis. During cutting, grinding and polishing the specimens are exposed to water and other chemicals. The specimens that were grinded and polished ended up with a useless fracture surface due to corrosion. The fracture surface should be considered coated with electroless Ni to protect the surface during polishing, especially if only one side of the fracture is available and both fracture surfaces and microstructure are of interest.
- Further investigation of smooth surfaces should be carried out. An attempt was made to perform a hardness test on the smooth surfaces, but was unsuccessful, see chapter 5.4. A hardness test of the smooth surfaces and surroundings with nano-indentation could provide a better understanding of the microstructure.
- The constant K in the formula from Østby et al (2012) should be determined.
- Mapping of the areas around the straight cracks with an EBDS, as shown in chapter 6.8, to see if the same solution of elements applies here as well may be useful.
- Further development of the procedure for sorting AE signals should be conducted.

11 References

- AGBOOLA, O. 2010. The role of non-metallic inclusions in steel failure. *Am. Eurasian. J. Sci. Res.*, 5, 4.
- AKSELSEN, O. M. 2014. SMACC/ AM 2 - Evaluation of 420 MPa steel welds. SINTEF Materials and Chemistry: SINTEF.
- ANDERSON, T. L. 2005. *Fracture mechanics : fundamentals and applications*, Boca Raton, FL, Taylor & Francis.
- ASKELAND, D. R. & PHULÉ, P. P. 2006. *The science and engineering of materials*, Toronto, Ont., Thomson.
- BHADESHIA, H. K. D. H. & HONEYCOMBE, S. R. 2006. *Steels: Microstructure and Properties*, Elsevier Ltd.
- BRAMFITT, B. L. & MARDER, A. R. 1976. A Study of the Delamination Behavior of a Very Low Carbon Steel. *Metallurgical Transactions A*, 8A.
- BRANDT, K., SOLBERG, J. K., AKSELSEN, O. M. & ØSTBY, E. Initiation of Cleavage Fracture in a Weld Simulated Low Carbon Low Alloy Arctic Steel. Twenty-second (2012) International Offshore and Polar Engineering Conference: International Society of Offshore & Polar Engineers, 2012 Rhodes, Greece. 323-328.
- EASTERLING, K. 1992. *Introduction to Physical Metallurgy of Welding*, Butterworth - Heinemann Ltd.
- HELEN, J. 1989. *Scanning, elektron-mikroskopi*, Metallurgisk institutt, NTH.
- HELLIER, C. J. 2001. *Handbook of Nondestructive Evaluation*, McGraw-Hill Professional Publishing.
- HERØ, H., EVENSEN, J. & EMBURY, J. D. 1975. The Occurrence of Delamination in a Control Rolled HSLA Steel *Canadian Metallurgical Quarterly*, 14.
- JR, J. W. M., KINNEY, C., PYTLEWSKI, K. & ADACHI, Y. 2013. Microstructure and cleavage in lath martensitic steels. *Science and Technology of Advanced Materials*.
- JUN, H. J., KANG, J. S., SEO, D. H., KANG, K. B. & PARK, C. G. 2005. Effects of deformation and boron on microstructure and continuous cooling transformation in low carbon HSLA steels. *Materials Science and Engineering A*, 422, 6.
- KUNISHIGE, K., FUKUDY, M. & SUGISAWA, S. 1979. 19. *Transactions of the Iron and Steel Institute of Japan*, 324.
- LAMBERT-PERLADE, A., GOURGUES, A. F., BESSON, J., STUREL, T. & PINEAU, A. 2004. Mechanisms and Modeling of Cleavage Fracture in Simulated Heat-Affected Zone Microstructures of a High-Strength Low Alloy Steel. *Metallurgical and Materials Transactions A*, VOLUME 35 A, 15.
- LOPEZ, V. V. 2014. *Microstructure Characterisation of Bainitic HSLA Steel for Pressure Vessels*. Master, Norwegian University of Science and Technology.
- MARTIN-MEIZOSO, A., OCAÑA-ARIZORRETA, I., GIL-SEVILLANO, J. & FUENTES-PÉREZ, M. 1994. Modeling Cleavage Fracture of Bainitic Steels. *Acta metall. mater.*, 42, 11.
- PALMER, A. C. & KING, R. A. 2008. *Subsea Pipeline Engineering* PennWell.
- ROSENFELD, A. R., SHETTY, D. K. & SKIDMORE, A. J. 1983. Fractographic observations of cleavage initiation in the ductile-brittle transition region of a reactor-pressure-vessel steel. *Metallurgical Transactions A*, 14a.
- SOFTWARE, A. 2004. Installation, Operation and User's Reference Manual. Physical Acoustics Corporation.
- THAULOW, C. & VALBERG, H. 2012. *TMM4140 Plastisk deformasjon og brudd (pdf)*, Norwegian University of Science and Technology - Department of Engineering Design and Materials.
- YOKOYAMA, K. & NAGUMO, M. 1998. Brittle fracture initiation associated with the strain localization in a heat-affected zone of a low carbon steel. *Metallurgical and Materials Transactions A*, 29, 8.
- ZHANG, X. Z. & KNOTT, J. F. 1999. Cleavage fracture in bainitic and martensitic microstructures. *Acta Materialia*, 47, 13.
- ÖSTBERG, A. & MODIN, U. Etching Handbook. In: STEEL, A. S. (ed.). AB Sandvik Steel.

ØSTBY, E., AKSELSEN, O. M. & KRISTENSEN, T. A. 2013. Monitoring of cleavage microcrack arrest in weld thermal simulated microstructures by means of acoustic emission. *The International Society of Offshore and Polar Engineers*.

ØSTBY, E., THAULOW, C. & AKSELSEN, O. M. 2012. Quantitative relations between acoustic emission signal amplitude and arrested cleavage microcrack size. *International Journal of Fracture*, 177:73-80.

12 Appendix

12.1 Master contract



MASTERKONTRAKT

- uttak av masteroppgave

1. Studentens personalia

Etternavn, fornavn Larsen, Andreas Vrenne	Fødselsdato 30. apr 1988
E-post	Telefon 97978955

2. Studieopplysninger

Fakultet Fakultet for ingeniørvitenskap og teknologi	
Institutt Institutt for produktutvikling og materialer	
Studieprogram Produktutvikling og produksjon	Studieretning Materialer

3. Masteroppgave

Oppstartsdato 14. jan 2015	Innleveringsfrist 10. jun 2015
Oppgavens (foreløpige) tittel Akustisk emisjon fra arktiske stål	
Oppgavetekst/Problembeskrivelse Sammendrag av prosjektoppgaven er: * Sammendrag av resultatene fra prosjektoppgaven og lag modeller som skal undersøkes i masteroppgaven * Utvikle en eksperimentell test for å oppdage mikrosprekker stanset av defekter og utfør tester. Dette kan også inkludere AE overvåkning under nanomekanisk testing * Sett resultatene i sammenheng med teoretiske modeller for sprøbrudd/FE modellering av mikrosprekker, inkludert et estimat av lokale verdier for stans av sprekkvekst. * Sammenheng mellom mikrostruktur og observerte AE målinger	
Hovedveileder ved institutt Professor Christian Thaulow	Medveileder(e) ved institutt
Merknader 1 uke ekstra p.g.a påske.	

4. Underskrift

Student: Jeg erklærer herved at jeg har satt meg inn i gjeldende bestemmelser for mastergradsstudiet og at jeg oppfyller kravene for adgang til å påbegynne oppgaven, herunder eventuelle praksiskrav.

Partene er gjort kjent med avtalens vilkår, samt kapitlene i studiehåndboken om generelle regler og aktuell studieplan for masterstudiet.

Trondheim 2011-15

Sted og dato

Student

Andreas Vrenne Larsen

Hovedveileder

Dr. Christer S

Originalen lagres i NTNUs elektroniske arkiv. Kopi av avtalen sendes til instituttet og studenten.

Side 2 av 2

12.2 Risk assessment

NTNU	Risk assessment		Prepared by	Number	Date
			HSE section	HMSIV/2603E	04.02.2011
HSE/AS			Approved by		Replaces
			The Rector		01.12.2006

Unit: Department of Engineering Design and Materials

Date: 20/2-2015

Line manager:

Participants in the identification process:

Short description of the main activity/main process: Master project for student Andreas Vrenne Larsen. Project title: Acoustic Emission from Arctic Steels

Is the project work purely theoretical? NO

Signatures: Responsible supervisor: 

Student: 

ID nr.	Activity/process	Responsible person	Existing documentation	Existing safety measures	Laws, regulations etc.	Comment
1	Cutting activity at metallography lab	Nousha Kheradmand	Risk assessment for lab and mandatory HSE course	Proper use of equipment, manual, safety glasses		Training w/with phd students
2	Grinding and polishing at metallography lab	Nousha Kheradmand	Risk assessment for lab and mandatory HSE course	Proper use of equipment, manual, safety glasses and gloves		Training w/with phd students
3	Fume-hood activity (Etching) at metallography lab	Nousha Kheradmand	Risk assessment for lab and mandatory HSE course	Proper use of equipment, manual, safety glasses, gloves and lab coat		Performed in fume-hood. Training w/with phd students
4	Fume-hood activity (Cleaning) at metallography lab	Nousha Kheradmand	Risk assessment for lab and mandatory HSE course	Proper use of equipment, manual, safety glasses, gloves and lab coat		Training w/with phd students
5	Acoustic Emission testing at material lab	Tore Andre Kristensen (SINTEF)	Mandatory HSE course	Safety glasses		Training w/with phd students
6	SEM lab	Nousha Kheradmand	Course with phd student			

Unit: Department of Engineering Design and Materials Date: 20/2

Line manager:

NTNU		Date	
		04.02.2011	
HSE/KS		Number	Replaces
		HMSRV2603E	01.12.2006
Prepared by		Approved by	
		The Rector	

Risk assessment

Participants in the identification process:

Short description of the main activity/main process: Master project for student Andreas Vrenne Larsen. Project title: Acoustic Emission from Arctic Steels

Signatures: *Dr. Thaulus* Responsible supervisor: *Andreas Vrenne Larsen* Student:

Activity from the identification process form	Potential undesirable incident/strain	Likelihood (1-5)	Consequence:			Risk Value (human)	Comments/status Suggested measures
			Human (A-E)	Environment (A-E)	Economy/material (A-E)		
1	Flying Debris	1	A	A	A	A1	
2	Wearing of finger tip	3	A	A	A	A3	Use gloves
3	Skin irritation	1	C	A	A	C1	Use gloves, lab coat and safety glasses
4	Splash of solvent	3	A	A	A	A3	Use gloves, lab coat and safety glasses
5	General danger for a workshop	2	A	A	A	A2	Use safety glasses
6	Wrong use of equipment	1	A	A	D	D1	Good training from phd students

Likelihood, e.g.:

1. Minimal
2. Low
3. Medium
4. High
5. Very high

Consequence, e.g.:

- A. Safe
- B. Relatively safe
- C. Dangerous
- D. Critical
- E. Very critical

Risk value (each one to be estimated separately):

Human = Likelihood x Human Consequence
 Environmental = Likelihood x Environmental consequence
 Financial/material = Likelihood x Consequence for Economy/material

NTNU				Risk assessment			
HSE/KS						Prepared by	Number
		HSE section	HMSRV2603E	04.02.2011			
		Approved by		Replaces			
		The Rector		01.12.2006			

Potential undesirable incident/strain
Identify possible incidents and conditions that may lead to situations that pose a hazard to people, the environment and any materiel/equipment involved.

Criteria for the assessment of likelihood and consequence in relation to fieldwork

Each activity is assessed according to a worst-case scenario. Likelihood and consequence are to be assessed separately for each potential undesirable incident. Before starting on the quantification, the participants should agree what they understand by the assessment criteria:

Likelihood	Low 2	Medium 3	High 4	Very high 5
Minimal 1	Once every 50 years or less	Once every 10 years or less	Once a month or less	Once a week

Consequence

Grading	Human	Environment	Financial/material
E Very critical	May produce fatality/ies	Very prolonged, non-reversible damage	Shutdown of work >1 year.
D Critical	Permanent injury, may produce serious serious health damage/sickness	Prolonged damage. Long recovery time.	Shutdown of work 0.5-1 year.
C Dangerous	Serious personal injury	Minor damage. Long recovery time	Shutdown of work < 1 month
B Relatively safe	Injury that requires medical treatment	Minor damage. Short recovery time	Shutdown of work < 1 week
A Safe	Injury that requires first aid	Insignificant damage. Short recovery time	Shutdown of work < 1 day

The unit makes its own decision as to whether opting to fill in or not consequences for economy/materiel, for example if the unit is going to use particularly valuable equipment. It is up to the individual unit to choose the assessment criteria for this column.

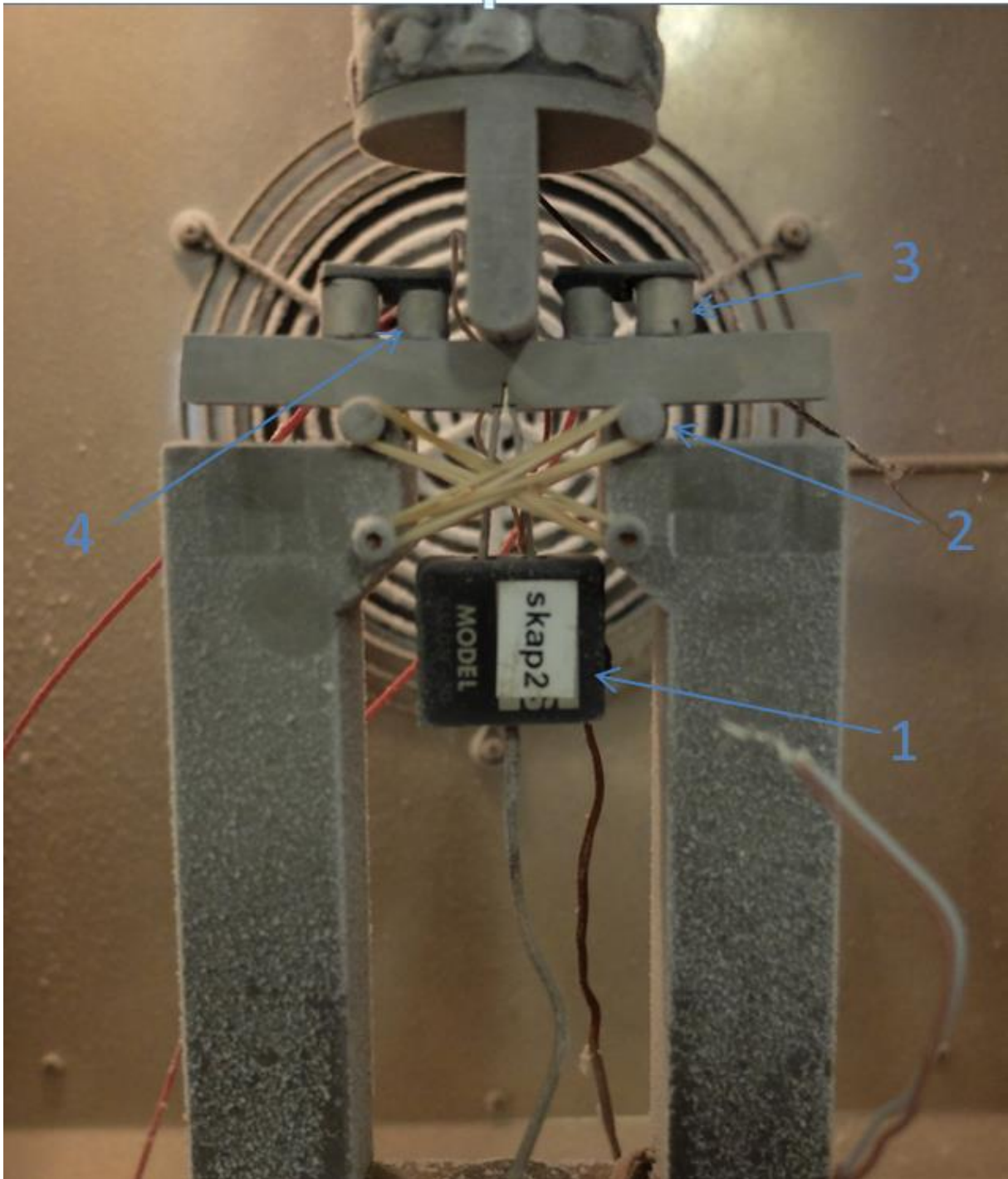
Risk = Likelihood x Consequence

Please calculate the risk value for "Human", "Environment" and, if chosen, "Economy/materiel", separately.

About the column "Comments/status, suggested preventative and corrective measures":

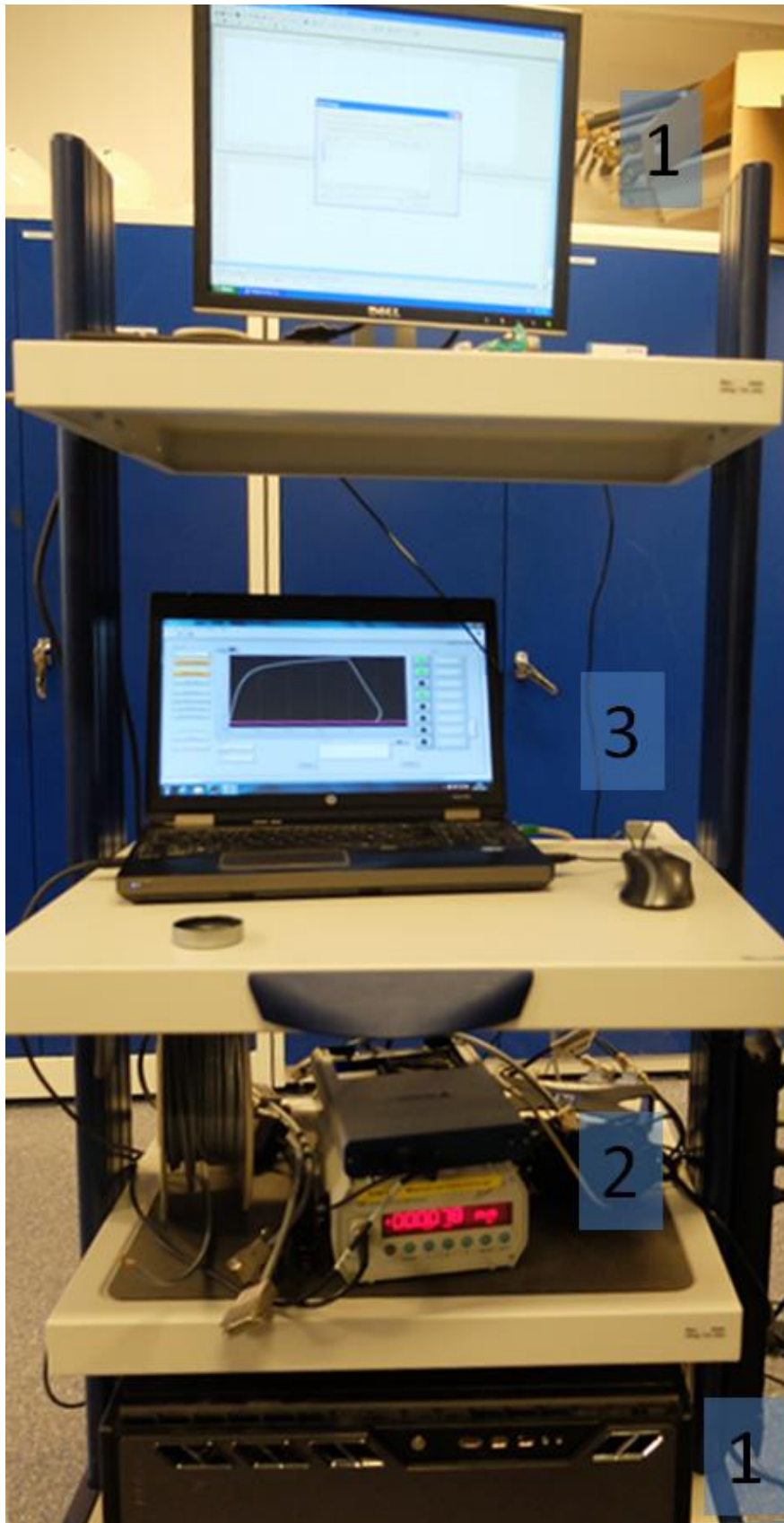
Measures can impact on both likelihood and consequences. Prioritise measures that can prevent the incident from occurring; in other words, likelihood-reducing measures are to be prioritised above greater emergency preparedness, i.e. consequence-reducing measures.

12.3 Test setup SENB



1. Pinch gauge for CMOD measurement
2. Circular bars, support for specimen
3. Magnetic clamps for AE sensors
4. AE sensors

12.4 AE equipment



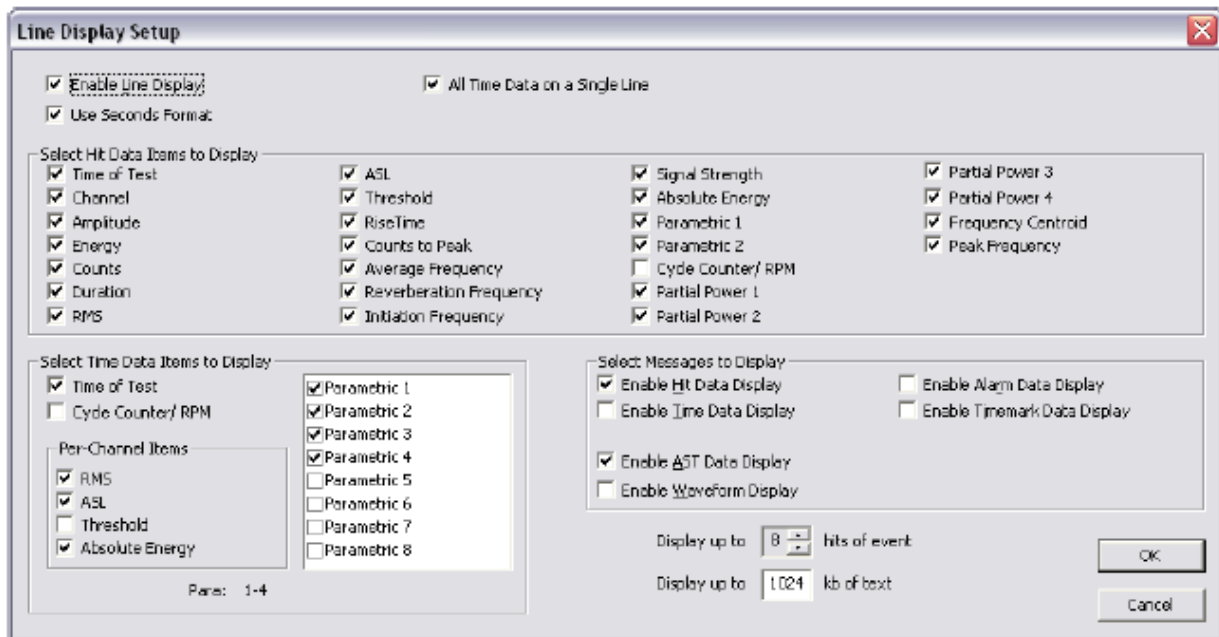
1. Stationary computer with AEwin software and monitor.
2. Amplifier for signal from CMOD pinch gauge.
3. Laptop which log stress – displacement curve independent of AE recording.

12.5 Geometrical factor used in SINTEF spreadsheet

This formula is found on page 3-29 in Thaulow and Valberg (2012).

$$f\left(\frac{a}{W}\right) = 3\left(\frac{a}{W}\right)^{1/2} \times \frac{1.99 - (a/W) \times (1 - a/W) \times [2.15 - 3.93\left(\frac{a}{W}\right) + 2.7(a/W)^2]}{2\left(1 + \frac{2a}{W}\right) \times (1 - a/W)^{3/2}}$$

12.6 Line display setup



The dialog box is titled "Line Display Setup" and contains several sections for configuring the display. At the top, there are two checked options: "Enable Line Display" and "All Time Data on a Single Line". Below this is a checked option "Use Seconds Format".

The "Select Hit Data Items to Display" section contains a grid of 12 items, all of which are checked:

<input checked="" type="checkbox"/> Time of Test	<input checked="" type="checkbox"/> ASL	<input checked="" type="checkbox"/> Signal Strength	<input checked="" type="checkbox"/> Partial Power 3
<input checked="" type="checkbox"/> Channel	<input checked="" type="checkbox"/> Threshold	<input checked="" type="checkbox"/> Absolute Energy	<input checked="" type="checkbox"/> Partial Power 4
<input checked="" type="checkbox"/> Amplitude	<input checked="" type="checkbox"/> Rise Time	<input checked="" type="checkbox"/> Parametric 1	<input checked="" type="checkbox"/> Frequency Centroid
<input checked="" type="checkbox"/> Energy	<input checked="" type="checkbox"/> Counts to Peak	<input checked="" type="checkbox"/> Parametric 2	<input checked="" type="checkbox"/> Peak Frequency
<input checked="" type="checkbox"/> Counts	<input checked="" type="checkbox"/> Average Frequency	<input type="checkbox"/> Cycle Counter/ RPM	
<input checked="" type="checkbox"/> Duration	<input checked="" type="checkbox"/> Reverberation Frequency	<input checked="" type="checkbox"/> Partial Power 1	
<input checked="" type="checkbox"/> RMS	<input checked="" type="checkbox"/> Initiation Frequency	<input checked="" type="checkbox"/> Partial Power 2	

The "Select Time Data Items to Display" section has two sub-sections. The first has "Time of Test" checked and "Cycle Counter/ RPM" unchecked. The second, "Per-Channel Items", has "RMS", "ASL", and "Absolute Energy" checked, and "Threshold" unchecked. To the right is a list of 8 parametric items, with Parametric 1, 2, and 3 checked, and Parametric 4 through 8 unchecked. Below this list is the text "Param: 1-4".

The "Select Messages to Display" section has "Enable Hit Data Display" and "Enable Δ ST Data Display" checked, while "Enable Time Data Display", "Enable Alarm Data Display", and "Enable Timemark Data Display" are unchecked. "Enable Waveform Display" is also unchecked.

At the bottom right, there are two spinners: "Display up to 8 hits of event" and "Display up to 1024 kb of text". There are "OK" and "Cancel" buttons at the bottom right.

12.7 Other parameters in AEwin

- “ASL” = This is a measurement of the signal continuous amplitude and is measured in dB. The average value is adjusted constantly during testing with a gap of 10 – 1000 milliseconds depending on the settings. This parameter gives an indication of the activity in the material due to processes with amplitude below the threshold value.
- “RMS” = This is an easy mathematical calculation of the tension in the signal. The amplitude is squared for each signal and summed up.

12.8 Power law

12.8.1 General procedure

Microsoft Excel was used to obtain a power law which describes the trend line linked to the points. The following steps were made:

1. Define a formula for the power law. The general function $y = A + Bx^n$ where chosen. $A, B, n = constants$ while y and $x = value\ on\ y -\ and\ x -\ axis$.
2. Three columns were made for the x and y data in addition to one column which were called "y_model". The power law was inserted in this column to calculate the "y_model".
3. The constants A, B and n was set at each rows and defined with the value 1.
4. The names and the appurtenant cells were defined by using "Create from Selection", found under the "Formulas" tab.
5. "y_model" were calculated.
6. A minimum value were found by the following equation: " $=SUMPRODUCT(y-y_model;y-y_model)$ ".
7. This "minimum value" was reduced by changing the variables A, B and n . This was done with the add in "Solver". If the add in is not present under the "Data" tab it can be found by "File" -> "Options" -> "Add-Ins" -> set "Manage" to "Excel Add-ins" and click «Go..." -> tick the box and click "ok".
8. In the "Solver" the following steps were done:
 - a. Choose the cell which contains the minimum value in the field "Set Objective:"
 - b. Tick the "Min" tab
 - c. Choose the cells which contains the value defining the constants A, B and n in the field "By Changing Variable Cells"
 - d. "Select a Solving Method" were set to "GRG Nonlinear"
 - e. In "Options" under the "GRG Nonlinear" tab were the number in "Convergence" field reduced by adding zeroes and "Central" were chosen for "Derivatives"
 - f. The "Solve" tab was clicked to start the calculations.
9. After the calculations was executed were the new "minimum value" checked in addition to comparing the y values with the new y_model values.

12.8.2 From Østby et al., 2012

Five attempts were made to achieve a satisfying result, starting with all of the points and removing those points which are thought to differ largely from the trend. See Table 7-2, page 100, for a list of the points. The results of the five tests are shown below.

1. attempt					2. attempt				
x	y	y_model			x	y	y_model		
64	32	26.778	A	0	64	32	28.049	A	0
78	35	61.231	B	7.52652E-07	79	55	66.932	B	9.72067E-07
79	55	64.580	n	4.180752	90	87	114.677	n	4.13039
90	87	111.3774686			97	125	156.256		
93	89	127.7418162	Min.	9759.5861	109	232	252.964	Min.	261266.6102
97	125	152.3329888			111	260	272.694		
109	232	248.0669833			112	354	282.985		
111	260	267.6592108							
112	354	277.8858323							
3. attempt					4. attempt				
x	y	y_model			x	y	y_model		
64	32	30.149	A	0	64	32	30.122	A	0
79	55	72.262	B	9.56921E-07	109	232	277.905	B	8.73993E-07
109	232	274.974	n	4.15152	112	354	311.246	n	4.17310
112	354	307.783							
			Min.	4284.2029				Min.	3938.7125
5. attempt									
x	y	y_model							
64	32	34.148	A	0					
112	354	353.364	B	9,80085E-07					
			n	4.17572					
			Min	5.01768					

Table 12-1 - Attempts to acquire a power law based on Østby et al., 2012

12.9 Overview all SENB05 tests

12.9.1 From project thesis

Identification	OK?	Comment	Number of screened out signals	Total number of signals
30-5sec1cyc -60	No	Straight to macro-fracture	1	1
31-5sec1cyc -60	No	Straight to macro-fracture	5	5
32-5sec1cyc -60	No	Straight to macro-fracture	1	1
17-10sec1cyc -60	No	Straight to macro-fracture	3	3
18-10sec1cyc -60	Yes	No macro-fracture	23	32
19-10sec1cyc -60	No	Straight to macro-fracture	1	1
5-15sec1cyc -60	No	Straight to macro-fracture	1	1
6-15sec1cyc -60	No	Straight to macro-fracture	1	1
7-15sec1cyc -60	Yes	Macro-fracture	51	53
36-5sec2cyc -60	No	Straight to macro-fracture	5	5
37-5sec2cyc -60	No	Straight to macro-fracture	1	1
38-5sec2cyc -60	No	Straight to macro-fracture	1	1
23-10sec2cyc -60	No	Straight to macro-fracture	1	1
24-10sec2cyc -60	Yes	No macro-fracture	15	28
25-10sec2cyc -60	Yes	Macro-fracture	1	2
11-15sec2cyc -60	No	Straight to macro-fracture	2	2
12-15sec2cyc -60	Yes	Macro-fracture	1	3
13-15sec2cyc -60	No	Straight to macro-fracture	2	2

Table 12-2 - Overview of tests run to macroscopic fracture – project

12.9.2 Conducted during writing of master thesis

Tests run to macroscopic fracture

Identification	OK?	Comment	Number of screened out signals	Total number of signals
58-5sec1cyc RT	No	Signal from de-loading	2	2
59-5sec1cyc RT	Yes	No macro-fracture	0	1
60-5sec1cyc RT	Yes	No macro-fracture	0	1
94-15sec1cyc RT	Yes	No macro-fracture	0	1
95-15sec1cyc RT	No	Straight to macro-fracture	1	1
96-15sec1cyc RT	No	No signal	0	0
54-5sec1cyc 0c	Yes	No macro-fracture	0	2
55-5sec1cyc 0c	Yes	No macro-fracture	0	5
57-5sec1cyc 0c	Yes	Macro-fracture	2	6
91-15sec1cyc 0c	No	Macro-fracture	1	1
92-15sec1cyc 0c	No	No signal	0	0
93-15sec1cyc 0c	Yes	No macro-fracture	2	3
49-5sec1cyc - 30c	No	Straight to macro-fracture	1	1
51-5sec1cyc - 30c	No	Straight to macro-fracture	1	1
52-5sec1cyc - 30c	No	Straight to macro-fracture	1	6
88-15sec1cyc - 30c	No	Straight to macro-fracture	1	1
89-15sec1cyc - 30c	Yes	Macro-fracture	2	4
90-15sec1cyc - 30c	Yes	No macro-fracture	0	8
129-25sec1cyc - 30c	Yes	No macro-fracture	0	5
130-25sec1cyc - 30c	Yes	No macro-fracture	3	4

131-25sec1cyc - 30c	Yes	No macro-fracture	0	8
135-25sec1cyc - 45c	Yes	Macro-fracture	1	3
136-25sec1cyc - 45c	Yes	No macro-fracture	0	8
137-25sec1cyc - 45c	Yes	Macro-fracture	1	6
132-25sec1cyc - 60c	No	Straight to macro-fracture	1	1
133-25sec1cyc - 60c	Yes	Macro-fracture	1	3
134-25sec1cyc - 60c	Yes	No macro-fracture	4	16
138-25sec1cyc - 75c	Yes	Macro-fracture	3	5
139-25sec1cyc - 75c	Yes	Macro-fracture	4	5
140-25sec1cyc - 75c	No	Straight to macro-fracture	1	1

Table 12-3 - Overview - SENB 05 tests run to macroscopic fracture - master

Interrupted tests

Identification	OK?	Comment	Number of screened out signals	Total number of signals
166 5sec1cyc – 30c	Yes	Macro-fracture	1	2
167 5sec1cyc – 30c	Yes	No macro-fracture	0	1
168 5sec1cyc – 60c	No	Straight to macro-fracture	3	3
169 5sec1cyc – 60c	No	Straight to macro-fracture	1	1
170 5sec1cyc – 30c	Yes	Macro-fracture	1	3
171 5sec1cyc – 30c	No	Straight to macro-fracture	1	1
172 5sec1cyc – 30c	No	Straight to macro-fracture	1	1
125 15sec1cyc – 30c	Yes	Macro-fracture	4	5
125 15sec1cyc – 30c	Yes	No macro-fracture	0	1
127 15sec1cyc – 30c	No	Straight to macro-fracture	2	2
128 15sec1cyc – 30c	No	Straight to macro-fracture	2	2
180 15sec1cyc – 60c	Yes	No macro-fracture	0	1
182 15sec1cyc – 60c	Yes	Macro-fracture	11	13
183 15sec1cyc - 60c	No	Straight to macro-fracture	2	2
184 15sec1cyc - 60c	No	Straight to macro-fracture	2	2
185 15sec1cyc - 60c	Yes	No macro-fracture	6	8
191 25sec1cyc - 60c	Yes	No macro-fracture	0	1
191 25sec1cyc - 60c	Yes	No macro-fracture	0	1
191 25sec1cyc - 60c	No	Straight to macro-fracture	1	1
216 5sec2cyc - 60c	No	Straight to macro-fracture	3	3
217 5sec2cyc - 60c	Yes	No macro-fracture	0	1

218 5sec2cyc - 60c	No	Straight to macro-fracture	1	1
219 5sec2cyc - 60c	No	Straight to macro-fracture	2	2
220 5sec2cyc - 60c	No	No data		
221 5sec2cyc - 60c	Yes	Macro -fracture	1	2
222 5sec2cyc - 30c	Yes	No macro-fracture	0	3
223 5sec2cyc - 60c	No	Straight to macro-fracture	1	1
224 5sec2cyc - 60c	Yes	No macro-fracture	1	2
225 5sec2cyc - 60c	Yes	No macro-fracture	1	3
333 15sec2cyc - 60c	Yes	No macro-fracture	1	2
334 15sec2cyc - 60c	Yes	Macro -fracture	1	2
335 15sec2cyc - 60c	Yes	No macro-fracture	0	1
336 15sec2cyc - 60c	Yes	No macro-fracture	0	1
337 15sec2cyc - 30c	Yes	No macro-fracture	0	2
338 15sec2cyc - 30c	No	No macro-fracture -RISE	2	2
339 15sec2cyc - 45c	Yes	No macro-fracture	0	1
340 25sec2cyc - 45c	Yes	No macro-fracture	0	2
341 25sec2cyc - 60c	No	Straight to macro-fracture	1	1
342 25sec2cyc - 60c	No	Straight to macro-fracture	1	1
343 25sec2cyc - 60c	No	Straight to macro-fracture	1	1
344 25sec2cyc - 60c	Yes	Macro-fracture	1	2
345 25sec2cyc - 60c	No	Straight to macro-fracture	1	1
346 25sec2cyc - 60c	Yes	No macro-fracture	0	1
347 25sec2cyc - 60c	No	Straight to macro-fracture	1	1

348 25sec2cyc - 60c	No	Straight to macro-fracture	1	1
348 25sec2cyc - 60c	No	Straight to macro-fracture	1	1

Table 12-4 - Overview - SENB 05 Interrupted tests – master

12.10 EDS - Average values, smooth and rough surfaces

Element	Smooth surface				Rough surface			
	Wt %	Atomic %	Net Int.	Error %	Wt %	Atomic %	Net Int.	Error %
C K	2.55	10.42	0.90	44.21	1.56	6.48	0.51	65.20
O K	1.31	4.04	2.08	39.27	1.46	4.59	2.18	32.22
AlK	0.35	0.64	0.74	86.06	0.30	0.56	0.59	90.77
SiK	0.39	0.68	1.12	78.45	0.38	0.69	1.04	78.35
P K	0.23	0.36	0.70	83.42	0.19	0.31	0.53	85.48
NbL	0.32	0.17	0.56	77.03	0.30	0.16	0.50	80.39
MoL	0.34	0.18	0.65	74.61	0.34	0.18	0.60	75.13
S K	0.01	0.01	0.02	99.99	0.01	0.01	0.02	99.99
CaK	0.61	0.75	1.96	57.10	0.75	0.95	2.19	49.04
CrK	0.71	0.67	2.12	57.20	0.97	0.95	2.60	41.77
MnK	1.96	1.76	3.47	38.19	2.24	2.08	3.61	32.34
FeK	89.15	78.60	127.91	3.37	88.94	80.80	117.52	3.38
CoK	1.07	0.89	1.26	68.18	1.50	1.31	1.63	56.77
NiK	1.01	0.84	0.96	70.14	1.07	0.93	0.95	69.25

Table 12-5 - EDS on smooth and rough surfaces - Test no. 126

Element	Smooth surface				Rough surface			
	Wt %	Atomic %	Net Int.	Error %	Wt %	Atomic %	Net Int.	Error %
C K	2.13	8.78	2.65	31.84	2.41	9.18	1.75	37.93
O K	1.14	3.58	8.52	23.88	2.21	6.35	7.17	23.56
AlK	0.22	0.41	1.38	81.62	0.27	0.47	1.20	81.65
SiK	0.25	0.45	2.54	72.82	0.31	0.54	2.16	68.99
P K	0.12	0.20	1.09	76.74	0.14	0.22	1.02	80.05
NbL	0.17	0.09	0.94	73.91	0.22	0.12	0.99	74.81
MoL	0.23	0.12	1.31	67.84	0.30	0.16	1.43	68.88
S K	0.00	0.00	0.03	99.99	0.00	0.00	0.02	99.99
CaK	0.38	0.48	3.80	54.81	0.57	0.72	5.04	43.86
CrK	0.50	0.48	5.39	50.79	0.77	0.75	6.24	39.50
MnK	1.78	1.63	13.42	22.71	2.01	1.82	9.32	28.46
FeK	91.37	82.33	593.73	2.48	88.81	77.98	319.62	2.71
CoK	1.05	0.90	5.39	51.77	1.20	1.03	3.92	49.53
NiK	0.64	0.55	2.24	66.13	0.76	0.65	1.89	63.23

Table 12-6 - EDS on smooth and rough surfaces - Test no. 180

Element	Smooth surface				Rough surface			
	Wt %	Atomic %	Net Int.	Error %	Wt %	Atomic %	Net Int.	Error %
C K	0.91	3.63	1.67	28.19	2.04	8.30	2.16	22.12
O K	0.60	1.84	3.13	30.16	1.85	5.69	8.98	13.09
AlK	0.13	0.17	0.76	59.36	0.21	0.38	1.32	63.26
SiK	0.17	0.22	1.27	48.21	0.25	0.44	2.16	51.80
P K	0.04	0.06	0.35	71.28	0.09	0.15	0.82	66.59
NbL	0.09	0.10	0.79	54.40	0.13	0.07	0.71	65.39
MoL	0.19	0.15	1.43	44.58	0.20	0.10	1.08	59.77
S K	0.50	0.46	2.62	55.56	0.00	0.00	0.01	99.99
CaK	30.80	27.55	130.30	28.98	0.19	0.23	1.76	54.36
CrK	0.37	0.34	2.28	38.97	0.31	0.30	2.80	42.01
MnK	0.88	0.81	4.44	29.00	1.52	1.38	7.90	16.36
FeK	46.66	42.77	203.22	0.97	92.21	82.11	388.00	1.94
CoK	0.39	0.34	1.39	21.37	0.60	0.51	2.12	55.92
NiK	Not valid	Not valid	Not valid	Not valid	0.39	0.33	1.13	62.46

Table 12-7 - EDS on smooth and rough surfaces - Test no. 339

Element	Smooth surface				Rough surface			
	Wt %	Atomic %	Net Int.	Error %	Wt %	Atomic %	Net Int.	Error %
C K	4.40	16.17	5.33	23.94	5.49	20.66	2.85	23.01
O K	0.92	2.72	12.46	36.72	0.85	2.42	1.78	38.16
AlK	0.23	0.41	5.67	68.78	0.19	0.32	0.58	91.38
SiK	0.19	0.34	6.36	59.13	0.29	0.48	1.225	76.87
P K	0.07	0.11	2.33	75.74	0.115	0.17	0.51	85.66
NbL	0.09	0.05	1.75	81.61	0.16	0.08	0.405	80.84
MoL	0.13	0.07	2.38	77.28	0.21	0.10	0.54	74.95
S K	0.00	0.01	0.03	99.99	0	0.01	0.02	99.99
CaK	0.44	0.54	9.43	50.30	0.85	0.97	3.86	33.05
CrK	0.80	0.74	13.95	35.72	0.98	0.865	4.105	32.53
MnK	2.10	1.83	23.74	19.27	2.62	2.17	6.57	21.82
FeK	88.50	75.27	841.05	2.48	85.79	69.87	174.45	2.95
CoK	1.57	1.28	12.65	36.99	1.48	1.15	2.495	49.11
NiK	0.56	0.46	3.57	60.42	0.98	0.76	1.355	68.25

Table 12-8 - EDS on smooth and rough surfaces - Test no. 167

Element	Smooth surface				Rough surface			
	Wt %	Atomic %	Net Int.	Error %	Wt %	Atomic %	Net Int.	Error %
C K	3.84	14.69	1.31	40.27	2.63	10.27	1.34	39.46
O K	1.29	3.73	1.90	47.22	1.02	3.03	3.04	36.03
AlK	0.36	0.63	0.74	86.11	0.23	0.41	0.68	63.01
SiK	0.40	0.66	1.12	79.24	0.26	0.44	1.15	55.14
P K	0.19	0.29	0.55	84.60	0.07	0.11	0.27	65.02
NbL	0.30	0.16	0.52	79.73	0.12	0.06	0.27	68.24
MoL	0.30	0.15	0.53	77.15	0.14	0.07	0.40	68.21
S K	0.01	0.01	0.03	99.99	0.00	0.00	0.01	88.03
CaK	0.48	0.57	1.44	63.89	0.22	0.27	1.61	62.38
CrK	0.62	0.59	1.71	60.90	0.48	0.46	3.52	49.07
MnK	1.83	1.60	2.99	42.92	1.62	1.50	7.72	34.89
FeK	88.38	75.28	118.95	3.43	91.75	82.16	327.55	2.61
CoK	1.18	0.97	1.26	67.66	0.93	0.79	2.68	51.58
NiK	0.82	0.67	0.75	74.43	0.53	0.44	0.99	68.92

Table 12-9 - EDS on smooth and rough surfaces - Test no 217

12.12 EDS of inclusion in arrested microcracks – test no 167

Element	Side 1				Side 2			
	Wt %	Atomic %	Net Int.	Error %	Wt %	Atomic %	Net Int.	Error %
C K	2.51	8.01	5.74	15.95	4.45	14.68	13.66	12.63
O K	8.15	19.16	55.31	10.62	6.14	16.79	79.74	9.06
AlK	7.00	9.80	131.91	8.28	2.63	5.06	85.76	10.19
SiK	0.41	0.55	9.50	17.44	0.16	0.33	7.18	40.17
P K	0.03	0.03	0.61	92.03	0.02	0.03	0.84	83.59
NbL	0.04	0.02	0.50	88.18	0.04	0.01	0.27	89.93
MoL	1.31	0.58	18.58	29.10	0.94	0.26	10.38	21.92
S K	3.98	4.80	107.27	6.26	1.56	1.19	31.04	10.77
CaK	12.52	12.14	275.76	2.77	2.72	3.30	100.70	4.94
CrK	0.41	0.33	7.17	43.28	0.55	0.30	9.13	22.17
MnK	1.22	0.89	14.68	15.02	14.47	1.13	22.66	11.74
FeK	61.76	43.23	627.37	1.98	65.28	56.20	948.79	1.74
CoK	0.52	0.36	4.43	49.92	0.90	0.64	9.34	18.85
NiK	0.15	0.10	1.05	65.00	0.14	0.09	1.20	62.35

Table 12-10 - EDS on lower inclusion – Test no. 167

Element	Side 1				Side 2			
	Wt %	Atomic %	Net Int.	Error %	Wt %	Atomic %	Net Int.	Error %
C K	4.07	12.12	8.09	14.56	4.42	13.96	8.34	14.82
O K	8.19	17.68	36.25	12.22	4.04	9.56	19.27	13.78
AlK	8.00	10.30	150.35	7.78	1.74	2.45	34.97	10.19
SiK	0.35	0.43	7.70	22.16	0.01	0.01	0.18	65.64
P K	0.06	0.06	1.32	77.81	0.00	0.00	0.00	4.32
NbL	0.03	0.01	0.39	87.39	0.00	0.00	0.00	99.99
MoL	2.06	0.78	26.62	7.38	0.00	0.00	0.01	99.99
S K	6.29	7.24	156.79	6.30	15.08	17.84	434.80	3.86
CaK	22.20	19.93	420.30	2.46	20.27	19.17	433.45	2.57
CrK	0.91	0.64	12.16	15.18	0.72	0.53	11.30	15.42
MnK	1.54	1.01	15.49	13.47	1.57	1.09	18.21	12.39
FeK	45.37	29.23	395.70	2.24	51.03	34.70	508.67	2.15
CoK	0.77	0.47	5.62	23.80	0.95	0.61	7.91	18.27
NiK	0.17	0.10	1.09	62.10	0.17	0.11	1.21	61.59

Table 12-11 - EDS on upper inclusion – Test no. 167

12.13 EDS of fracture of inclusion – test no. 167

Element	Wt %	Atomic %	Net Int.	Error %
C K	1.44	4.36	1.45	27.38
O K	5.13	11.50	9.33	17.32
AlK	1.96	2.61	31.53	9.67
SiK	0.15	0.20	2.64	45.84
P K	0.07	0.08	1.24	77.87
NbL	0.01	0.00	0.07	99.99
MoL	3.51	1.37	34.96	6.60
S K	22.13	25.08	440.56	3.35
CaK	38.39	35.45	473.01	2.67
CrK	0.53	0.42	3.52	51.59
MnK	1.07	0.77	6.27	23.00
FeK	24.94	17.69	136.01	3.34
CoK	0.51	0.35	2.12	53.14
NiK	0.18	0.11	0.78	64.04

Table 12-12 - EDS on fracture of inclusion - Test no. 167

12.14 EDS on unknown facet – test no. 217

Element	Fracture facet				Rough facet			
	Wt %	Atomic %	Net Int.	Error %	Wt %	Atomic %	Net Int.	Error %
C K	4.98	18.73	1.77	30.11	2.75	10.93	0.96	44.04
O K	1.75	4.94	2.65	33.03	1.26	3.75	1.94	46.52
AlK	0.51	0.86	1.09	80.04	0.37	0.67	0.77	85.65
SiK	0.34	0.54	0.99	80.75	0.32	0.55	0.90	82.51
P K	0.16	0.23	0.46	86.65	0.12	0.19	0.34	93.24
NbL	0.18	0.09	0.32	87.97	0.28	0.15	0.48	82.21
MoL	0.23	0.11	0.43	77.15	0.21	0.11	0.38	82.17
S K	0.01	0.01	0.03	99.99	0.01	0.01	0.02	99.99
CaK	0.20	0.23	0.65	76.91	0.51	0.65	1.58	65.59
CrK	0.31	0.27	0.93	74.54	0.53	0.52	1.58	66.35
MnK	1.31	1.08	2.31	58.40	1.90	1.73	3.31	44.94
FeK	88.52	71.75	126.07	3.43	89.74	79.03	126.49	3.40
CoK	0.79	0.61	0.94	74.07	1.09	0.94	1.28	68.79
NiK	0.75	0.58	0.72	74.50	0.91	0.78	0.87	69.58

Table 12-13 - EDS on unknown facet – Test no. 217

12.15 X80 TPI

These three specimens were polished and etched in Nital for investigation of microstructure. It was going to be used to compare with the R50A 420 from Ruukki. Unfortunately there was not enough time. The three corresponding fracture surfaces were prepared for investigation in SEM and overview pictures were taken. This can be found on the USB stick.

Vickers Hardness			
Specimen	Line number	HV	Standard Deviation
15-2cyc 5sec	1	297.9HV0.1	10.43
15-2cyc 5sec	2	216.9HV0.1	17.34
25-2cyc 10sec	1	283.6HV0.1	20.88
25-2cyc 10sec	2	215.1HV0.1	14.88
11-2cyc 15sec	1	285.1HV0.1	17.97
11-2cyc 15sec	2	187.2HV0.1	11.23

Table 12-14 - Vickers Hardness X80 TPI

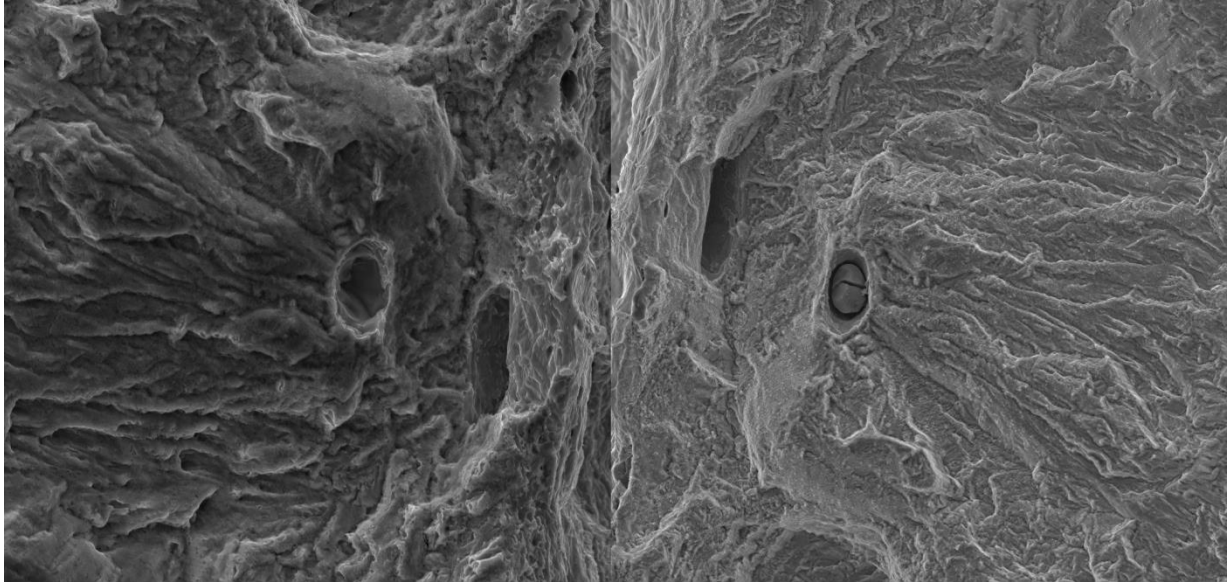
Weldability for X80 TPI

In the datasheet provided from Posco for X80 TPI are CE = 0.43 which is somewhat more than what Palmer (2008) recommend for a pipe steel. On the other hand are PCM = 0.17 which are below what he stated as a maximum.

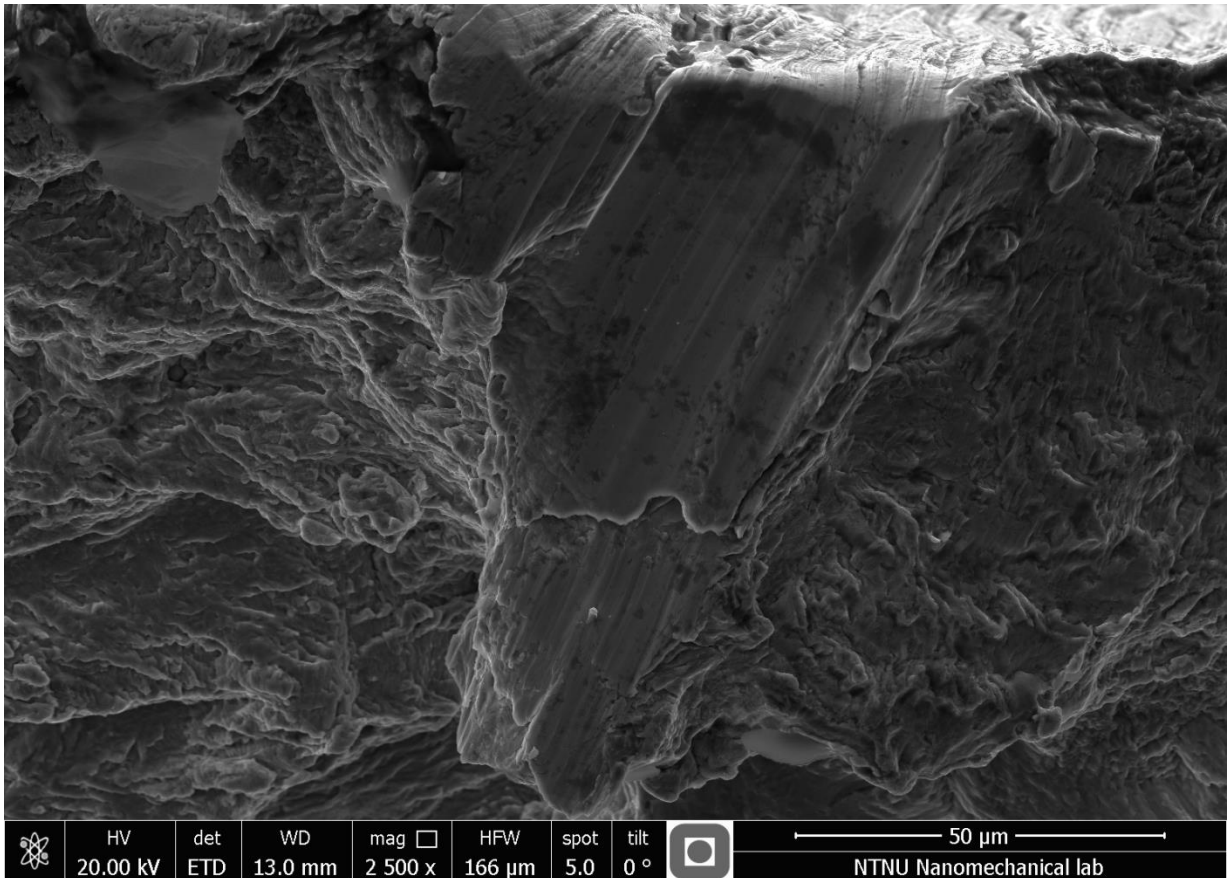
12.16 Additional pictures taken in SEM

12.16.1 Missing inclusion

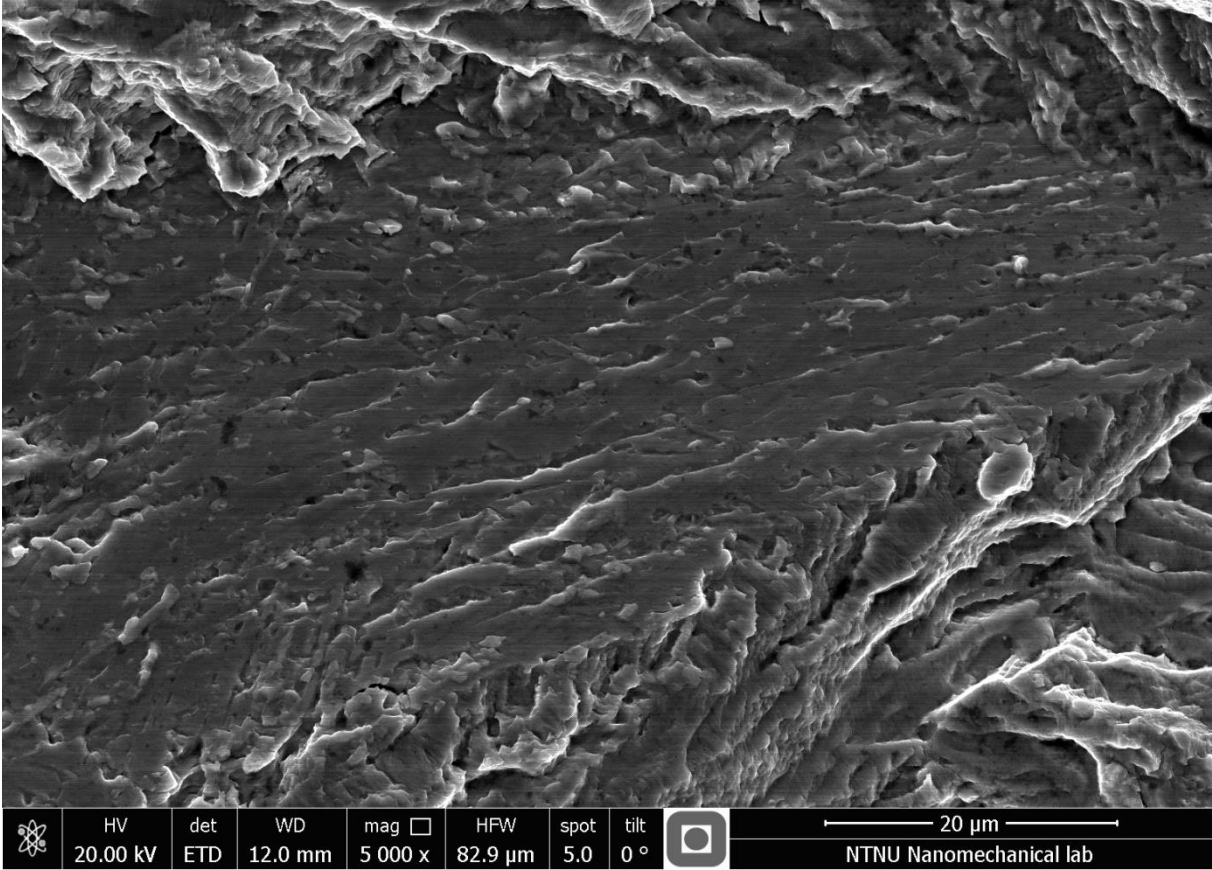
Taken at magnification 5000X, but the left with 20.00kV and the right with 10.00 kV, hence the difference in brightness.



12.16.2 Deformed edge



12.16.3 Test no. 217 – smooth surface enlarged.



12.17 Form for crack depth measurement



Måleskjema for bruddmekanisk prøving

SINTEF Materialer og kjemi
Laboratorium for materialprøving

Prosjektnr.:		Prosedyrer.:	
Testmaskin Id. Nr.:		SENT eller SENB:	
B og W måleverktøy Id. Nr.:		Klypemåler 1, id. nr.:	
Sprekkklengde måleverktøy Id. Nr.:		Klypemåler 2, id. nr.:	
SENB opplageravstand S:		Klypemåler 3, id. nr.:	
Test temp.T: °C	Rate: mm/min	Knivh. z ₁ og z ₂ :	mm

Prøvenummer		49		36		31	
Skårplassering							
Skårvinkel α °							
Skårretn. SN/TT							
Skår fra Cap/Rot							
Type brudd (m, u eller c)							
Bredde B mm							
Høyde W mm							
Erodert skårl. mm			Δa_{TOT}		Δa_{TOT}		Δa_{TOT}
a _{1%B} mm		4,845	-"-	4,635	-"-	4,800	4,990
a _{12.5%B} mm		5,055	-"-	4,825	-"-	4,925	5,655
a _{25%B} mm		5,030	-"-	5,015	-"-	5,000	5,905
a _{37.5%B} mm		4,975	-"-	5,115	-"-	5,045	5,850
a _{50%B} mm		4,875	-"-	5,125	-"-	5,045	5,820
a _{62.5%B} mm		4,900	-"-	5,070	-"-	5,030	5,850
a _{75%B} mm		4,835	-"-	4,900	-"-	5,100	6,810
a _{87.5%B} mm		4,795	-"-	4,720	-"-	5,055	5,590
a _{99%B} mm		4,550	-"-	4,525	-"-	4,870	5,135

Merknader:

DATO:.....

SIGN:.....

12.18 Calculated CTOD

Calculation of CTOD from CMOD of a SENB05 after BS7448:1991

Specimen number 7

Distance between supports: $S_s := 40\text{mm}$

Height of plate: $W_h := 10\text{mm}$

Crack depth: $a := 5.03\text{mm}$

Applied force $P := 6.689\text{kN}$

Plate thickness: $B := 10\text{mm}$

E - modulus - assumed $E := 208000 \frac{\text{N}}{\text{mm}^2}$

Yield strength: $\sigma_{YS} := 498 \frac{\text{N}}{\text{mm}^2}$

Plastic rotation factor, BS 7448 $r_p := 0.4$

Poisson number - assumed $\nu := 0.3$

Hight of clamps $z := 0$

CMOD $V_p := 1.8316\text{mm}$

F(a/W):

$$F_{\text{ratio}} := \frac{3 \cdot \frac{S_s}{W_h} \cdot \sqrt{\frac{a}{W_h}}}{2 \left(1 + 2 \cdot \frac{a}{W_h}\right) \left(1 - \frac{a}{W_h}\right)^{\frac{3}{2}}} \left[1.99 - \frac{a}{W_h} \left(1 - \frac{a}{W_h}\right) \left[2.15 - 3.93 \left(\frac{a}{W_h}\right) + 2.7 \left(\frac{a}{W_h}\right)^2 \right] \right] = 10.8$$

Stress intensity factor: $K_1 := \frac{P}{B \cdot \sqrt{W_h}} \cdot F_{\text{ratio}} = 71.921 \cdot \text{MPa} \cdot \sqrt{\text{m}}$

$$E_{ps} := \frac{E}{1 - \nu^2} = 2.286 \times 10^5 \cdot \frac{\text{N}}{\text{mm}^2}$$

CTOD: $\delta_{\text{CTOD}} = \delta_{\text{el}} + \delta_{\text{pl}}$

$$\delta_{\text{CTOD}} := \frac{K_1^2 \cdot (1 - \nu^2)}{2 \cdot \sigma_{YS} \cdot E_{ps}} + \frac{r_p \cdot (W_h - a) \cdot V_p}{r_p \cdot (W_h - a) + a + z} = 0.5395 \cdot \text{mm}$$